Optimization of PECVD Boron-Phosphorus Doped Silicon Oxynitride

for Low-Loss Optical Waveguides

Mohamed Gamar Hussein

Graduation committee:

Chairman and Secretary:	
Prof. Dr. ir. A.J. Mouthaan	University of Twente
Promotor:	
Prof. Dr. A. Driessen	University of Twente
Assistant Promotor:	
Dr. K. Wörhoff	University of Twente
Members:	
Prof. Dr. J. Schmitz	University of Twente
Prof. Dr. ing. D.H.A. Blank	University of Twente
Prof. Dr.-Ing. habil. J. Müller	Technische Universität Hamburg-Harburg
Prof. Dr. P.V. Lambeck	University of Twente/OptiSense B.V.
Prof. Dr. H.W.M. Salemink	TU Delft

The research described in this thesis was carried out at the Integrated Optical Microsystems (IOMS) Group, Faculty of Electrical Engineering, Mathematics and Computer Science, MESA+ Research Institute for Nanotechnology, University of Twente, P.O. Box 217, 7500 AE Enschede, The Netherlands.

This work was financially supported by the European TIOM project for the first two years and by the Dutch National Freeband Communication project "Broadband Photonics" for the last two and half years.

Printed by PrintPartners IPSKAMP, Enschede, The Netherlands.

ISBN: 978-90-365-2473-5

OPTIMIZATION OF PECVD BORON-PHOSPHORUS DOPED SILICON OXYNITRIDE FOR LOW-LOSS OPTICAL WAVEGUIDES

DISSERTATION

to obtain
the doctor's degree at the University of Twente,
on the authority of the rector magnificus,
prof. dr. W. H. M. Zijm,
on account of the decision of the graduation committee,
to be publicly defended
on Friday 23 February 2007 at 15:00

by

Mohamed Gamar Hussein

born in Taloudi, Sudan

This dissertation is approved by:

the promotor: Prof. Dr. A. Driessen

the assistant promotor: Dr. K. Wörhoff

To my daughter Lara

Contents

1 Introduction

This chapter gives an introduction to this thesis. The basic concepts of integrated optical waveguide structures will be given as well as the main characteristics of silicon oxynitride for integrated optics. The relevant aspects concerning the silicon oxynitride deposition technology are described. Also the objectives of the present work will be presented. Finally, an outline of the thesis will be given.

1.1 Silicon oxynitride for integrated optics

Since the concept of integrated optics was first proposed in 1969 [1], extensive studies have been undertaken on a variety of optical materials. Most of these materials have been successfully employed in integrated optics and usually classified as low-contrast (e.g., doped silica [2-7], lithium niobate [8-11] or high-contrast (e.g., III-V semiconductor materials [12, 13]).

The basic concept in integrated optical devices is the same as in optical fibers: the confinement of light. A medium that possesses a certain refractive index, surrounded by media with lower refractive indices, can act as a light trap, where the light cannot escape from the structure due to the phenomena of total internal reflection at the interfaces. This effect confines light propagation within high refractive index media (core layer), and can be used to fabricate optical waveguides that transport light from point to point, for long distances in optical fibers or in compact optical circuits in the case of integrated optic devices. Figure 1.1 shows the basic structures for the most common planar optical waveguide geometries. In a slab waveguide structure [Figure 1.1(a)] the light is confined only in the vertical direction. To control light propagation in the lateral dimension, a channel waveguide has to be patterned [see Figure 1.1(b)].

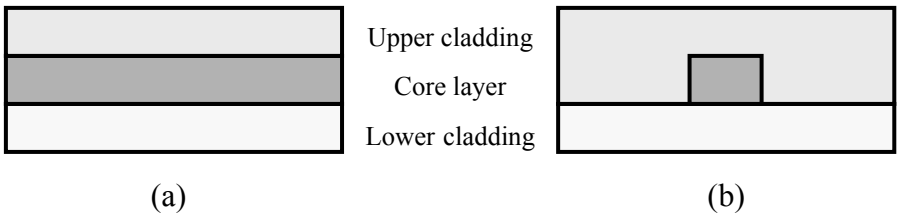

Figure 1.1 Schematic cross-section of basic waveguide structures: (a) slab waveguide; (b) channel waveguide.

Materials must satisfy the following requirements in order to be successfully applied in integrated optics: high transparency, possibility for accurate waveguide definition, high physical, chemical, mechanical and thermal stability, compatibility with other materials used in microelectronics and fiber technology, easy processing and reasonably low cost. Moreover, integrated optics devices for application in telecommunication are highly demanding on low insertion loss, low polarization dependent loss, efficient

fiber-to-chip coupling and high integration density [14, 15]. The size of the waveguides is strongly dependent on the index contrast of the structure. In low index contrast waveguiding structures, the large channel cross-section of these waveguides matches well with the standard optical fiber, but due to the low index contrast large bending radii are required, leading to a low integration density. High-contrast systems on the other hand allow very small bending radii and hence compact devices, but high-efficiency fiber-chip coupling is difficult to obtain. This parameter, however, can be significantly improved by a proper design of the fiber-to-chip interface [16, 17]. These improvements make sense for active devices, such as semiconductor (mainly GaAs/AlGaAs and InP/InGaAsP) optical amplifiers and high speed modulators.

For passive devices, much attention has been paid to silicon based dielectrics in the last two decades. In particular, silicon oxynitride (SiO_xN_y or shortly SiON) has been emerging as a technologically reliable material for integrated optics application [18, 19]. This is mainly because of high transparency in the visible and near-infrared and the possibility of obtaining a broad range in the index of refraction (n) by changing the nitrogen/oxygen composition from SiO_2 (n = 1.45) up to Si_3N_4 (n = 2.0) [20, 21].

The main advantage of silicon-based integrated optical devices is the low cost of the silicon substrates, besides being a well-known material with a long tradition and experience developed from micro-electronic technology. In general, the first step in waveguide fabrication using silicon substrates is the deposition of a silicon dioxide layer with a thickness of a few micrometers. Alternatively, a SiO_2 layer can be obtained by direct oxidation of the silicon at high temperature (~ 1100 ^oC). This layer serves as buffer between the high refractive index silicon substrate and the SiON core layer by providing the low index region for light confinement. Since the refractive index of the SiON can be continuously varied in the range 1.45 – 2.0, a continuous index contrast from low to very high between the waveguide core and the surrounding SiO_2 layer with index 1.45 can be obtained. In this sense SiON offers the device designer a high degree of design freedom to optimize:

- The index contrast between the waveguiding and the cladding layers.
- The dimensions of the waveguide.
- The field confinement in the guiding layer.

The versatility of SiON together with easy and reproducible deposition methods makes it an attractive materials system that allows for compact and potentially low-cost integrated optics structures.

1.1.1 Choice of technology for SiON deposition

Silicon oxynitride can be deposited with a large number of deposition techniques, such as chemical vapor deposition (CVD), reactive sputtering, ion implantation and thermal oxidation/nitridation of silicon. Among them are

several which can currently be considered as standard methods in silicon-based integrated circuit technology, namely, plasma enhanced CVD (PECVD) or low pressure CVD (LPCVD). Both technologies have been successfully used for integrated optics devices and are available in the cleanroom of the MESA+ Research Institute [21-23]. The layer deposition by CVD is based on a chemical reaction between gaseous precursors that are mostly absorbed on the substrate surface. An overview of the gaseous precursors, the energy source for activation, the deposition temperature and pressure ranges of PECVD compared to LPCVD is given in Table 1.1.

Table 1.1 Comparison of characteristic parameters for PECVD and LPCVD.

	Technology		
Parameter	PECVD	LPCVD	References
Gas flow	SiH_4, N_2O, N_2 and NH_3	$SiCl_2H_2$, (O_2 or N_2O) and NH_3	[21, 23-25]
Energy	Electrical (plasma)	Thermal	[21, 24, 26]
Deposition temperature	200 – 400 ^oC	700 – 900 ^oC	[21, 24, 26]
Pressure	33.3 - 266.6 Pa	6.7 – 26.7 Pa	[21, 24, 26]

The major advantage in using PECVD over LPCVD is the ability to deposit at much lower temperatures than would be required for LPCVD. In PECVD the reaction is promoted by the plasma, hence higher deposition rates can be obtained, typically > 30 nm/min in contrast to < 10 nm/min for LPCVD. Moreover, low temperatures make the deposition possible on metallized substrates with low melting points, such as aluminum. The higher temperature in the LPCVD process results, in principle, in higher quality layers, but it appears that these films have also a larger tensile stress, which restricts the layer thickness that can be deposited [24]. One disadvantage of PECVD is target surface contamination. However, this is remedied because a benefit of PECVD is the ability to easily clean the reactor. In practice, preferentially use is given to PECVD as it allows for relatively high deposition rates at low temperatures (< 400 ^oC).

1.1.2 Tetrahedron model of silicon oxynitride

It is known that SiO_2, Si_3N_4 and SiON in amorphous thin films possess a characteristic chemical order, whose basic units are tetrahedra with silicon in the center and oxygen or nitrogen atoms at the vertices. This microscopic structure is called the tetrahedron model [27].

The Tetrahedra can be identified as the fundamental units, which determine the optical response of the layers. For example, it has been shown

that there is a linear relationship between the molar composition and refractive index of the SiON layer (Figure 1.2). Assuming that SiON is a physical mixture of two distinct phases SiO_2 and Si_3N_4, the refractive index of stoichiometric SiO_xN_y (n_{SiON}) can be obtained within a good approximated from the following relations [28]:

$$n_{SiON} = X_{SiO_2} n_{SiO_2} + X_{Si_3N_4} n_{Si_3N_4} \tag{1.1}$$

$$X_{SiO_2} + X_{Si_3N_4} = 1 \tag{1.2}$$

where X_{SiO_2} and $X_{Si_3N_4}$ are the mole fractions, and n_{SiO_2} and $n_{Si_3N_4}$ are the refractive indices of SiO_2 and Si_3N_4 respectively.

From Equations (1.1) and (1.2) the refractive index of SiON can be derived as a function of the mole fraction of SiO_2:

$$n_{SiON} = n_{Si_3N_4} + (n_{SiO_2} - n_{Si_3N_4}) X_{SiO_2} \tag{1.3}$$

Relation (1.3) can be plotted for a given $n_{SiO_2} = 1.45$ and $n_{Si_3N_4} = 2.00$ at a wavelength of 632.8 nm. It demonstrates that the refractive index of stoichiometric SiO_xN_y (n_{SiON}) can be varied continuously between 1.45 –2.0 depending on the relative mole fractions of the oxide and the nitride (see Figure 1.2).

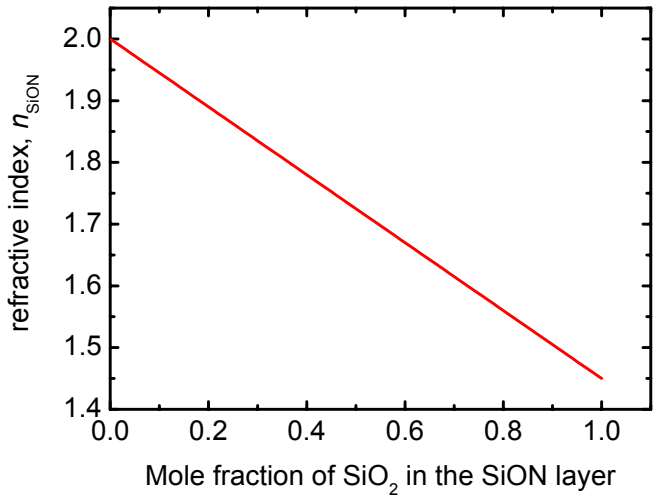

Figure 1.2 The refractive index at 632.8 nm of a SiON layer as a function of the mole fraction of SiO_2 obtained with the aid of Eq. (1.3)

The tetrahedron model has been extended to include hydrogen-rich silicon oxynitride (SiO_xN_y:H). In fact, hundreds of possible tetrahedra should be considered when three or more species can surround the central atom (e.g., O, N, H and NH for SiO_xN_y:H). An example of a SiON tetrahedron with a stretching as well as a bending mode vibration is shown in Figure 1.3.

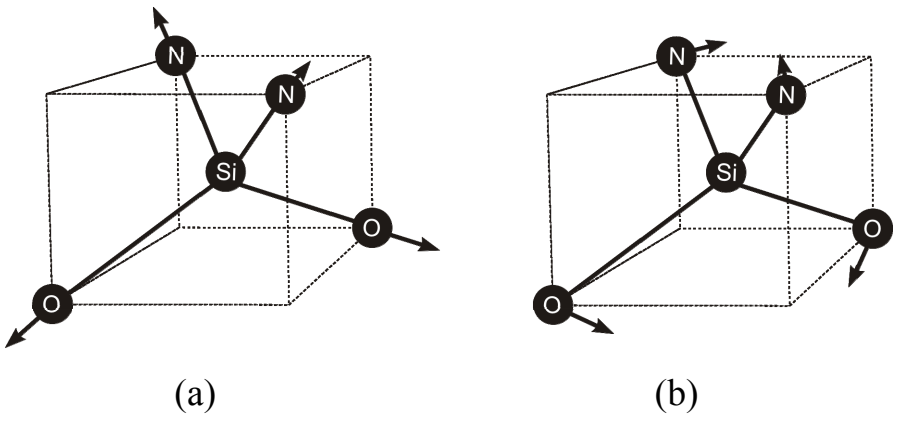

Figure 1.3 Example of SiON tetrahedron (Si-O_2N_2): (a) stretching mode vibration (b) bending mode vibration.

The following tetrahedra (Table 1.2) are considered for silicon-oxynitride [29], where ν= 0, 1, 2, and 3:

Table 1.2 The possible Si-centered tetrahedra in SiON

Si-$Si_{4-\nu}N_\nu$	Si-$HN(NH)_2$
Si-$N_{4-\nu}(NH)_\nu$	Si-$SiO_2(NH)$
Si-$HO_2(NH)$	Si-$SiN_2(NH)$
Si-$SiO(NH)_2$	Si-$O_{4-\nu}N_\nu$
Si-$SiN(NH)_2$	Si-$HO(NH)_2$
Si-$Si_{4-\nu}O_\nu$	Si-$HN_2(NH)$
Si-$O_{4-\nu}(NH)_\nu$	Si-$Si(NH)_3$

1.1.3 Optical properties of PECVD SiON

Refractive index

For integrated optics application the refractive index of the waveguiding layers is one of the main optical parameters. The PECVD SiON refractive index can be adjusted by tuning the N_2O flow, as can be seen from the results given in Figure 1.4. This change is caused by a change in composition from Si_3N_4 to SiO_2. The dependence of the refractive index on the N_2O flow can be divided into two regimes.

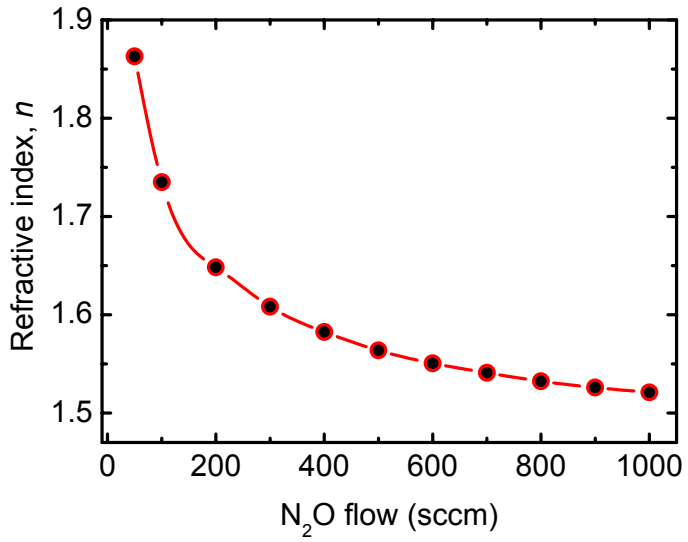

Figure 1.4 Refractive index of PECVD deposited silicon oxynitride as a function of the nitrous oxide flow.

At low N_2O flows, the refractive index change varies rapidly with the N_2O flow. Here, the reproducibility of the refractive index of the silicon oxynitride layers is doubtful because a small change in flow causes a large effect on the refractive index. The slope of the refractive index curve decreases gradually with increased N_2O flow. In the lower refractive index range, the index changes only slightly with the N_2O flow; therefore, the reproducibility will be significantly better. From that point of view, the PECVD process should be applied for integrated optics waveguide fabrication in the refractive index range up to 1.7 [21].

Hydrogen induced optical losses in PECVD SiON layers

Although PECVD SiON is highly transparent in the visible and near-infrared, for applications in the 3rd telecommunication window PECVD SiON layers suffer from the incorporation of hydrogen, especially in the form of N-H and Si-H bonds with stretching modes around 3400 cm^{-1} and 2280 cm^{-1}, respectively [30-33]. Their first and second overtones at 1510 and 1500 nm, respectively, contribute substantially to the absorption in the third telecommunication window around 1550 nm [19, 21, 23, 34]. Figure 1.5 shows a typical optical loss spectrum of a Low Frequency (LF) PECVD SiON layer (n = 1.52). In addition, O-H bonds in PECVD SiON are responsible for optical loss around 1400 nm (see Figure 1.5).

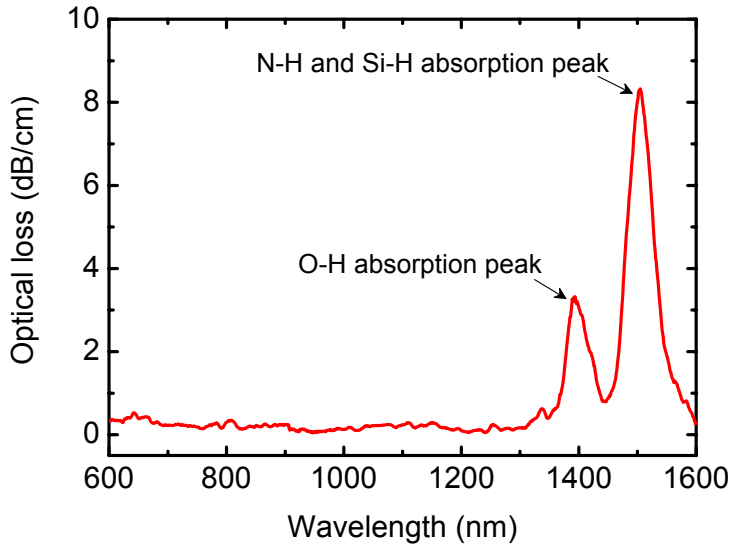

Figure 1.5 Typical optical loss spectrum of an as deposited PECVD SiON layer (n = 1.52).

1.2 Objectives of the present work

The main objective of this thesis is to develop new processes for the realization of PECVD silicon oxynitride thin films for use in low loss optical waveguides.

In the previous section has been explained that the hydrogen incorporation in the SiON matrix is responsible for optical losses in the second and the third telecommunication window. In general, this hydrogen content of as-deposited SiON layers can be reduced significantly by heat treatment at 1150 °C [21, 23, 31, 34]. Annealing, however, at this high temperature for several hours leads to

undesired interface diffusion and to an unwanted strong increase of the stress in the layers that might result in micro-cracks in the material. Therefore, new approaches have to be implemented. One of the means of reducing the hydrogen content in the as-deposited PECVD SiON layers is the introduction of phosphorus doping [35-37]. In our study the process development includes optimization of the undoped SiON, to be a starting point for phosphorus and boron doping.

For practical applications in integrated optics, channels have to be defined by an etching process such as Reactive Ion Etching (RIE). Generally, sidewall quality is critical to device performance, as the scattering loss increases due to sidewall roughness. Hence, a process for smoothing the device structure is needed. Undoped SiON has a prohibitive high melting temperature whereas for doped-silica it is known that by controlling the dopant concentration of phosphorus or boron, a suitable reflow temperature can be obtained [34, 38-40]. That is another reason for introducing phosphorus and boron doping.

Furthermore, after deposition and etching of the core layers, an upper cladding layer of PECVD SiO_2 or low index SiON has to be grown. Problems arise if the aspect ratio is large (see Figure 1.6) resulting in incomplete covering and voids. That means that realization of some important devices, such as arrayed waveguide gratings [41] and microring resonators, where sub-micron gaps between a large numbers of waveguides or the gap between a microring and a straight waveguide have to be completely filled without any void, would even be impossible with the conventional PECVD technology.

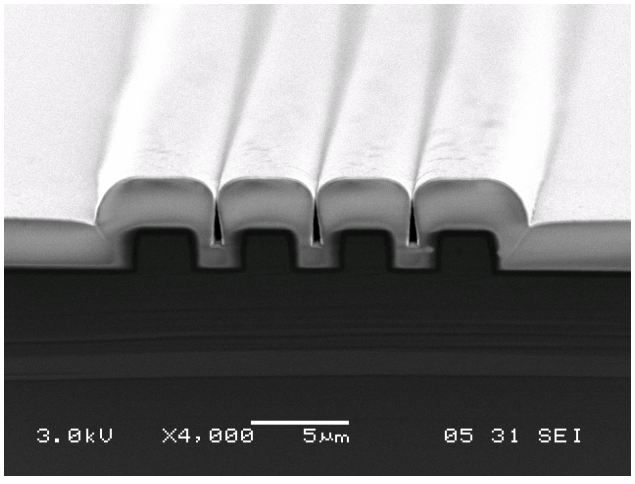

Figure 1.6 As-deposited test structure for PECVD SiON cladding on Si-ridges

1.3 Outline of the thesis

In accordance with the objectives, this thesis is structured as follows:

Chapter 2 describes the deposition technology that has been used to deposit silicon oxynitride layers and techniques used to characterize those layers. A brief description of the PECVD system configuration and its fundamental aspects are presented section (2.1). In order to optimize the fabrication of passive optical waveguides, a number of physical parameters of the deposited layers must be characterized. Methods and experimental setups for the determination of the properties of slab-waveguides are described section (2.2). The refractive index and the layer thickness are both determined by spectroscopic ellipsometry and prism coupler techniques. The stoichiometric composition of the layer material is characterized by X-ray Photoelectron Spectroscopy (XPS) and Rutherford Backscattering Spectroscopy (RBS). The hydrogen induced optical losses are determined by Fourier Transform InfraRed (FTIR) spectroscopy in the deep infrared, whereas the overtones absorption of these hydrogen bonds are measured by the prism coupler technique in the near infrared.

Chapter 3 describes the optimization process of undoped PECVD silicon oxynitride layers, a base material for P and BP-doping. For integrated optics applications, the properties of the silicon oxynitride must be investigated. The uniformity and reproducibility of the refractive index and the thickness of the layers are highly important parameters. The structural and optical properties, like the index and loss, of the PECVD SiON layers are strongly dependent on the layer composition. This, in turn can be controlled by the parameters of the PECVD process, like the flow-rate and the ratio of the process gases, the chamber pressure, the RF power and the substrate temperature. A serious drawback of the chosen deposition process is the incorporation of undesirable N-H and Si-H bonds in the layers which significantly increase the optical loss in the spectral region of interest for telecom applications.

Chapter 4 describes our results on the PECVD deposition process of low and high index P-doped SiON layers. We first focus on the composition and the chemical environment of phosphorus, silicon, oxygen, nitrogen, and hydrogen in these layers. These data were obtained by XPS, RBS and FTIR. Thereafter an analysis is given for the as-deposited as well as annealed layers with respect to the hydrogen content and optical losses.

Chapter 5 describes our results on the PECVD deposition and reflowing of BP-doped SiON layers. We first focus on the composition and the chemical environment of boron, phosphorus, silicon, oxygen, nitrogen, and hydrogen in these layers. These data were obtained by XPS and FTIR. Thereafter an

analysis is given for the as-deposited as well as annealed layers with respect to reflowing properties, the hydrogen content and optical losses.

Finally **Chapter 6** provides a summary and conclusions of the significant contributions of this research work.

2 Deposition technology and characterization techniques

This chapter describes the deposition technology that has been used to deposit silicon oxynitride layers and techniques used to characterize those layers. A brief description of the PECVD system configuration and its fundamental aspects are presented in section (2.1). In order to optimize the fabrication of passive optical waveguides, a number of physical parameters of the deposited layers must be characterized. Methods and experimental setups for the determination of the properties of slab-waveguides are described in section (2.2). The refractive index and the layer thickness are both determined by spectroscopic ellipsometry and prism coupler techniques. The stoichiometric composition of the layer material is characterized by XPS and RBS. The hydrogen induced optical losses are determined by FTIR in the deep infrared, whereas the overtones absorption of these hydrogen bonds are measured by the prism coupler technique in the near infrared.

Parts of this chapter are adopted from:

M.G. Hussein, K. Wörhoff, G. Sengo and A. Driessen, "*Optimization of plasma-enhanced chemical vapor deposition Silicon Oxynitride layers for integrated optics applications*" Accepted for publication in Thin Solid Films (2006).

2.1 Plasma enhanced chemical vapor deposition

The PECVD process has been used to deposit a large number of insulators, semiconductors, and conductors. There are two basic plasma arrangements of PECVD, the direct (parallel plate) and the remote (down-steam) plasma process. In a parallel plate reactor the plasma is produced in the part of the system which contains the substrate. Therefore, the substrate is subject to physical processes such as ion bombardment. In remote PECVD the plasma is produced in a chamber which is connected to the depositing chamber. Therefore, the plasma generation is remote from the substrate.

The focus, in our study, will be on the PECVD parallel plate reactor, since it is the most widely used plasma configuration for depositing PECVD SiON layers and it will be used in this work.

2.1.1 Reactor configuration

The PECVD configuration used in this work is a parallel plate type reactor (Oxford Plasmalab System 133 PECVD reactor). The schematic layout of the reactor is shown in Figure 2.1 . It consists of a process chamber in which two parallel plate electrodes of 210 mm diameter are placed horizontally with a spacing of 20 mm. The upper electrode is connected to a Radio Frequency (RF) generator (GEN) operating at high frequency (13.56 MHz) via an Automatic Matching Unit (AMU) to ensure maximum power transfer. Alternatively a Low Frequency (LF) generator at 100 – 400 KHz can be connected to the upper electrode. This electrode is also functioning as showerhead for the inlet of process gases such as silane SiH_4, N_2, nitrous oxide (N_2O), ammonia (NH_3), phosphine (PH_3) and diborane (B_2H_6). These highly pure gases are mixed in a gas pod and introduced to the chamber via the showerhead. Table 2.1 shows the available gas lines for our system. The lower electrode (substrate electrode) contains the heating element and is grounded. The system is integrated with a load-lock wafer transporter, allowing fast system pump-down. The process chamber pumping configuration consists of a dry combination of roots/rotary pumps and a turbo pump for the load-lock. The pressure in the system is monitored by a Capacitance Manometer (CM) and Penning gauges.

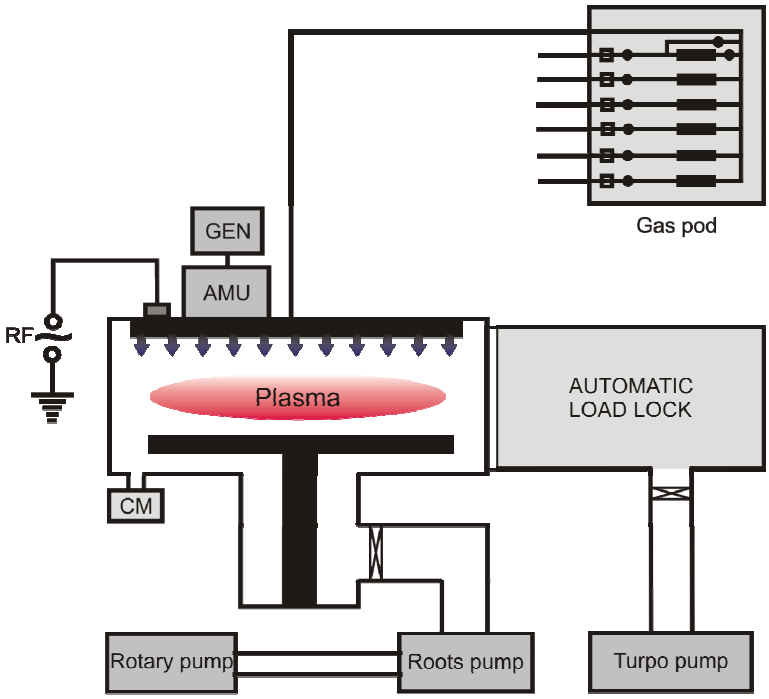

Figure 2.1 Schematic layout of the Oxford Plasmalab System 133 PECVD reactor.

The system is controlled by Programmable Logic Controller (PLC) hardware and PC2000 software. This software has been designed to provide intuitive user interaction with the system via advanced graphics and process recipe pages.

Table 2.1 Gas lines available for our Oxford 133 PECVD system.

Gas line	Gas	Percentage (%)	Diluted in	Maximum flow (sccm)	Purpose
1	CF_4	80	O_2	500	Cleaning
2	N_2O	100		3000	Deposition
3	N_2	100		2000	Deposition
4	SiH_4	2	N_2	3000	Deposition
5	NH_3	100		100	Deposition
6	N_2O	100		200	Deposition
7	SiH_4	2	He	3000	Deposition
8	SiH_4	2	Ar	3000	Deposition
9	GeH_4	5	Ar	100	Doping
10	PH_3	5	Ar	100	Doping
11	B_2H_6	5	Ar	100	Doping
12	-	-	-	-	-

2.1.2 Fundamentals of plasma CVD

In the plasma, electrons gain energy rapidly through the RF electric field and lose energy through elastic collisions. In addition, the high-energy electrons are capable of inelastic collisions that cause the reactant gas molecules to dissociate and ionize, producing secondary electrons by various electron-impact reactions. In this way, highly reactive chemical species are produced for deposition of layers at temperatures lower than those possible with thermally driven CVD. Furthermore, the chemical processes occurring at surfaces exposed to the plasma are modified by ion bombardment. There are many possible inelastic interactions between electrons and gas species in a glow discharge. The following examples are believed to be important for PECVD [42]:

Excitation: $$A + e^- \rightarrow A^* + e^- \quad (2.1)$$

Ionization: $$A + e^- \rightarrow A^+ + 2e^- \quad (2.2)$$

Dissociation: $$A_2 + e^- \rightarrow 2A + e^- \quad (2.3)$$

Electron attachment: $$A + e^- \rightarrow A^- \quad (2.4)$$

Dissociative attachment: $$A_2 + e^- \rightarrow A + A^- \quad (2.5)$$

The chemistry and physics of plasma deposition are extraordinarily complex, since the glow discharges include both chemical and physical processes. However, a reasonable set of steps for plasma CVD that can be used to understand the deposition mechanisms are the following (Figure 2.2):

1. Creation of the reactive species within the plasma phase by electron impact ionization and dissociation.
2. Gas phase reaction and transport of the reactive species by diffusion to the wafer surface.
3. Adsorption of reactive species on the wafer surface sites and the reaction of these species with surface atoms or with other adsorbed species to form a reaction product.
4. Surface diffusion of the adsorbed species and reaction products. Nuclei grow into islands and islands merge into a continuous thin film.

Desorption of the volatile reaction products and transport of byproducts away from the growth region.

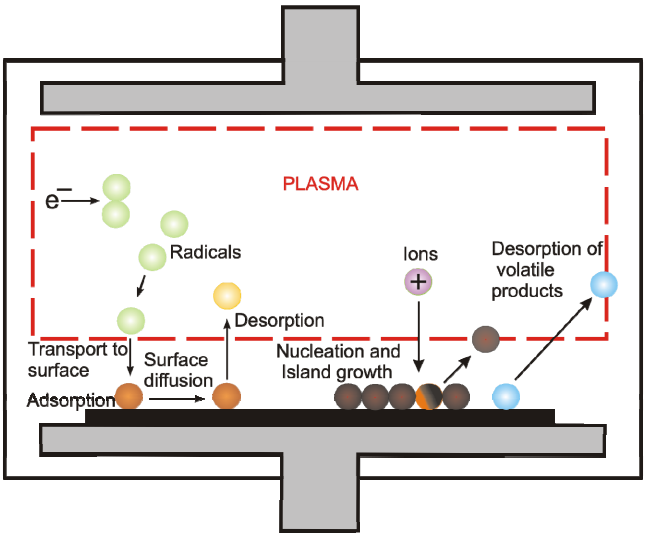

Figure 2.2 Schematic picture of a parallel plate reactor with the basic processes in plasma CVD.

2.2 Characterization techniques

2.2.1 Refractive index and layer thickness measurements

In general the refractive index of a material is expressed in terms of its real and imaginary components:

$$\tilde{n} = n - i\kappa \tag{2.6}$$

where the real part n accounts for the normal dispersion and the imaginary part, κ, is related to the absorption.

A light wave propagating though a medium along the z-direction can be described by an electric field representing a plane wave:

$$E = E_0 e^{i(\omega t - \tilde{k}z)} \tag{2.7}$$

where $\tilde{k}$ is the complex wave vector, $\tilde{k} = \frac{\omega}{c}\tilde{n} = k_o\tilde{n}$, ($k_o$ is the free space wave vector), ω is the angular frequency and c is the velocity of light in vacuum. Equation (2.7) can be rewritten as:

$$E = E_0 e^{i(\omega t - \frac{\omega}{c}\tilde{n} z)} = E_0 \underbrace{e^{i(\omega t - \frac{\omega}{c} n z)}}_{1} \underbrace{e^{-(\frac{\omega}{c}\kappa z)}}_{2} \tag{2.8}$$

where the first exponential term gives the phase of a running plane wave, whereas the second is the decay term which is related to the absorption for $\kappa > 0$.

A well known dispersion relation to determine the wavelength dependence of *n* is Cauchy's dispersion formula [43]:

$$n(\lambda) = A + \frac{B}{\lambda^2} + \frac{C}{\lambda^4} + \ldots \tag{2.9}$$

Where A, B, C, … are constants, which can be determined experimentally. Higher order terms can be omitted, since these are becoming very small.

2.2.1.1 Ellipsometry

An ellipsometer is a well known instrument for the characterization of thin dielectric layers regarding refractive index and thickness. The principle is based on the fact that the intensity of the reflected light at a dielectric interface depends on the polarization of the incoming beam, while the transmission of light through a transparent layer changes the phase of the incoming wave depending on the refractive index and the thickness of the layer. An ellipsometer can be used to measure layers as thin as 0.5 nm and thick as several microns [44].

In ellipsometry linearly polarized light is incident at an oblique angle on the surface to be analyzed. The reflected light becomes elliptically polarized. Ellipsometry determines the amplitude ratio, psi (ψ), and the phase difference, delta Δ [45]. Paul Drude derived the following relationship between the thickness of the layer, d, and the optical constants *(n_1, n_2, n_3)* of the structure air/layer/substrate (e.g., air/SiON/Si in our case (see Figure 2.3) [45]:

$$\tan\left(\psi \cdot e^{i\Delta}\right) = \frac{\left(r_{p31} + r_{p12} e^{-2ix}\right) \cdot \left(1 + r_{s31} \cdot r_{s13} e^{-2ix}\right)}{\left(1 + r_{p31} \cdot r_{p12} e^{-2ix}\right) \cdot \left(r_{s31} + r_{s12} e^{-2ix}\right)} \tag{2.10}$$

Where $x = \frac{2\pi}{\lambda} \cdot d \cdot \left(n_1^2 - n_3^2 \sin^2 \phi_3\right)^{1/2}$ and $r_{p,s31}$ and $r_{p,s12}$ are the Fresnel reflection coefficients for the air-layer interface and layer-substrate interface respectively.

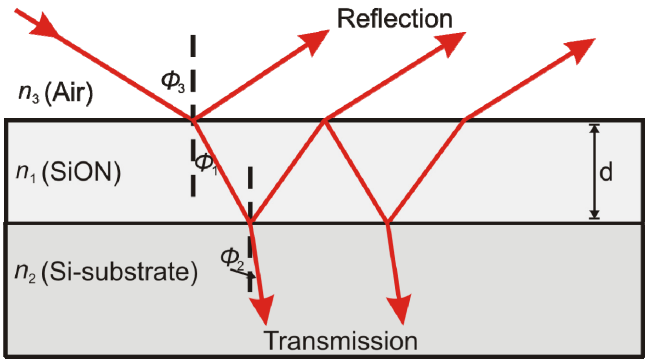

Figure 2.3 Reflection and transmission of a plane wave by an air (n_3), SiON (n_1) and Si-substrate (n_2) structure with parallel-plane boundaries where d is the layer thickness, ϕ_3 is the angle of incidence in the air and ϕ_1, ϕ_2 are the angles of refraction in the SiON layer and the substrate, respectively.

Our spectroscopic ellipsometer (Woollam M-44) operates in the spectral range from 601.1 to 1098.4 nm. The setup that has been applied for the SiON layers characterization is shown in Figure 2.4. A broad band white light source is used to illuminate the selected wafer area. The light from the source is first converted to a collimated beam by the collimator, and then linearly polarized by passing through the polarizer.

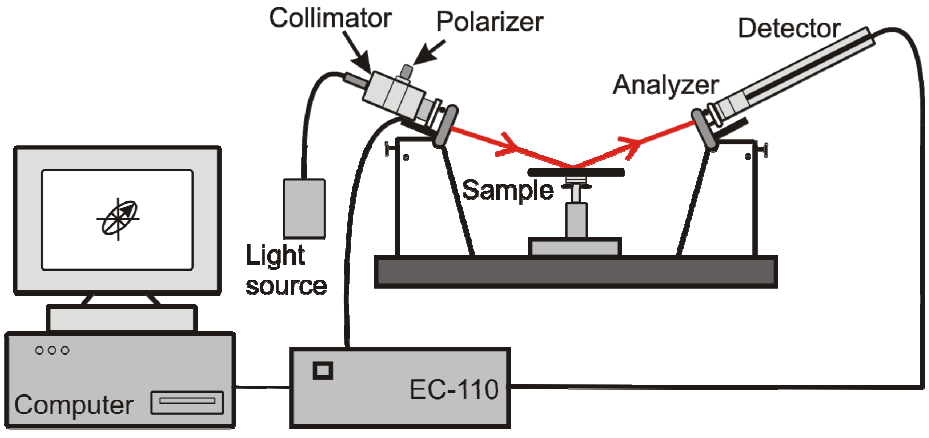

Figure 2.4 Woollam M-44 spectroscopic ellipsometer experimental setup.

The light that reflects from the structure under test changes its polarization dependent on the layer thickness and the refractive indices of the layer stack and the substrate. This light then passes through the analyzer, which determines the polarization state of the light resulting in values for ψ and Δ. Analyzing software supplied by Woollam allows to obtain the layer thickness and the refractive index by knowing the optical constants of the substrate. The calculations are done by fitting the measured data to a theoretical model which describes the layer structure in detail; the results are a dispersion curve, the layer thickness and the errors.

The accuracy in ellipsometric measurements is strongly dependent on the specific layer structure and can not be given for arbitrary cases. For the layer structures depicted in Figure 2.3 we obtain with our multi-wavelength ellipsometer typically an accuracy of 0.002 for the index and 1% for the thickness.

2.2.1.2 *Prism coupling techniques*

The prism coupling technique is a well known method for characterizing a slab-waveguiding structure. Figure 2.5 shows the two possible prism shapes to determine the refractive index and the thickness of the guiding layer [43, 46, 47].

The method is based on the excitation of guided modes by an external optical beam using a prism with a refractive index, n_p. In order to obtain convenient coupling angles ϕ the refractive index of the prism must be higher than the refractive index of the guiding layer, n_1, (which can be the SiON layer). The prism is separated from the waveguide by an air gap, with index n_3. The lower cladding, with index n_2 can be SiO_2 [Figure 2.5 (a)]. In the case of Attenuated Total Reflection (ATR) [Figure 2.5 (b)] the lower cladding can be SiO_2 or silicon.

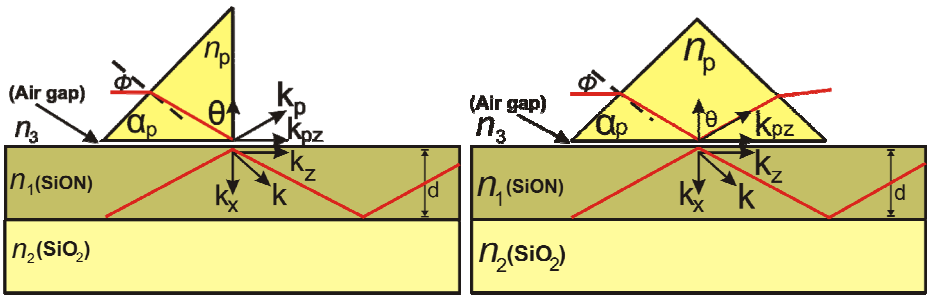

Figure 2.5 Prism coupler method for refractive index and thickness measurement on a slab-waveguide: (a) halved prism coupler (b) ATR set-up.

When an optical beam passes through the prism to its base (prism/air boundary) at an angle exceeding the critical angle, the evanescent fields that extend below the prism base couple efficiently to the waveguiding modes in the structure if the phase matching condition is fulfilled. This happens when the z-component of the wave vector is equal to the mode propagation constant β_m, where m is an integer. The propagation constant (k_z) is given by:

$$k_z = k_o n_p \sin\theta = k_p \sin\theta = k_{pz} \tag{2.11}$$

where k_p is the wavevector inside the prism. In the case of phase matching it follows:

$$k_z = \beta_m = k_o n_p \sin\theta_m = k_o n_{eff} \tag{2.12}$$

From equation (2.12) the phase matching can be written in terms of the effective index n_{eff} of the guided mode n_p and θ as:

$$n_{eff_m} = n_p \sin\theta_m \tag{2.13}$$

With known parameters of the prism (n_p and prism angle α) the phase matching condition in equation (2.13) can be rearranged to give a relation between n_{effm} and the measured incident angle ϕ_m, the so called coupling angle, for the case that the energy transferred to the guiding layer is at maximum [48]:

$$n_{eff_m} = n_p \cdot \sin\left[\alpha_p + \sin^{-1}\left(\sin\phi_m / n_p\right)\right] \tag{2.14}$$

The refractive index and the thickness (d) of the guided layer can be determined from a set of n_{effm} (at least two modes) from the dispersion relation for planar waveguide given by [43, 48, 49]:

$$n_{eff_m}^2 = -\frac{1}{4k_0^2 d^2}\left(2m\pi + 2\varphi_{m_{12}} + 2\varphi_{m_{13}}\right)^2 + n_1^2 \tag{2.15}$$

where m is an integer, $\varphi_{m_{12}}$ and $\varphi_{m_{13}}$ are the phase shifts of the total internal reflection at the lower and the upper cladding respectively. The calculations are done by fitting the measured data to a theoretical model which describes the structure.

Prism coupling setup (halved prism method)

Our experimental arrangement for prism coupling measurements (halved prism method) is shown in Figure 2.6. It consists of lasers, chopper, polarizer, focusing lens, in- and out-coupling prisms, two detectors, two trans-impedance amplifier, two digital multi-meters, lock-in amplifier and a rotation table with its stepper motor driver. The lasers provide the monochromatic light at the desired wavelength, which can be polarized (TE or TM) by a polarizer.

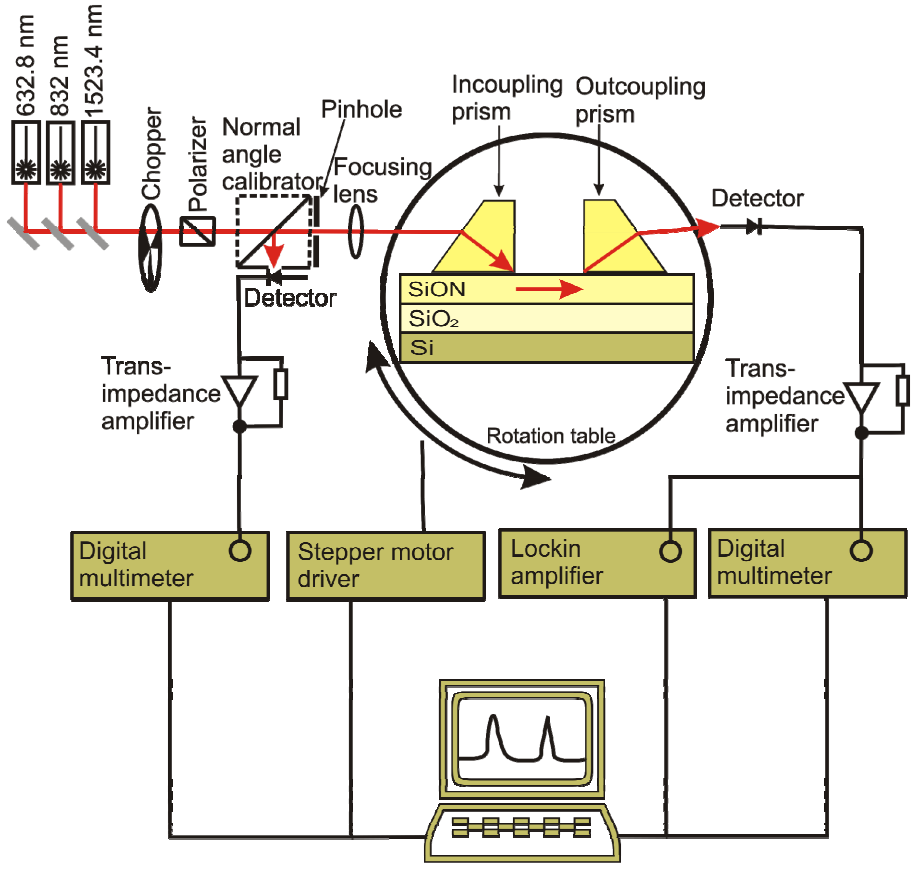

Figure 2.6 Prism-coupling (halved prism) setup.

An in-coupling prism is loaded on the structure by means of a spring in order to adjust the air gap for obtaining an optimum coupling efficiency. An out-coupling prism is placed at a variable distance from the in-coupling prism to couple out the guided mode, which can be detected by a suitable photodiode. All together (the structure, in-coupling and out-coupling prism

and the detector) are fixed on the sample holder, which can be rotated with respect to the incident beam to vary the external incident angle ϕ, which is controlled by a stepper-motor using a step size of 0.01°. The incident beam is focused into the prism by a lens with focus just on the prism base corner. For improved sensitivity a phase sensitive detection scheme is employed making use of a chopper. The out-coupling light is measured as a function of rotation angle by a suitable photodiode to give the peaks indicating the coupling angle and/or the position of the modes. The measurement results can be fitted using a computer software program (Indexfit software) [50]. Another photodiode is used to detect the reflected light from the prism to the normal angle calibrator in order to determine the zero position.

The prism coupling technique has an important advantage in comparison to other techniques, such as ellipsometry. It requires only the determination of the coupling and reference angles, which can be done easily with an accuracy of $\Delta\phi=0.01^{o}$, the resolution of the stepper motor used to drive the rotation holder. When the core is thick enough to support more than two modes of the same polarization, the method becomes self-consistent, since the two unknowns *n* and d are then determined from more than two independent measurements. Moreover, the prism coupling measurement gives the possibility to measure the materials birefringence.

The relative measurement accuracy of this method is approximately 1×10^{-4} in the refractive index and 0.25% in the layer thickness. Being very accurate, the method nevertheless has some inconveniences. The method needs relatively thick layers as at least two modes are needed for the determination of the thickness and the refractive index. If, however, one of these parameters already is known, a measurement of a single mode structure is still meaningful. In addition, Difficulties in the out-coupling may occur due to excessive losses in the layer.

Prism coupling setup (ATR)

The commercial experimental setup for ATR measurements (Metricon 2010 setup) is shown in Figure 2.7. The advantage of the ATR configuration is the possibility to characterize layers with high attenuation or those providing leaky modes (e.g. SiO_2 buffer layers). In the ATR prism the input beam is completely reflected when no phase matching at the prism/air interface occurs. The reflected beam is detected by the photodiode. When there is phase matching to a guiding or leaky mode the reflectivity drops, resulting in a dip in the spectrum (intensity as a function of coupling angle).

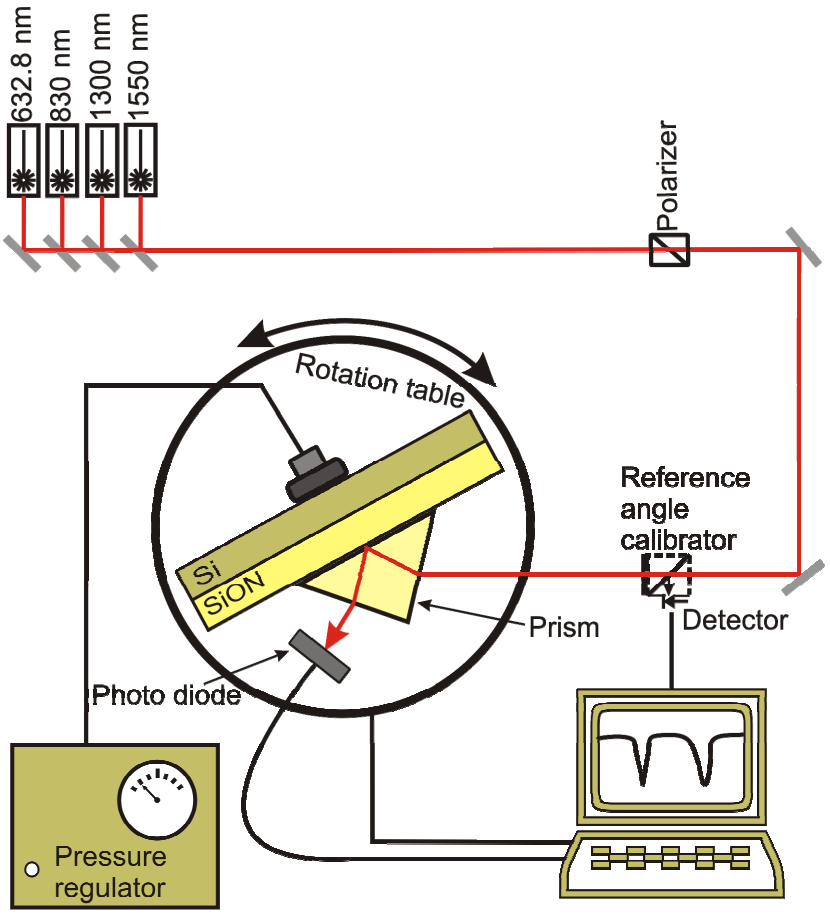

Figure 2.7 Schematic picture of the Metricon 2010 prism coupler.

2.2.2 Analysis of the composition of the layers and their hydrogen content

2.2.2.1 Fourier Transform Infrared Spectroscopy

Infrared (IR) spectroscopy deals with the interaction between a molecule and infrared radiation with frequencies lying in the range from 400 to 4000 cm^{-1} [51]. The IR spectra are commonly divided into three main regions. The high-frequency region between 1300 and 4000 cm^{-1} (2-7.7 μm), is called the functional group region as characteristic stretching frequencies for important functional groups such as C=O, O-H, N-H and Si-H occur in this region. The middle-frequency region, between 900 and 1300 cm^{-1} (7-11 μm) is known as the fingerprint region, in which the absorption spectra are complex and normally due to combinations of interacting vibrational modes, providing a unique fingerprint for every molecule. The spectrum in this region is especially

valuable if examined in reference to other regions. The region between 650 and 900 cm^{-1} (11-15 µm) provides a general classification of molecules from the pattern of absorptions, such as substitution patterns on a benzene ring (see Figure 2.8) [52].

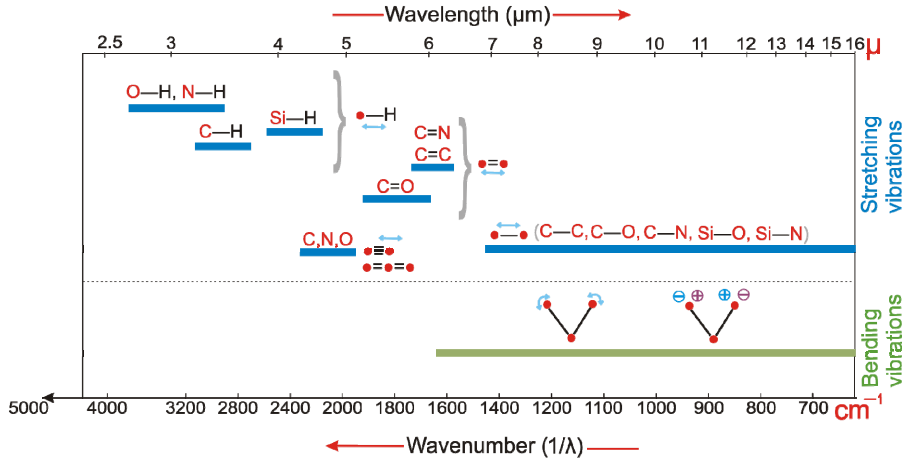

Figure 2.8:Typical features in the IR absorption spectra of molecules.

Most of the simple molecules have a certain fundamental vibrational frequency. When infrared light is incident on such a molecule, the frequency that matches its fundamental vibration will be absorbed resulting in molecular vibrations. The vibrational frequency of the molecule is related to the energy of the transition by the following relation:

$$E_{final} - E_{initial} = h\frac{c}{\lambda} = hc\tilde{\nu} \tag{2.16}$$

where $E_{initial}$ and E_{final} are the initial and the final energy state, h is the Planck constant and $\tilde{\nu}$ is the wavenumber in cm^{-1}.

This absorption causes a molecule to undergo a net change in the dipole moment as a result of vibrational or rotational motion. Because only a few molecules exhibit pure rotational bands, the vibrational absorption bands are of more practical interest. Vibrations can be subdivided into two classes, depending on whether the bond length or the position of the atom relative to the original bond axis is changing. The first type of vibration is a stretch mode that produces a change of bond length. Such a mode is a periodic symmetric or asymmetric movement along the line between the atoms so that the interatomic distance is either increasing or decreasing. The second type of vibration is a bending mode, resulting in a change in bond angle. These are also sometimes called scissoring, rocking, wagging or twisting motions.

FTIR is a well-known method of obtaining infrared spectra by measuring the interferogram of the sample using an interferometer. Thereafter a Fourier transform on the interferogram is performed in order to obtain the spectrum [53]. Generally FTIR can be classified into the following two categories:

- Qualitative analysis - where the aim is to identify the sample.
- Quantitative analysis - where the absorption is related to the concentration of certain species in the layer.

FTIR is based on an interferometer (mostly a Michelson interferometer), which splits the IR beam in two paths to recombine them later so that the intensity variation can be determined as a function of the path difference. The interferometer contains two orthogonal mirrors: one movable and one fixed. Because one beam travels always a fixed length and the other is constantly changing as the mirror moves, the signal which exits from the interferometer is the result of interference between the two beams. The resulting signal is called an interferogram (see Figure 2.9).

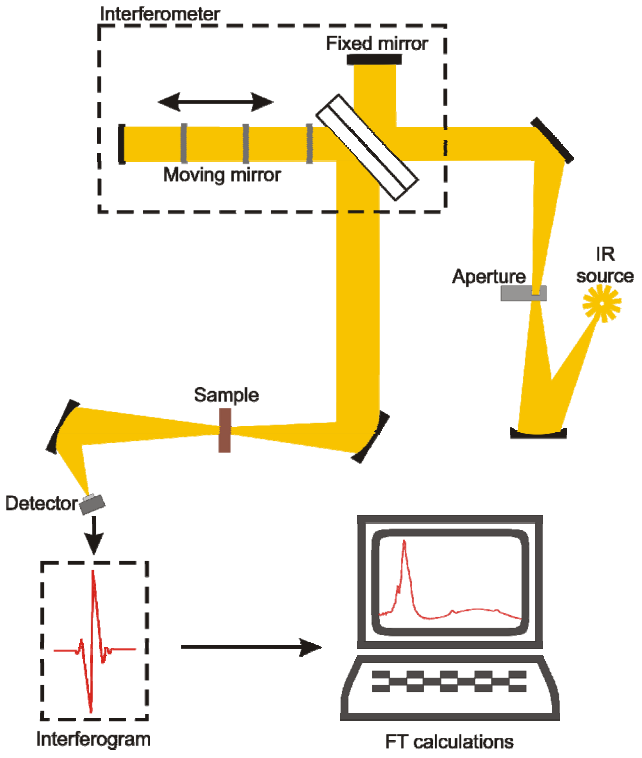

Figure 2.9 Schematic picture of the FTIR experimental setup used for absorption measurements

The mirror moves with constant velocity to generate a complete interferogram. The intensity of the signal as a function of the optical path difference (δ) is given by:

$$I'(\delta) = \frac{I_0(\tilde{\nu})}{2}\left[1 + \cos\left(2\pi\left(\frac{\delta}{\lambda}\right)\right)\right] \tag{2.17}$$

Sine $\tilde{\nu} = 1/\lambda$ equation (2.17) becomes:

$$I'(\delta) = \frac{I_0(\tilde{\nu})}{2}\left[1 + \cos\left(2\pi\tilde{\nu}\delta\right)\right] \tag{2.18}$$

So the interferogram of monochromatic source can be expressed by the following equation:

$$I'(\delta) = B(\tilde{\nu}) \cdot \cos\left(2\pi\tilde{\nu}\delta\right) \tag{2.19}$$

where the parameter $B(\tilde{\nu})$ is the intensity of the source at a given wavenumber.

Now the source can be polychromatic so that the interferogram at each point is the sum of the interference from all incoming wavelengths. Therefore one gets:

$$I(\delta) = \int_{-\infty}^{\infty} B(\tilde{\nu}) \cdot \cos\left(2\pi\tilde{\nu}\delta\right) \cdot d\tilde{\nu} \tag{2.20}$$

This expression is called an interferogram and its Fourier transform gives the FTIR spectrum, i.e. the absorbance or transmittance as a function of wavenumber. A typical example of a FTIR spectrum of SiON layer is indicated in Figure 2.10.

Because each different material has a unique combination of atoms, no two compounds produce the same infrared spectrum. Therefore, infrared spectroscopy can result in a positive identification (qualitative analysis) of every different kind of transparent material. In addition, the area of the peaks in the spectrum is a direct measure for the bonds concentration in the material. With reference measurements and some computer algorithms, infrared spectroscopy is an excellent tool for quantitative analysis.

In this work, the hydrogen concentration and the nature of the atomic bonds of the layers were determined with a Digilab FTS-575C FTIR spectrometer. The measurements were carried out at room temperature in a nitrogen atmosphere by transmission through the deposited layer and the silicon substrate with a spectral resolution of 4 cm^{-1}.

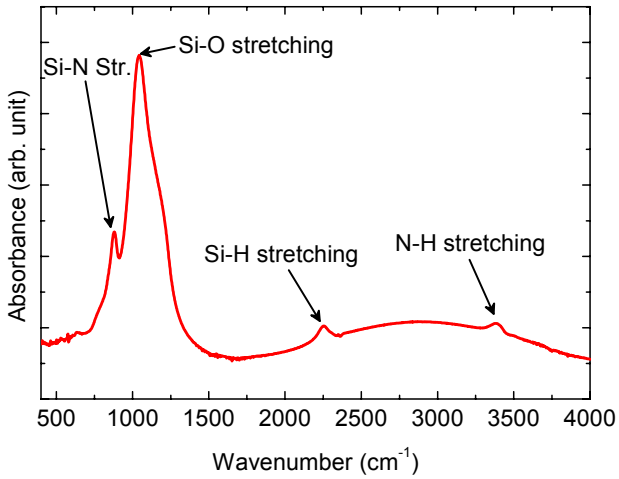

Figure 2.10: FTIR spectrum of PECVD silicon oxynitride layer

The basis of the quantitative analysis is Beer's law, which relates the concentration to absorbance and is usually written as:

$$A = a\, d\, C \tag{2.21}$$

where A is the measured absorbance, defined by: ($A = \log {}^{I_0}\!/_{I}$), I_0 the incident and I the transmitted intensity, a the wavenumber-dependent absorptivity coefficient, d the layer thickness and C the concentration of the molecules in the layer [51, 53].
For the quantitative analysis it is convenient to use infrared absorption, since the absorbance is linearly proportional to concentration [see Equation (2.21)]. The transmittance (T), however, does not show the linear dependence:

$$A = \log \frac{I_o}{I} = \log \frac{1}{T} = a\, d\, C \tag{2.22}$$

With the aid of the FTIR spectra, the hydrogen concentration for the SiON layers can be determined by the integrated absorption coefficient over the band of interest. The N-H and Si-H bonds concentrations can be estimated with the method given by Lanford and Rand [54] by using the following expression:

$$[X-H] = \frac{1}{2.303\,\sigma_{X-H}} \times \int_{band} a(\tilde{\nu})\, d\tilde{\nu} \tag{2.23}$$

where $a(\tilde{\nu})\,d\tilde{\nu}$ is the normalized absorption band intensity, $a = \left(\frac{2.303}{d}\right) A$ the absorption coefficient and σ the absorption cross-sections. The absorption cross-sections for N-H and Si-H bonds are $\sigma_{N-H} = 5.3 \times 10^{-18}\ cm^2$ and $\sigma_{Si-H} = 7.4 \times 10^{-18}\ cm^2$ respectively.

2.2.2.2 *X-ray photoelectron spectroscopy*

XPS is one of the most frequently used techniques to characterize SiON layers [55-57]. The method is suitable for determining the chemical composition and the nature of different chemical bonds of the layer. XPS is based on the photoelectric effect, i.e., the ejection of an electron from a core level by an X-ray photon of energy $h\nu$. The energy of the emitted photoelectrons is then analyzed by an electron spectrometer and the data is presented as intensity (usually expressed as counts or counts/s) versus the binding energy of the electron (see Figure 2.11). If E_K is the kinetic energy of the leaving electron (experimentally determined by the spectrometer), $h\nu$ the photon energy and W the spectrometer work function, then the binding energy E_B of the electron is given by [58]:

$$E_B = h\nu - E_K - W \tag{2.24}$$

As all three quantities on the right-hand side of the equation are known or measurable, it is a simple matter to calculate the binding energy of the electron.

The XPS experiments described in this thesis are carried out on a PHI Quantera Scanning ESCA (electron spectroscopy for chemical analysis) Microprobe. A monochromatic Al X-ray source ($h\nu$ = 1486.6 eV) at 26.4 W was used, with a beam diameter of 100 μm and a 45° take-off angle. The total pressure in the main chamber during analysis was 1.6 × 10^{-10} Pa. The spectrometer was calibrated using the Au $4f_{7/2}$ peak position at 84.00 eV. The samples were analyzed after 6 minute (~ 70 nm in depth) sputtering by Argon ions beam accelerated at 3 keV and beam current of 15 nA. The atomic concentration values of the layers were calculated from the ratio of the experimental core level areas with PHI Multipak software using factory calibrated values for the sensitivity factors of the respective elements. For detailed analysis of the chemical state of elements in the layers, the core-level spectra were deconvolved into separate components representing the contribution of different chemical environments.

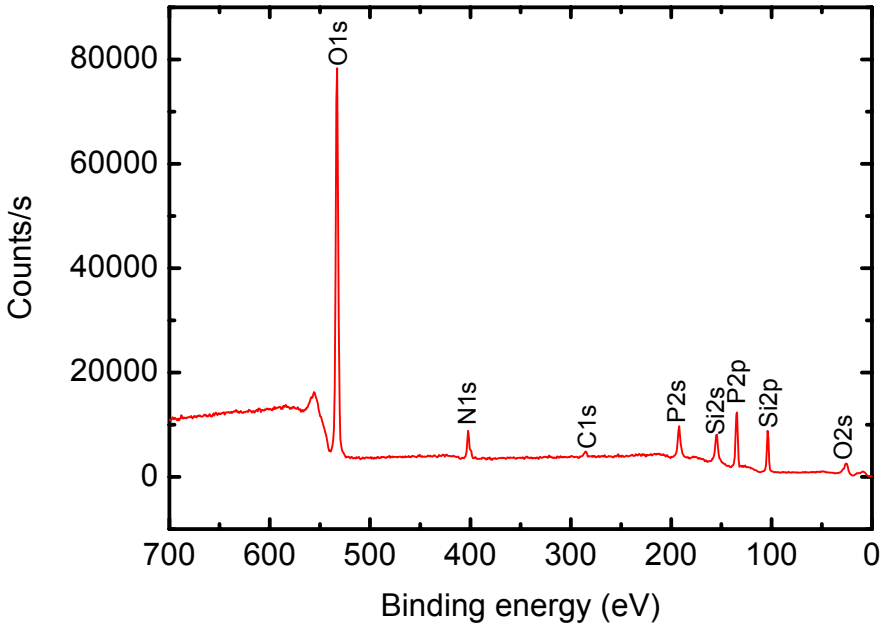

Figure 2.11 Typical XPS surface survey spectrum created by an Al X-ray source for a PECVD P-doped SiON layer

2.2.2.3 Rutherford backscattering spectrometry

RBS analysis is a powerful tool for the characterization of the SiON layers [32, 59, 60]. RBS is based on collisions between atomic nuclei. It involves measuring the number and energy of ions in a beam which backscatter after colliding with atoms in the near-surface region of a sample at which the beam has been targeted. With this information, it is possible to determine atomic mass and elemental concentrations versus depth below the surface.

The RBS measurements, were performed with a He^+ beam with energy E = 2.0 MeV, charge Q = 20 μC, current I = 20 nA and detection angle of 15^o. The RBS data were analyzed by the Rump program.

A typical RBS spectrum together with its fitting curve, obtained utilizing the Rump program are shown in Figure 2.12.

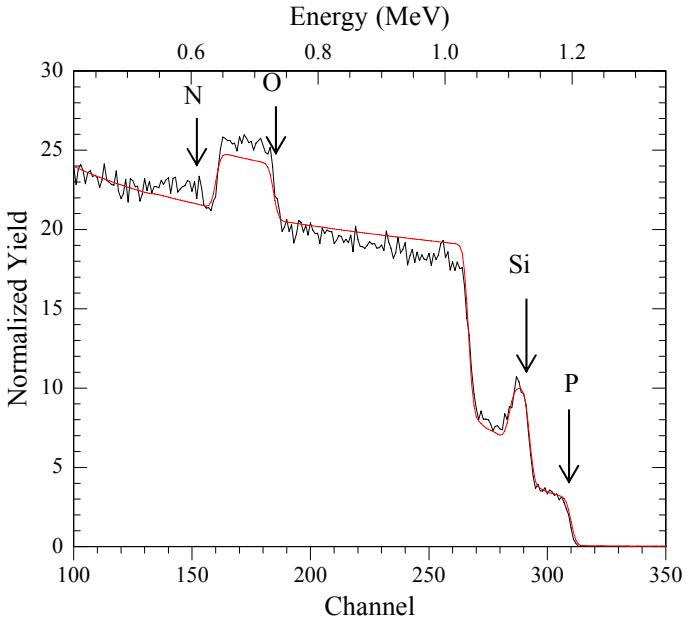

Figure 2.12 RBS spectrum of PECVD P-doped SiON layer deposited on a silicon substrate.

2.2.3 Optical loss measurements

The waveguide attenuation or optical loss is one of the most important characteristics of the waveguide evaluation regarding its usefulness for integrated optics applications. As the optical beam propagates through the waveguide, photons can be scattered, absorbed or radiated, resulting in losses. Scattering loss occurs as a result of inhomogeneities in the material or roughness of the layer boundaries and it is proportional to λ^{-4} [43, 61]. The absorption loss is due to the vibrational frequency of the molecules or bonds in the material in the case of dielectrics. Also impurities can contribute to absorption. Semiconductors are transparent at energies below the gap energy. Materials with free charges are always highly absorbing. Losses may also occur if the tail of the evanescent field in the waveguide structure leads to undesired coupling to radiation modes. So the thickness of the buffer layer has to be well designed when characterizing SiON/SiO_2/Si structures since Si has the highest refractive index in the structure.

Moving prism method

A moving prism setup is used to determine the optical loss of the slab-waveguide. The light is coupled into the waveguide with the in-coupling prism, and then is coupled out with a second prism (see Figure 2.13). A broad-band (polychromatic) source is used to perform the measurements. The out-coupled light is transmitted to the spectrometer by a liquid fiber bundle. The intensity of the out-coupled light can be determined at different positions along the streak. Thus the waveguide attenuation spectrum $\alpha(\lambda)$ can be given as [61]:

$$\alpha(\lambda) = \frac{-10 \cdot \log\left(I_{L_i}(\lambda) \Big/ I_{L_1}(\lambda) \right)}{(L_i - L_1)} \qquad [dB/cm] \qquad (2.25)$$

where I_{L_1} is the incident intensity and I_{L_i} is the intensity at a propagation length L, i is the measurement number (i > 1).

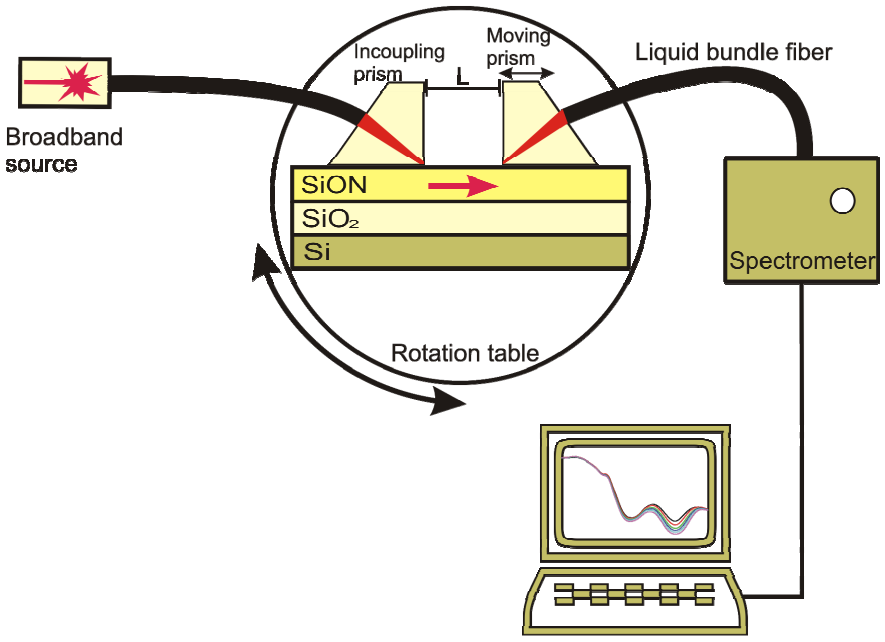

Figure 2.13 Experimental setup for measuring the optical loss of the slab-waveguides.

A set of waveguide transmission spectra recorded for various prism positions (L_i) along the streak is presented in Figure 2.14(a). From these transmission spectra the waveguide optical loss (dB/cm) can be determined as shown in Figure 2.14(b).

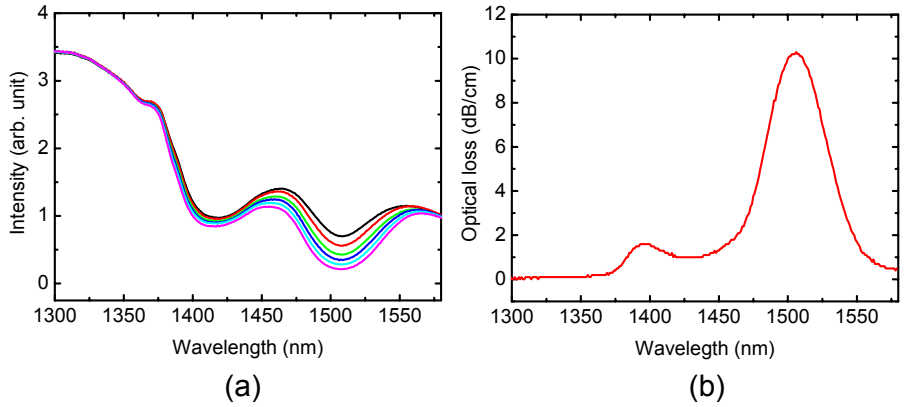

Figure 2.14 Determination of the optical loss spectrum: (a) transmission spectrum recorded at increasing prism positions; (b) optical loss spectrum obtained by analysis of (a)

The optical loss spectrum of Figure 2.14(b) is obtained by performing, at each wavelength of the spectrum, a linear fit of the measured loss as function of the prism distance. The result of this fit process is shown for a wavelength of 1550 nm in Figure 2.15.

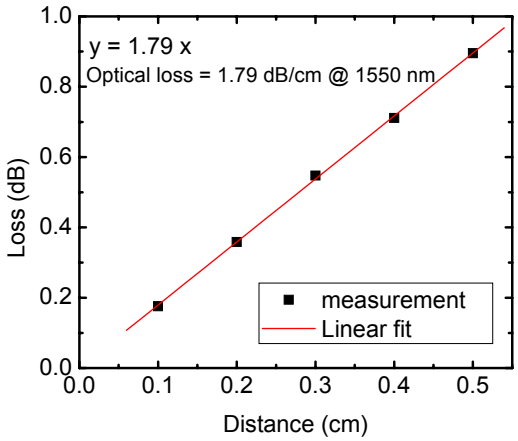

Figure 2.15 Fit result (solid line) obtained by an analysis of Figure 2.14(a) at a wavelength of 1550 nm.

The correlation (r^2) between the linear fit and the measurement results is close to unity (= 0.9995) which indicates that the coupling efficiency of the moving prism has been constant.

Although the moving prism method can give accurate results - the measurement limit of this method is approximately 0.2 dB/cm -, some problems might occur when the prism is moved:

- Pressing the out-coupling prism on the layer may changes the in-coupling efficiency, so the out-coupling pressure has to be low and constant. For this the use of index-matching oil is preferable.
- The out-coupling prism has to deliver a constant fraction of the out-coupling intensity to the spectrometer. To get more accurate and reproducible measurements the liquid fiber bundle has to be fixed close to the prism with an optimized non-changing angle, so the out-coupling prism and the liquid fiber bundle have to be considered as a single piece of equipment sliding along the streak.

3 Optimization of undoped PECVD silicon oxynitride layers

For integrated optics applications, the properties of the silicon oxynitride must be investigated in detail. The uniformity and reproducibility of the refractive index and the thickness of the layers are highly important parameters. The structural and optical properties, like the index and loss, of the PECVD SiON layers are strongly dependent on the layer composition. This, in turn can be controlled by the parameters of the PECVD process, like the flow-rate and the composition of the process gases, the chamber pressure, the RF power and the substrate temperature. A serious drawback of the chosen deposition process is the incorporation of undesirable N-H and Si-H bonds in the layers which significantly increase the optical loss in the spectral region of interest for telecom applications. This chapter describes the optimization process of undoped PECVD silicon oxynitride layers, a base material for P and BP-doping.

Parts of this chapter are adopted from:
M.G. Hussein, K. Wörhoff, G. Sengo and A. Driessen, "*Optimization of plasma-enhanced chemical vapor deposition Silicon Oxynitride layers for integrated optics applications*" Accepted for publication in Thin Solid Films, 2006.

3.1 Deposition and characterization of undoped SiON from silane and nitrous oxide using 13.56 MHz generator

In this section, we focus on the correlation between the deposition parameters and the PECVD SiON layer properties, in order to identify those trends which lead to materials properties optimized for integrated optics applications. Based on the optimized deposition parameters, a series of layers with a broad range of refractive index between 1.48 and 1.66 has been fabricated. The optical and compositional properties of this series of SiON samples have been characterized by spectroscopic ellipsometry, XPS, FTIR spectroscopy and prism coupler techniques.

3.1.1 Deposition mechanism

It has been described in Section (2.1.2) that the deposition mechanisms for a PECVD process can be considered to consist of five major steps [42, 62]. In the case that silicon oxynitride is obtained from N_2O – SiH_4/N_2 gases mixtures the deposition process can be summarized as follow:

Step 1 include the electron-impact ionization and dissociation of silane and nitrous oxide molecules, which can be written by the following equations [62, 63]:

$$\begin{aligned} &e + SiH_4 \rightarrow SiH_m^+ + (4-m)H + e + e \qquad m = 1,2,3 \\ &e + N_2O \rightarrow N_2 + O^+ + e + e \\ &e + N_2O \rightarrow NO^+ + N + e + e \end{aligned} \tag{3.1}$$

$$\begin{aligned} &e + SiH_4 \rightarrow SiH_m + (4-m)H + e \qquad m = 1,2,3 \\ &e + N_2O \rightarrow N_2 + O + e \\ &e + N_2O \rightarrow NO + N + e \end{aligned} \tag{3.2}$$

Step 2 is dealing with the gas phase reaction and transport of the reactive species by diffusion to the silicon wafer surface. The complex electro-chemical reactions which take place during the plasma deposition do not allow a detailed description. Instead we will focus on the gas molecules dissociation when utilizing N_2O and SiH_4/N_2 gaseous mixtures and describe the most favorable chemical reactions. The plasma contains SiH_m, O and N radicals, which can react to form energetically favorable bonds.

Table 3.1 Strength of chemical bonds occurring during plasma deposition of SiON

Chemical bonds	Bond Strengths (kJ/mol)
Si-O	799.6
Si-N	470.0
Si-Si	325.0
Si-H	299.2
N-H	339.0
O-H	427.6

According to Table 3.1 [64], the most favorable chemical reaction is between SiH_m and O radicals leading to the formation of Si-O bonds. Thus, for large N_2O:SiH_4/N_2 flow ratios with an excess of O radicals in comparison with SiH_m radicals, only Si-O bonds will be formed. For decreasing flow ratios, the number of SiH_m radicals per O radical will increase, leading to oxygen deficiency, and thus to appearance of Si-N and Si-H bonds in the layers. However, decreasing the flow ratio even further leads to a deficiency of both oxygen and nitrogen radicals. Thus, homonuclear SiH_m reactions become favorite leading to silicon-rich SiO_xN_y:H [65].

Step 3 is the adsorption of reactive species on wafer surface sites. There they can react with surface atoms or with other adsorbed species. The chemical reactions at the surface can be enhanced by ion bombardment. The coexistence of Si-H, N-H and Si-OH bonds offer the possibility for eliminating H_2 and H_2O [66, 67]. In this way additional Si-N, Si-Si and Si-O-Si can be formed on the surface through the following reactions [67, 68]:

$$\begin{aligned} &Si-H+N-H \rightarrow Si-N+H_2^{\nearrow} \\ &Si-H+Si-H \rightarrow Si-Si+H_2^{\nearrow} \\ &Si-H+Si-OH \rightarrow Si-O-Si+H_2^{\nearrow} \\ &Si-OH+Si-OH \rightarrow Si-O-Si+(H_2O)^{\nearrow} \end{aligned} \tag{3.3}$$

Step 4 takes into account the surface diffusion of the adsorbed species and reaction products. By diffusion nuclei will form islands and islands will merge to form a continuous thin film.

Step 5, finally, deals with desorption of the volatile reaction products, such as H_2 and H_2O vapor. Gaseous byproducts diffuse and flow out of the reactor.

3.1.2 Influence of the deposition parameters on layers properties

The influence of the deposition parameters such as the RF power, chamber pressure, gas flow ratio and deposition temperature on the layer properties as well as for the chemical reaction will be discussed in this section. Since all these parameters are under control of the user, reproducible and precise results can be achieved.

3.1.2.1 Plasma power and frequency

The plasma is generated by applying an electric field at zero (DC), radio, or microwave frequency or a combination of these to the gas mixture. In our reactor we use a RF field to generate the plasma.

The rate at which the excited species, ions and free radicals can be formed is estimated by using a reaction rate equation [42, 67]. For example, the rate at which A* is created from reaction Equation (2.1) can be described by:

$$\frac{d[A^*]}{dt} = k_d[A][e^-] \tag{3.4}$$

where k_d is the reaction rate coefficient, [A] is the concentration of the species A, and [e^-] is the electron concentration. It is clear that an increase in power leads to dissociation of more gas molecules which enhances the deposition rate.

As common in PECVD equipment, our reactor can be operated at two RF frequencies, low frequency (LF) (25 – 500 KHz) or high frequency (HF) around 13.56 MHz. It has been shown that, there is a large difference in the layer composition and density between layers deposited below and above 4 MHz, the transition frequency at which ions cannot follow the RF field. At low frequencies (< 4 MHz) , ions and electrons can follow the RF field and, therefore, ion bombardment can take place on the depositing layer [66, 67].

3.1.2.2 Chamber pressure

The average distance that a particle can travel before colliding with another particle, the so-called the Mean Free Path (MFP), is inversely proportional to the pressure. The mean free path of an electron is very short at atmospheric pressure (101325 Pa). Only at low pressure, the acceleration of the electrons between two collisions is sufficiently high to ionize gases molecules and to create glow discharge plasma. At higher pressures, the discharge voltage increases, making it difficult to start the plasma, since the impedance between the parallel plates decreases due to the higher gas concentration [69]. This results in a material with low density [67].

3.1.2.3 Gas flow ratio

Silicon oxynitride consist of a stoichiometric mixture of silicon, nitrogen and oxygen atoms, i.e. all silicon atoms are bonded to oxygen or nitrogen atoms. Depending on the process used to deposit the oxynitride layers a varying amount of hydrogen is present. It has been shown that the O/N ratio influences the optical prosperities of the material; this change is caused by a change in composition. Therefore the hydrogen distribution in silicon oxynitride is expected to depend on the O/N ratio [32].

It has been reported that when silicon oxynitride is prepared with the two gases SiH_4 and N_2O, the excited oxygen reacts with silane to form disiloxane ($H_3Si–O–SiH_3$) forming in this way Si–O bonds [32, 70, 71]. When the N_2O/SiH_4 flow increases, the excited oxygen atom density increases too, leading to a disiloxane increase with respect to the SiH_2 and SiH_3 precursors. In this way the formation of Si-O becomes favored leading to a layer composition close to SiO_2, where the hydrogen is mainly bonded to nitrogen and oxygen. At low N_2O/SiH_4 ratios formation of Si-Si and Si-H bonds becomes more favorable [see also section (3.1.1), step 2]. When silicon oxynitride is prepared with three gases (SiH_4, N_2O and NH_3), oxidation and nitridation are in competition. N_2O dissociates to form oxygen and nitrogen, which reacts with SiH_m radicals to form Si-O bonds and few Si-N bonds. Beside N_2O also NH_3 is a nitrogen source. Thus, homonuclear SiH_m reactions become unlikely, and Si-N, N-H or $N=H_2$ bonds will be preferentially be formed in comparison with Si-H bonds with increasing NH_3 gas flow ratio.

3.1.2.4 Deposition Temperature

PECVD is a chemical vapor deposition process that is enhanced by the plasma, resulting in an increased dissociation rate of the reactive gases. The gases combine and form the desired layer on the surface of a substrate, which can be held at a relatively low substrate temperature (< 400 °C). Because of this low deposition temperature and the hydrogenated precursors used to deposit the PECVD SiON layers, considerable amount of hydrogen becomes incorporated in the PECVD SiON layers [21, 33, 62, 67, 72]. Variation of the deposition temperature was found to have a weak influence on the layer properties [67], which can be explained by the fact that the mean electron temperature (T_e) that is related to the degree of ionization and dissociation, is much higher than the mean gas temperature (T_g); typically, $T_e/T_g > 10$.

3.1.3 Design of experiment

In order to obtain an optimum technology with the Oxford PECVD system 133 for undoped SiON to be a base material for fabricating P and BP-doped SiON optical waveguides. A series of experiments are conducted according to the Graeco-Latin square [73, 74], in which several significant parameters, each with different values (levels) are selected and arranged in a way to have

minimum experimental efforts for a desired results reliability. The results of the experiments are either the optimized deposition parameter set or guide to the best direction for a follow-up experiment.

3.1.3.1 Determination the number of factors and levels

A design of experiment (DOE) was implemented to investigate how the deposition parameters (independent variables or factors) influence the layer properties such as refractive index (*n*), deposition rate (R) and thickness non-uniformity (δd) of the PECVD SiON layers. These properties are strongly dependent on the layer composition [75], which, in turn can be controlled by the parameters of the PECVD process, like the flow-rate and the ratio of the process gases, the RF power, the chamber pressure and the substrate temperature. For process optimization four factors were selected for the DOE. These factors are RF power, chamber pressure, 2%SiH_4/N_2O and N_2O gas flow. Four levels have been given to each factor. The following variables and ranges (Table 3.2) were chosen for the DOE based on tool company guidance, previous published work and preliminary variation of the process parameters:

Table 3.2 Variable settings used for the experimental design

		Levels			
Factors		1	2	3	4
Power	(W)	20	30	40	50
Pressure	(Pa)	100	120	140	160
2% SiH_4/N_2 flow	(sccm)	1000	1200	1400	1600
N_2O flow	(sccm)	300	800	1300	1800

3.1.3.2 Choosing and randomizing an experimental design

When a full factorial design experiment is conducted to 4 factors and 4 levels, all levels of a factor should be "crossed" with all levels of the other factors, which means that $4\times4\times4\times4=4^4=256$ experimental runs are required. This is unacceptable for both cost and time consumption. To reduce the number of the experimental runs while the influence of each factor on the layers properties can still be investigated, a Graeco-Latin square is adopted for SiON deposition (Table 3.3).

Table 3.3 Matrix layout of the 4×4 Graeco-Latin square design

Power	Pressure			
	1	*2*	*3*	*4*
1	S(1)N(1)	S(2)N(3)	S(3)N(4)	S(4)N(2)
2	S(2)N(2)	S(1)N(4)	S(4)N(3)	S(3)N(1)
3	S(3)N(3)	S(4)N(1)	S(1)N(2)	S(2)N(4)
4	S(4)N(4)	S(3)N(2)	S(2)N(1)	S(1)N(3)

* S≡2% SiH_4/N_2 gas flow and N ≡ N_2O gas flow

With this arrangement, the main effect of RF power, chamber pressure, 2%SiH_4/N_2O and N_2O gas flow on the layer properties can be analyzed from only 16 run of experiments, see Table 3.4.

Table 3.4: 4×4 Graeco-Latin square experimental sequence and the responses

		Matrix (Factors)				Responses		
No.	Run sequ.	Power	Press.	SiH_4	N_2O	*n*	R (nm/min)	δd%
1	13	1	1	1	1	1.567	40.73	1.74
2	5	1	2	2	3	1.500	57.22	1.09
3	14	1	3	3	4	1.497	61.84	1.21
4	6	1	4	4	2	1.531	72.76	1.20
5	7	2	1	2	2	1.518	49.82	1.77
6	16	2	2	1	4	1.478	70.45	1.58
7	9	2	3	4	3	1.505	86.85	1.37
8	15	2	4	3	1	1.589	85.93	1.40
9	2	3	1	3	3	1.504	57.20	1.48
10	1	3	2	4	1	1.637	72.88	1.44
11	11	3	3	1	2	1.473	97.12	1.53
12	8	3	4	2	4	1.475	98.56	1.26
13	12	4	1	4	4	1.496	66.49	1.81
14	4	4	2	3	2	1.495	103.17	1.44
15	10	4	3	2	1	1.525	108.94	1.41
16	3	4	4	1	3	1.457	107.82	1.29

To control the bias error that will inevitably appear in the experiment, a complete randomization of the experimental sequence is necessary. A number of methods of randomization are available. In this experiment, 16 pieces of paper with the matrix number of Table 3.4 were put in a box and well shuffled. The random test sequence was established by taking a piece of paper

out of the box once a time. The experiment sequence is listed in the 2nd column of Table 3.4. The 16 run were performed according to the randomized experiment sequence as presented in Table 3.4. All layers were deposited at 300 °C on p-type <100> oriented 100 mm silicon wafers. The basic properties (*n*, R and δd) are listed as responses in Table 3.4. The thickness and refractive index have been determined by spectroscopic ellipsometry (Woollam M44) on approximately 250 nm thin layers directly deposited on silicon wafers. The measurement error is approximately 2×10^{-3} in refractive index and 0.1% in layer thickness. The variance in thickness δd has been measured by a single-wavelength ellipsometric profiler (Plasmos 2000), and is given by the half difference between maximum and minimum deviation of the thickness values measured over a 70×70 mm² area with a 15×15 points grid on the 100 mm wafers. The run-to-run reproducibility has been determined by measuring the deviations of *n* and d at the same position on samples grown in two adjacent runs.

3.1.3.3 Data analysis

Analysis of variance (ANOVA) [74, 76] were performed on the experimental data of Table 3.4, a summary of this analysis that indicates significant effects at the 5% level or less for the thickness non-uniformity is presented in Table 3.5, where *df* is degree of freedom, *SS* stands for sum of squares, *MS* is the mean square. From these data *F* ratio is calculated from the variation due to an experimental treatment or effect (mean sum of squares of each factor) divided by the variation due to experimental error (mean sum of the error) [73, 74, 76].

Table 3.5 Significant test of factors for the thickness non-uniformity

Factor	*df*	*SS*	*MS*	*F*	$F_c(0.05)$	Significant
Power	3	0.1096	0.03654	24.4972	9.28	Yes
Pressure	3	0.3888	0.12961	86.8883	9.28	Yes
SiH_4	3	0.0634	0.02114	14.1732	9.28	Yes
N_2O	3	0.094	0.03134	21.0112	9.28	Yes
Error	3	0.0045	0.00149			
Total	15	0.6604	0.04403			

This analysis has also been done for the refractive index and the deposition rate. The calculations indicate that the N_2O flow rate has a significant effect on the refractive index and both RF power and chamber pressure were found to have a significant effect on the deposition rate, whereas all factors have a significant effect on the thickness non-uniformity as presented in Table 3.5. Since all factors were found to influence the thickness uniformity. The combination (1 2 2 3), which gave a better thickness uniformity will be used in

the next section to vary the process parameters, in order to have a better look to the principal effects and the contribution of each parameter to the layer properties.

3.1.4 Process optimization by correlation analysis

The objective of our investigation is to optimize the PECVD SiON deposition process over a wide index range (1.46 - 1.7) to arrive at layers with thickness uniformity within 1% and a deposition rate sufficiently high for technical applications (> 50 nm/min).

Silicon oxynitride layers have been deposited with an Oxford Plasmalab System 133 PECVD reactor which has been described in section 2.1.

All layers were deposited on p-type <100> oriented 100 mm silicon wafers. In order to determine the optimum processing parameters for the SiON deposition process, the following set [combination (1 2 2 3), see Section 3.1.3] of input parameters has been established after a preliminary study:

- RF power: 20 W
- Chamber pressure: 120 Pa
- Total gas flow: 2500 sccm
- Substrate temperature: 300 °C
- Gas flow ratio: 54 for N_2O/SiH_4 (calculated from the flow rates of N_2O and the $2\%SiH_4/N_2$ mixture).

Thereafter a systematic variation of the parameters has been made within the parameter window given in Table 3.6 This study, which should result in a better understanding of the principal effects and the contribution of each parameter to the layer properties, was carried out according to Pearson's correlation method [77].

Table 3.6 Variation ranges of the PECVD deposition parameters used to optimize PECVD SiON layers

Input parameter	Range of variation
RF power	20 - 100 W
Chamber pressure	93.3 – 146.6 Pa
Total gas flow	1666.7 - 3333.3 sccm
Substrate Temperature	300 - 400 ^{0}C
N_2O/SiH_4 gas flow ratio	19.4 - 75

This analysis is carried out by changing systematically the process parameters of Table 3.6 and observing the influence on the refractive index (n), deposition rate (R) and thickness non-uniformity (δd) of the layers. Table 3.7 shows the resulting correlations with range between -1.00 to +1.00. A value -1.00 represents a perfect negative correlation for two variables, while +1.00

represents a perfect positive correlation. A value of 0.00 represents a total lack of correlation [77].

Table 3.7 Correlation analysis results relating the PECVD input deposition parameters with the deposited SiO_xN_y:H layers properties (n, R *and* δd*)*

	Output		
Input	*n*	R	δd
RF Power	-0.943	0.963	0.979
Pressure	-0.984	0.958	-0.997
Total flow ($2\%SiH_4/N_2 + N_2O$)	0.977	0.982	-0.584
Substrate Temperature	-0.347	0.102	0.456
Flow ratio (N_2O/SiH_4)	-0.918	0.784	-0.263

From the correlation results (Table 3.7) the following conclusions can be drawn:

- The RF power, the pressure and the total gas flow have a significant effect on the layer properties (*n*, R and δd). The N_2O/SiH_4 gas flow ratio has only a weak influence on δd and significant effect on n and R. The substrate temperature has only a minor effect to the layer properties within the range studied.
- The RF power shows a positive correlation with the deposition rate, thickness non-uniformity and a negative one with the refractive index; that means that R and δd increase and n decreases with increasing power. The increase of the deposition rate at higher RF power, while the partial pressure for both, silane and nitrous oxide, is kept constant, can be attributed to the increase of the concentration of the active reaction species and the plasma density with the power. The observed decrease of the refractive index at higher power can be understood when the dissociation efficiencies of both gases are taken into account. It is well known that silane has higher dissociation efficiency than nitrous oxide [78] resulting in an domination of silane radicals at low power. By increasing the power, the relative concentration of oxygen radicals increases (see section 3.1.1, step 1) leading to a decrease of the refractive index.
- The chamber pressure shows a negative correlation with the refractive index and the thickness non-uniformity and a positive correlation with the deposition rate. At higher total pressure, the discharge voltage increases, making it difficult to start the plasma, since the impedance between the parallel plates decreases due to the higher gas concentration [69]. This results in a material with low density or a low refractive index with increasing pressure. On the other hand, the

residence time increases by increasing the total pressure. This explains the increase in the deposition rate with increasing total pressure.

- Both refractive index and deposition rate increase with increasing total gas flow. It is clear that the residence time decreases by increasing the total gas flow. Since the silane has higher dissociation efficiency than nitrous oxide, this leads to domination of silane radicals that increase the refractive index. The discharge is sustained by electrons making ionizing collisions in the gas [69]. The number of ionizing collisions will increase with increasing gas density (total gas flow) leading to increase of the deposition rate.
- The substrate temperature, studied in the range 300 to 400 °C with a gas flow ratio (N_2O/SiH_4 = 54) shows only a weak influence on the layer properties. This could be expected as the mean electron energy or electron temperature is much higher than the substrate temperature [67]. Our results confirm that in the experimental regime under investigation the electron-impact ionization and dissociation [Equations (3.1) and (3.2)] is independent of the substrate temperature.
- The gas flow ratio (N_2O/SiH_4) correlates negatively with the refractive index and thickness non-uniformity and positively with the deposition rate. When the N_2O/SiH_4 flow ratio increases, the excited oxygen atom density increases too, leading to increasing disiloxane compared to the SiH_2 and SiH_3 precursors. As a result the formation of Si-O becomes favored leading to a layer composition close to SiO_2 (see Section 3.1.1, step 2). When the N_2O/SiH_4 flow ratio decreases, the incorporation of nitrogen and silicon in the form of Si-H, Si-N, N-H and Si-Si becomes more probable, leading, as expected, to an increasing refractive index. The increase of the deposition rate with increasing N_2O/SiH_4 flow ratio is expected, as we suppose that our deposition conditions give rise to a complete dissociation of the silane and that the process is limited by the nitrous oxide concentration.

Based on the correlation analysis, the optimal deposition conditions were selected to be: RF power 20 W, chamber pressure 140 Pa, total gas flow 2500 sccm and deposition temperature 350 °C. Since the N_2O/SiH_4 gas flow ratio does not influence the thickness non-uniformity significantly but has a large impact on the refractive index, this input parameter will be varied in order to study the properties of silicon oxynitride films with different composition in more detail.

3.1.5 Properties of optimized SiON layers

In this section we will show detailed results on the compositional and optical properties of various SiO_xN_y:H layer deposited under optimized processing conditions. The basic properties (optical constants, deposition rate and thickness uniformity) of five sets of layers (S1 to S5) that have been

prepared by varying the N_2O/SiH_4 input ratio are shown in Table 3.8. As can be seen, high quality SiO_xN_y:H layers could be obtained for a wide range of index of refraction with sufficiently high deposition rate and excellent uniformity. The run-to-run reproducibility of the refractive index and the layer thickness is < 6×10^{-4} and ~1%, respectively for the entire deposited layers. The run-to-run reproducibility has been determined by measuring the deviations of the refractive index and the layer thickness at the same position on samples deposited in two adjacent runs.

Table 3.8 N_2O/SiH_4 gas flow, refractive index (real n, and imaginary part κ), deposition rate and thickness non-uniformity of the 5 different SiO_xN_y:H layers studied

Sample	N_2O/SiH_4 gas flow ratio	λ=632.8 nm		R ± ΔR (nm/min)	δd (%)
		$n \pm \Delta n$	κ		
S1	75.0	1.4871±0.0016	0	62.64±0.19	1.00
S2	39.3	1.5129±0.0018	0	67.41±0.20	0.86
S3	28.1	1.5322±0.0019	0.0020	65.55±0.20	0.92
S4	19.4	1.5690±0.0019	0.0032	61.93±0.18	0.93
S5	12.5	1.6525±0.0022	0.0045	55.36±0.17	1.08

The atomic ratios of Si, O and N in the layers were determined by XPS from the corrected areas of the Si 2p, N 1s, and O 1s peaks. Table 5 summarizes the binding energies of the photoelectron peaks and the atomic concentrations ratio of the deposited SiO_xN_y:H layers. The relative concentrations were determined to an accuracy of ~ 10% for silicon, oxygen and nitrogen with a detection limit of ~ 0.1 atom%. It can be seen from Table 4 and 5 that with an increase in the refractive index (decrease of the N_2O/SiH_4 flow ratio) the nitrogen and the silicon content increased.

Table 3.9 Binding energies of the photoelectron peaks Si2p, N1s and O1s, the relative atomic concentrations and the empirical formula of the 5 different SiO_xN_y:H layers studied

Sample	Binding energy (eV)			Atomic (%)			Empirical formula
	Si2p	N1s	O1s	Si	O	N	
S1	103.3	398.4	532.6	32.9	65.0	2.1	$SiO_{1.97}N_{0.06}$
S2	103.0	398.1	332.2	34.0	61.4	4.6	$SiO_{1.80}N_{0.13}$
S3	102.8	398.0	532.2	34.1	59.3	6.6	$SiO_{1.74}N_{0.19}$
S4	102.4	398.0	532.2	35.8	56.0	8.2	$SiO_{1.57}N_{0.23}$
S5	102.3	398.0	532.1	37.9	52.9	9.2	$SiO_{1.40}N_{0.24}$

From the valences of silicon (+4), oxygen (-2) and nitrogen (-3), a stoichiometric composition of silicon oxynitride can be predicted, under the assumption that the sum of the positive valences must be equal to that of the negative ones and the sum of all atomic concentrations (Si, N and O) in the layer must be equal to 100. This can be represented by the following equations:

$$4X_{Si} = 3X_N + 2X_O \tag{3.5}$$

$$X_{Si} + X_N + X_O = 100 \tag{3.6}$$

where X_{Si}, X_O and X_N represent the atomic percentages of silicon, oxygen and nitrogen in the silicon oxynitride layer, respectively.

With the aid of Equations (3.5) and (3.6) it is possible to derive the silicon and oxygen atomic percentages from the nitrogen atomic percentage according to the following equations:

$$X_{Si} = \tfrac{100}{3} + \tfrac{1}{6} X_N \tag{3.7}$$

$$X_O = \tfrac{200}{3} - \tfrac{7}{6} X_N \tag{3.8}$$

With these equations the silicon or oxygen atomic percentage can now be plotted as a function of the nitrogen atomic percentage for stoichiometric silicon oxynitride as shown in

Figure 3.1(a) and (b) respectively. For comparison we include also the experimental data points determined by XPS for our 5 layers.

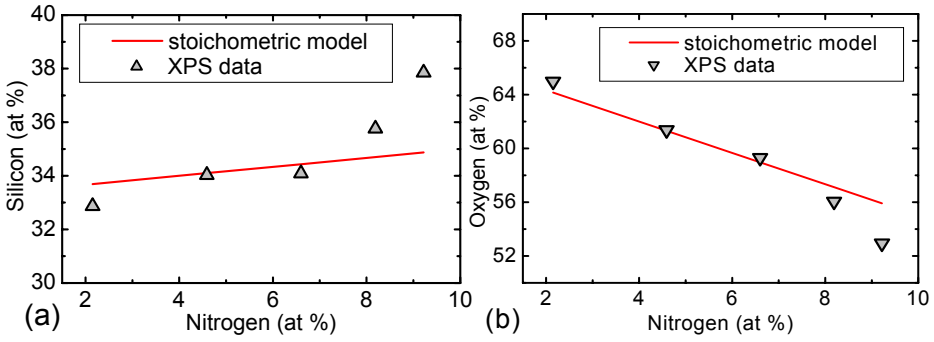

Figure 3.1 Atomic percentage of the 5 SiO_xN_y:H layers studied: (a) silicon and (b) oxygen as function of nitrogen concentration. The solid line represents stoichiometric SiO_xN_y, the triangles are experimental data points obtained by XPS.

Layers with low nitrogen concentration (lower refractive index, high N_2O/SiH_4 flow ratio) show good agreement between XPS data and the stoichiometric model. Higher refractive index layers with N_2O/SiH_4 < 20 deviate increasingly from the stoichiometry. This deviation can be attributed to the formation of silicon rich-silicon oxynitride (see section 3.1.1, step 2). For a quantitative analysis of the Si-Si bonds in the layers, a deconvolution of the Si 2p XPS spectra was performed Table 3.10.

Table 3.10 Results of the Si 2p peak fitting with relative binding energies (BE), the full width at half maximum (FWHM) and the corrected Si atomic concentration ratio of the 5 different SiO_xN_y:H layers studied

	Si 2p peak					
	Si bonded as SiO_xN_y			Si bonded as ≡Si–Si≡		
Sample	BE (eV)	FWHM (eV)	Atomic (%)	BE (eV)	FWHM (eV)	Atomic (%)
S1	103.2	2.7	32.9	-	-	0.0
S2	102.9	2.8	34.0	-	-	0.0
S3	102.8	2.8	33.9	99.4	1.1	0.2
S4	102.6	2.7	34.6	99.5	1.4	1.2
S5	102.3	2.8	34.7	99.8	2.4	3.2

Clearly the position of the Si 2p (SiO_xN_y) peak varies from 103.2 eV (sample S1) to 102.3 eV (sample 5). It is well known that the binding energy of Si 2p in the pure silicon is 99.3 eV [56, 58]. However this energy is shifted when silicon is bonded with other elements. For Si_3N_4 the Si 2p peak position is at 102 eV (a shift of 2.7 eV from silicon) and for SiO_2 at 103.3 eV (a shift of 4.0 eV) [56]. For SiO_xN_y the Si 2p peak can be expected to have a position between 102 eV and 103.3 eV, the actual position being dependent on the x and y values of the SiO_xN_y compound. The larger the y is, the closer it is to 102 eV, which is in agreement with our calculated empirical formulas of the studied samples (Table 3.9). The Si 2p peaks of sample S1 and S2 are well fitted with one Gaussian-Lorentzian shaped peak, while other samples (S3, S4 and S5) needed two Gaussian-Lorentzian peaks for fitting [Figure 3.2 (a) and (b)]. The additional peaks at 99.4, 99.5 and 99.8 eV were attributed to excess silicon (≡Si–Si≡) in sample S3, S4 and S5 respectively.

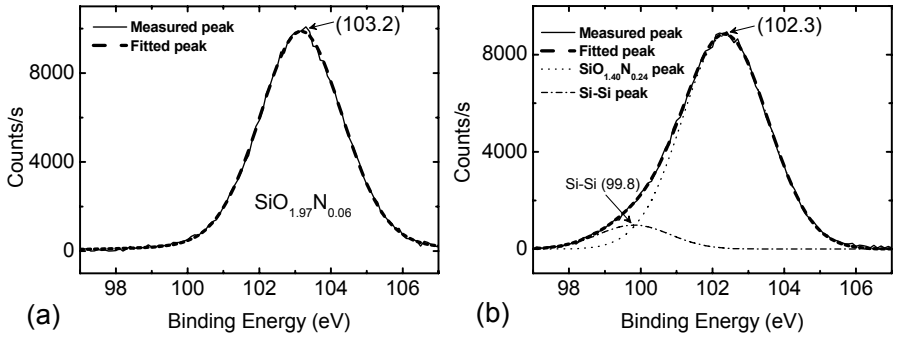

Figure 3.2 XPS Si 2p peak fitting for the measured spectrum collected for SiO_xN_y:H (a) sample S1 (b) sample S5

FTIR-spectroscopy has been performed on layers with the same composition as given in Table 3.9 (S1 to S5) to obtain direct information about compositional and vibrational properties of the deposited layers. The FTIR absorption spectra of the layers are shown in Figure 3.3. The dominant feature in these spectra is a broad Si-O stretching mode, which occurs at slightly decreasing position (1054, 1046, 1044, 1040 and 1038 cm^{-1}) with an increasing refractive index in the film from samples S1 to S5. The shift in position to higher energy with increasing oxygen content can be attributed to the increase of the electronegativity in the neighborhood of these bonds [70]. The increase in the peak width with the refractive index can be explained by the appearance of Si-N stretching bonds at 870 cm^{-1} at increasing nitrogen content.
The absorption peak at around 820 cm^{-1} in sample S1 is due to the Si-O bending mode. It is due to the excess amount of oxygen in this low index layer that makes the occurrence of Si-O bonds in two different forms (stretching and bending) more probable.

The absorption due to N-H stretching modes in the regions 3300 – 3400 cm^{-1} and that due to Si-H stretching modes in the regions 2150 – 2300 cm^{-1} are observed in all samples (S1 to S5). The vibrational overtones of these bonds are well known for their contribution to optical loss at the third telecommunication window around 1550 nm wavelength. It is therefore important to quantify the atomic concentration of hydrogen connected with the N-H and Si-H bonds in the layers.

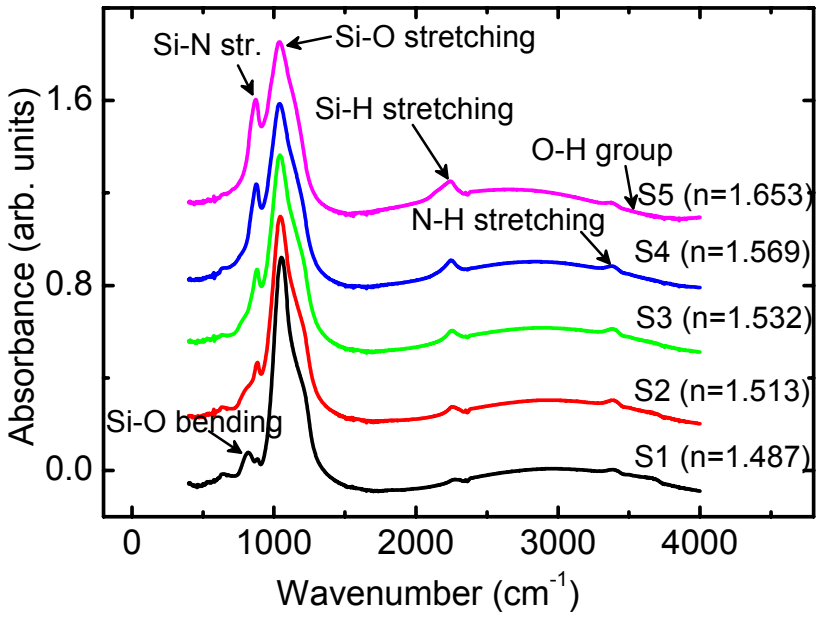

Figure 3.3 FTIR spectra of PECVD SiO_xN_y:H layers S1 to S5 with different refractive indices (for better visibility curves are plotted with an offset with respect to each others)

Like others [29, 32] we assume that the presence of N-N, O-O, H-H and N-O bonds in SiON can be excluded due to the high bond strength in N_2, O_2, H_2 and NO molecules, respectively. Also our XPS studies have shown no evidence for N-N and N-O bonds in the layers. Deconvolution of N1s XPS spectra obtained for sample S1 and S5 have shown the presence of two nitrogen peaks Figure 3.4. The peaks at 397.7 and 397.2 eV have been attributed to $N(\text{-Si})_3$ and those at 398.6 and 398.1 to Si-N(-H)_2 for sample S1 and sample S5 respectively [55].

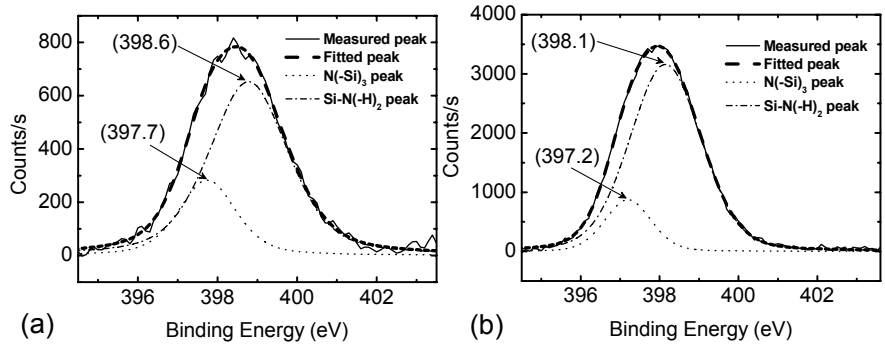

Figure 3.4 Deconvolution of N 1s XPS spectra for SiO_xN_y:H (a) sample S1 (b) sample S5

Therefore only Si-centred structures need to be considered. Consequently, taking into account the valences for Si, N, O, and H the atomic and bond concentrations are related by the following equations [79]:

$$\begin{aligned} 4[Si] &= 2[Si-Si]+[Si-O]+[Si-N]+[Si-H] \\ 3[N] &= [Si-N]+[N-H] \\ 2[O] &= [Si-O]+[O-H] \\ 1[H] &= [Si-H]+[N-H]+[O-H] \end{aligned} \tag{3.9}$$

O-H vibrations (~ 3500 cm^{-1}) were not detected by the FTIR; therefore the total hydrogen content according to equation (3.9) can be described in the following way:

$$[H] = [Si-H]+[N-H] \tag{3.10}$$

The N-H and Si-H bonds concentrations were determined from the FTIR measurements for all SiO_xN_y:H layers (S1 to S5) by using the method of Lanford and Rand [54] with the aid of equation (2.23).

The results are plotted in Figure 3.5. It appears that the total hydrogen content in the layers increases with increasing *n* and decreasing gas flow ratio (N_2O/SiH_4). Except for layers S1 and S2, the bonded hydrogen in SiO_xN_y:H is dominant in the form of Si-H bonds, which is in line with the PECVD process mechanisms (see section 3.1.1, step 2).

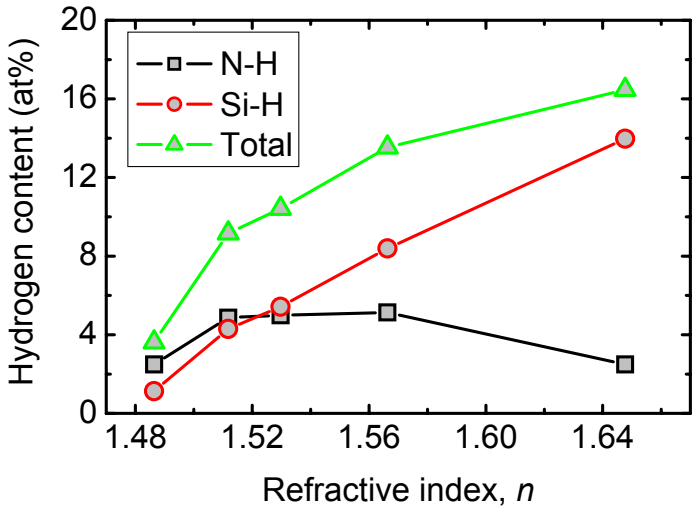

Figure 3.5 Hydrogen content as a function of the refractive index for SiO_xN_y:H samples S1-S5

It can be clearly seen in Figure 3.5 that the number of N-H bonds in the layers increases from layer S1 to S2 and decreases at larger *n*, while the nitrogen concentration is still increasing. We attribute this to the increase of Si-N bonds concentration as the gas flow ratio (N_2O/SiH_4) decreases. In the case of sample S1 and S2 there are sufficient oxygen radicals in the plasma and Si is preferably bonded as Si-O rather than Si-N (step 2), hence most of the nitrogen is bonded as N-H. When the gas flow ratio (N_2O/SiH_4) decreases the oxygen radicals in the reaction decreases too. The formation of Si-N (470 kJ/mol) will becomes more preferable over N-H (339 kJ/mol) in the gas phase (Table 2). On the other hand, N-H and Si-H bonds may react on the surface to form Si-N [see equation(3.3)].

The most important parameter for integrated optics application is the optical loss (α). In addition, loss measurements are very sensitive to the presence of hydrogen and excess silicon. The loss of PECVD SiO_xN_y:H (S1 to S5) slab-type waveguides structure has been determined by using a moving prism in/out-coupling technique. The measurements were performed on the fundamental TE modes at two wavelengths, 632.8 and 1550 nm. The measurement results are given in Table 3.11. It appears that the optical loss increases for both wavelengths with decreasing gas flow ratio (N_2O/SiH_4). The increase of the optical loss at 632.8 nm can be attributed to the increase in silicon content beyond stoichiometry and therefore increasing concentration of Si-Si bonds. These losses at visible light can be reduced by adding NH_3 to the (N_2O + SiH_4/N_2) gas mixture. In this way the probability of Si-Si bonds formation is reduced since Si is more likely to be bonded to nitrogen than to

silicon. Layers with a composition similar to S3, S4 and S5 have been prepared with the addition of NH_3 as process gas and losses below 0.2 dB/cm could be measured indicating the absence of excess silicon.

Table 3.11 Optical losses and Atomic concentration of the 5 different SiO_xN_y:H layers studied

Sample	N_2O/SiH_4 flow ratio	Si bonded as Si-Si (at %)	H (at %)	α @ 632.8 nm (dB/cm)	α @ 1550 nm (dB/cm)
S1	75.0	0.0	3.6	< 0.2	1.20
S2	39.3	0.0	9.2	< 0.2	1.68
S3	28.1	0.2	10.4	0.8	1.82
S4	19.4	1.2	13.5	6.9	2.41
S5	12.5	3.2	16.5	27.7	2.90

The optical loss at 1550 nm increases steadily with the hydrogen content. This is the well-known effect of the first and the second overtones of the N-H and Si-H frequencies respectively. By a post deposition thermal treatment [19, 21, 23, 72, 80] the hydrogen can be removed and the losses at 1550 nm can be reduced to below 0.2 dB/cm. Recent experiments on phosphorus doping of SiON layers show that that a significant reduction can be obtained in the hydrogen bonds concentration as well as the optical loss at 1550 nm, when compared to the undoped samples [81], which will be discussed in next chapter. The increase of the optical loss at 632.8 nm can be attributed to the increase in silicon content beyond stoichiometry and therefore increasing concentration of Si-Si bonds. These losses at visible light can be reduced by adding NH_3 to the (N_2O + SiH_4/N_2) gas mixture. In this way the probability of Si-Si bonds formation is reduced since Si is more likely to be bonded to nitrogen than to silicon. Layers with a composition similar to S3, S4 and S5 have been prepared with the addition of NH_3 as process gas and losses below 0.2 dB/cm could be measured indicating the absence of excess silicon. In the next section deposition of undoped SiON using ammonia will be described.

3.2 Deposition of undoped SiON using ammonia

PECVD silicon oxynitride were deposited from 2%SiH_4/N_2, N_2O and NH_3. The deposition conditions were similar to the optimized process (see Section 3.1.4), RF power 20 W (13.56 MHz), chamber pressure 140 Pa and deposition temperature 350 °C. The 2%SiH_4/N_2 flow rate of 600 sccm was kept constant in all deposition. The N_2O flow rate was varied from 240 to 600 sccm.

Figure 3.6 shows the dependence of the refractive index as a function of SiH_4/N_2O gas flow ratio for various NH_3 flow. The SiON layers (~ 250 nm) were deposited on silicon the thickness and the refractive index were measured with spectroscopic ellipsometry which has been described in Section 2.2.1.

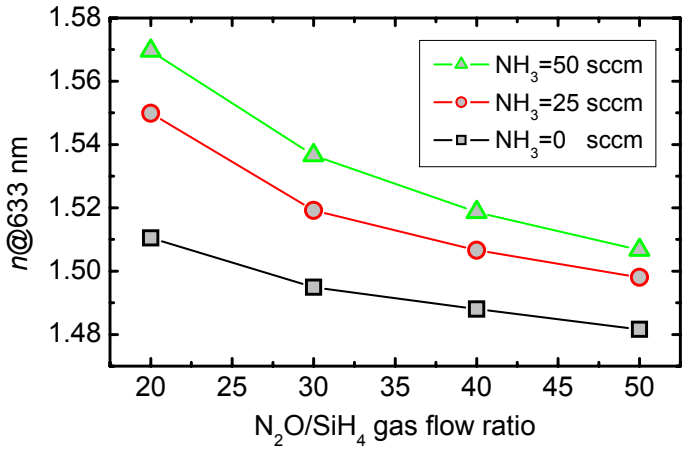

Figure 3.6 Refractive indices of SiON layers as a function of gas flow ratio N_2O/SiH_4 (The gas flow ratio of N_2O/SiH_4 was calculated using the real SiH_4 flow).

It can be clearly seen that the refractive index of the deposited SiON layer increases with the NH_3 gas flow rate. Indicating that a higher refractive index can be achieved by adding NH_3 to the PECVD process. The deposition rates were found to be ~ 55 nm/min for the given process parameters. The refractive index inhomogeneity and the thickness non-uniformity are 2-5×10^{-4} and 0.8 -1%, respectively, over a 70×70 mm^2 on 100 mm wafer. The run-to-run reproducibility of the refractive index and the layer thickness is < 6×10^{-4} and ~1%, respectively for the entire layers.

In order to study the effect of NH_3 on the PECVD SiON layer properties, a comparison is made between two samples (G1 and G2) with a similar refractive index (n=1.57), one is deposited from 2%SiH_4/N_2 and N_2O (G1) and the second one is deposited from 2%SiH_4/N_2, N_2O and NH_3 (G2). The XPS analysis described above has shown a decrease is the silicon concentration and an increase in the nitrogen atomic concentration with ammonia (see Table 3.12). Moreover, the XPS Si2p peak fitting shows no evidence of ≡Si–Si≡ in layer deposited with NH_3 (G2) indicating the absence of excess silicon. This corresponds well with the optical loss measurement obtained from the layers G1 and G2 (see Table 3.12).

Table 3.12 Atomic ratio and optical loss of two SiON layers with the same index of refraction deposited with two different processes.

Sample	*n* @ 632.8 nm	NH_3 flow (sccm)	Atomic concentration (%)			Si bonded as ≡Si–Si≡	α @ 632.8 nm (dB/cm)
			Si	O	N		
G1	1.57	0	35.76	56.05	08.19	1.2	6.9
G2	1.57	50	34.29	52.96	12.75	0.0	< 0.2

For the hydrogen concentration and the bond configurations FTIR spectroscopy has been used. Figure 3.7 shows FTIR spectra of the two samples which are deposited with and without NH_3.

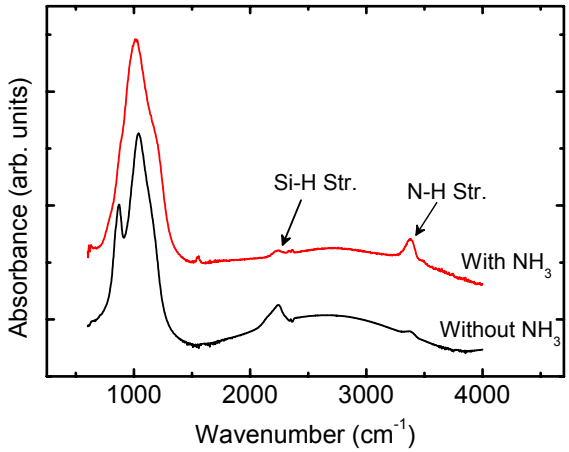

Figure 3.7 FTIR spectra of PECVD SiON layers G1 and G2 deposited by two different processes (for better visibility curves are plotted with an offset).

From Figure 3.7, it is clear to see that the bonded hydrogen in the SiON layer G1 deposited from 2%SiH_4/N_2 and N_2O is predominantly in the form of Si-H bonds, however, when NH_3 is added to the reaction, N-H bond become more favorable. This could be expected when there are more nitrogen radicals in the reaction. As presented in Table 3.1, the bond strength of Si-N> Si-Si and N-H > Si-H and consequently Si-N and N-H bonds are more likely to be formed instead of Si-Si and Si-H bonds respectively. Hence the Si atoms bonded to H and Si in the layer deposited from 2%SiH_4/N_2 and N_2O will be replaced by nitrogen atoms when ammonia is added to the process. In Table 3.13 a comparison is made between the two SiON layers G1 and G2 for the hydrogen bond concentration. The concentration of N-H and Si-H bonds was estimated using Equation(2.23).

Table 3.13 Hydrogen concentration of two the SiON layers with same index of refraction deposited by two different processes

Sample	NH_3 flow (sccm)	[N-H] ($\times 10^{21}$ atoms/cm^3)	[Si-H] ($\times 10^{21}$ atoms/cm^3)
G1	0	3.73	6.09
G2	50	8.31	2.77

In order to compare the absorbance of the Si-N bonds (~ 870 cm^{-1}), it has been necessary to carry out a deconvolution of the broad region of the absorption extending from 700 to 1500 cm^{-1}, see Fig. 3.7. For this purpose, 5 and 6 Gaussians bands have been employed for samples G1 and G2 respectively (see Figure 3.8). In this way, the Si-N normalized absorption band area was estimated. The result of the calculations indicates that the Si-N normalized absorption band area is increased from 30.6 for sample G1 to 87.0 cm^{-2} for sample G2. This can explain the elimination of Si-Si bonds when NH_3 is added to the reaction.

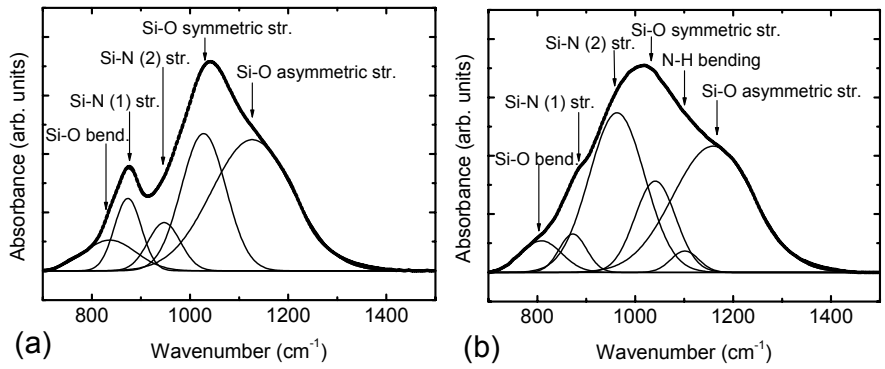

Figure 3.8 Gaussian deconvolution of the measured absorbance in the range from 700 to 1500 cm^{-1} for (a) sample G1 (b) sample G2

3.3 Deposition of undoped SiON using 187.5 KHz generator

Plasma enhanced deposition of silicon oxynitride has been investigated for various process parameters for a low RF frequency of 187.5 KHz [21, 82]. This frequency is sufficiently low to accelerate ions from the plasma to the electrode leading to significant ion bombardment on the substrate. The ion bombardment damages the SiON matrix and causes significant implantation of the accelerated ions [66, 67]. These effects are expected to have a significant contribution on the layer properties.

To investigate the influence of the LF deposition to the SiON layers, the depositions were carried out at low RF frequency starting from 2%SiH_4/N_2 and N_2O gas mixtures in an Oxford system 133 PECVD on p-type <100> oriented 100 mm silicon wafers. The optimization procedures were carried out in a similar way as presented in Sections 3.1.3 and 3.1.4. The influence of the flow-rate and the ratio of the process gases, the RF power, the chamber pressure and the substrate temperature were investigated.

The refractive index was found to decrease with RF power; the chamber pressure and gas flow ratio (N_2O/SiH_4) increases with increasing total gas flow (2%SiH_4/N_2 + N_2O). The deposition rate was found to increase with RF power, chamber pressure, gas flow ratio (N_2O/SiH_4) and total gas flow. However, none of the parameters have shown a significant effect on the thickness uniformity. The optimal deposition conditions were selected to be: RF power 60 W, chamber pressure 86.6 Pa, 2%SiH_4/N_2 gas flow 600 sccm, N_2O gas flow 125 – 600 sccm and deposition temperature 300 °C. Figure 3.9 shows the behaviors of refractive index and deposition rate of the deposited SiON layers as a function of the gas flow ratio.

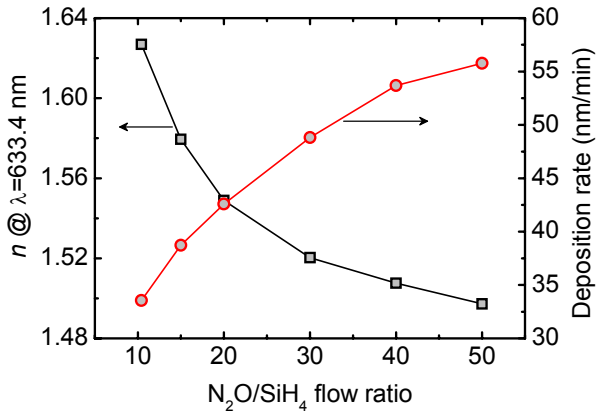

Figure 3.9 Refractive index and deposition rate of PECVD SiON layers deposited at low RF frequency as a function of gas flow ratio N_2O/SiH_4 (The gas flow ratio of N_2O/SiH_4 was calculated using the real SiH_4 flow)

The refractive index inhomogeneity, the thickness non-uniformity and the run-to-run reproducibility of SiON layers deposited by PECVD operating at low frequency are shown in Table 3.14.

Table 3.14 Uniformity and reproducibility of refractive index and thickness for SiON layers with different refractive indices.

	Uniformity on 100 mm wafer			Run-to-run reproducibility	
	Δn	δd (%)			
n	($\times 10^{-4}$)	50×50 mm²	70×70 mm²	Δn ($\times 10^{-4}$)	Δd (%)
1.4972	3	0.82	3.2	5	1.1
1.5076	2	0.86	3.0	4	0.9
1.5203	4	0.67	2.4	5	1.2
1.5489	6	0.83	3.7	6	1.7
1.5794	5	0.61	2.1	4	2.1
1.6269	6	0.72	3.8	6	2.0

When comparing PECVD SiON layers deposited by HF and LF power with a comparable refractive index, the absorption loss of the LF deposited layers were found to be lower than the HF layers. Figure 3.10 compares FTIR spectra of two SiON layers deposited by the two different processes. The N-H concentration has been determined by IR-spectroscopy as described in Section 2.2.2.1, the results are given in Table 3.15. Si-H bonds were not detected for the LF layer.

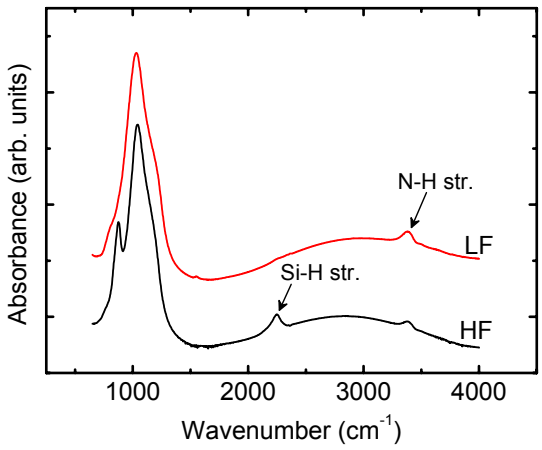

Figure 3.10 FTIR spectra of PECVD SiON layers with the same index of refraction deposited by two different processes (HF and LF) (for better visibility curves are plotted with an offset)

The optical loss of slab-type waveguides for both types of layers has been determined using a moving prism technique. The measurements were performed on the fundamental TE modes at two wavelengths, 632.8 and 1550 nm. The measurement results are also given in Table 3.15. It appears that the optical loss of LF SiON layer is lower than the HF SiON layer for both wavelengths. The decrease of the optical loss at 1550 nm is attributed to the reduction of the hydrogen concentration in the LF sample as a result of the ion bombardment [66]. The decrease in the optical loss at 632.8 nm can be attributed to the elimination of the Si-Si bonds in LF SiON layer. XPS Si2p peak fitting has shown no evidence of ≡Si–Si≡ bonds in the layers deposited with LF, indicating the absence of excess silicon.

Table 3.15 Hydrogen concentration and optical losses of two SiON layers with the same index of refraction deposited by two different processes.

Sample	*n*	[N-H] (atoms/cm^3)	[Si-H] (atoms/cm^3)	α @ 632.8 nm (dB/cm)	α @ 1550 nm (dB/cm)
HF	1.57	3.73×10^{21}	6.09×10^{21}	6.9	2.41
LF	1.57	5.91×10^{21}	0.00	0.2	1.94

3.4 Summary and conclusions

Optimized PECVD silicon oxynitride layers for integrated optics application have been deposited from 2%SiH_4/N_2 + N_2O and 2%SiH_4/N_2 + NH_3 + N_2O. The uniformity and homogeneity of the deposited layers and the reproducibility of the process are good.

The optical properties of SiON layers were found to depend largely on the deposition parameters, especially on the N_2O/SiH_4 gas flow ratio. The concentrations of the HF SiON layers deposited with high N_2O/SiH_4 flow ratio (> 20) can be described with the SiO_xN_y stoichiometric model. The deviation from the stoichiometric composition at lower N_2O/SiH_4 gas flow ratio is due to the formation of silicon rich silicon oxynitride. An increase of silicon content in the layers is accompanied by an increase in the number of Si-H bonds. The excess of silicon and the hydrogen content are responsible for raising the optical losses in the layers at wavelengths of 632.8 and 1550 nm, respectively. Both silicon and hydrogen increase with decreasing N_2O/SiH_4 gas flow ratio. PECVD SiON layers have been deposited without Si-Si bond by adding NH_3 to the (N_2O + SiH_4/N_2) gas mixture. PECVD silicon oxynitride with lower hydrogen concentration and without Si-Si bonds can be obtained by using a LF RF generator. That means that LF RF plasma is suitable for deposition of high refractive index SiON layers.

4 Phosphorus-doped PECVD silicon oxynitride for optical waveguides

This chapter describes our results on the PECVD deposition process of low and high index P-doped SiON layers. We first focus on the composition and the chemical environment of phosphorus, silicon, oxygen, nitrogen, and hydrogen in these layers. These data were obtained by XPS, RBS and FTIR. Thereafter an analysis is given for the as-deposited as well as annealed layers with respect to the hydrogen content and optical losses.

Parts of this chapter are adopted from:
M.G. Hussein, K. Wörhoff, G. Sengo and A. Driessen, "*Reduction of hydrogen-induced optical losses of plasma-enhanced chemical vapor deposition silicon oxynitride by phosphorus doping and heat treatment*" Journal of Applied Physics, vol. 101, pp. 023517, 2007.
M.G. Hussein, K. Wörhoff, G. Sengo, A. Driessen, "*Deposition and characterization of PECVD phosphorus-doped silicon oxynitride layers for integrated optics*", Proceedings of EUROCVD-15, The Electrochemical Society, Bochum, Germany, Sept. 2005.
M.G. Hussein, K. Wörhoff,, G. Sengo, A. Driessen, "*Fabrication and characterization of PECVD phosphorus-doped silicon oxynitride layers for integrated optics application*", proceedings 9th Annual Symposium of the IEEE/LEOS Benelux Chapter, December 2-3 2004, Pp. 91-94, Ghent University, Ghent, Belgium, ISBN Number: 9076546061, Dec. 2004.

4.1 Deposition and characterization of low index P-doped SiON layers

4.1.1 Experimental procedure

Low index PECVD undoped and P-doped SiON layers were deposited on p-type <100> oriented 100 mm silicon wafers at a substrate temperature of 350 °C, a chamber pressure of 140 mTorr and RF power of 20 W (HF). Optimized undoped SiON layers (P-00) could be obtained by gas mixtures of 600 sccm of silane (2% SiH_4 diluted in N_2), 600 sccm of nitrous oxide (N_2O), and 25 sccm of ammonia (NH_3) see Section 3.2. Phosphorus doping was obtained by adding phosphine (5% PH_3 diluted in Ar) to the gas mixtures. Three types of phosphorus doped layers P-10, P-30, and P-60 were deposited by adding 10, 30, and 60 sccm of phosphine (5% PH_3 diluted in Ar) to the gas mixtures.

In order to determine the composition, density and optical properties of the layers, several depositions of P-00, P-10, P-30, and P-60 type layers were carried out. The layer thickness and the index of refraction have been determined by spectroscopic ellipsometry on approximately 250 nm thin layers directly deposited on silicon wafers. Relatively thick layers (~ 1200 nm) deposited directly on silicon were used for the density and the atomic concentrations measurements, whereas for the optical loss measurements sufficiently thick layers on thermally oxidized wafers were prepared.

The density (ρ [g/cm^3]) was determined by weighting the silicon wafer before and after deposition, while the film volume was deduced from the film thickness. The nature of the hydrogen bonds and the hydrogen concentration of the layers were determined with FTIR. The atomic concentrations of Si, O and N of the layers were determined by XPS and RBS. For optical loss measurements the thickness of the thermal oxide has been chosen sufficiently thick so that the silicon substrate does not influence the modes. The SiON layer was approximately 2.5 μm thick to ensure single mode propagation. The measurement was performed on the TE mode using the sliding prism method.

4.1.2 Characterization of as-deposited layers

In order to study the phosphorus-doping effect on the PECVD SiON layer properties, a series of PECVD P-doped SiON layers (P-10, P-30, and P-60) were deposited. The as-deposited layers were analyzed and showed a refractive index in-homogeneity of less than 0.002 and a thickness non-uniformity of 1% for the entire layers. Figure 4.1 shows the atomic concentration determined by XPS and RBS. Both techniques give identical concentrations within the experimental error.

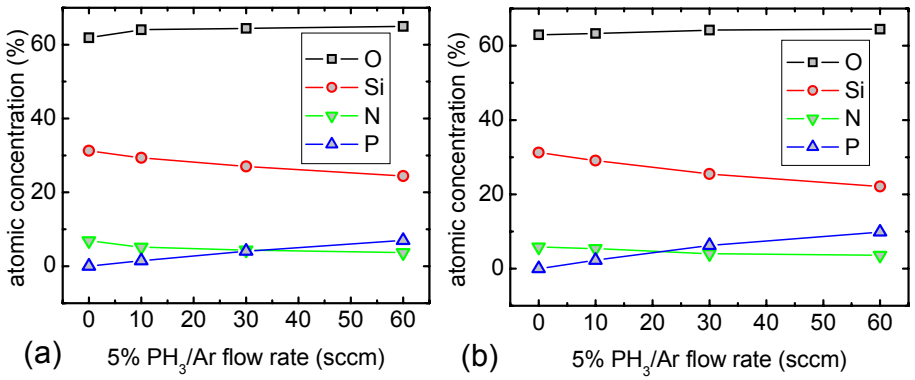

Figure 4.1 Atomic concentration of the studied layers as a function of the PH_3 (5% in Ar) flow ratio measured by: (a) XPS; (b) RBS

The atomic phosphorus concentration increases, as expected, with increasing PH_3/Ar gas flow rate. Figure 4.2 shows the refractive index obtained by spectroscopic ellipsometry and the density of the PECVD SiON layers with increasing P-doping.

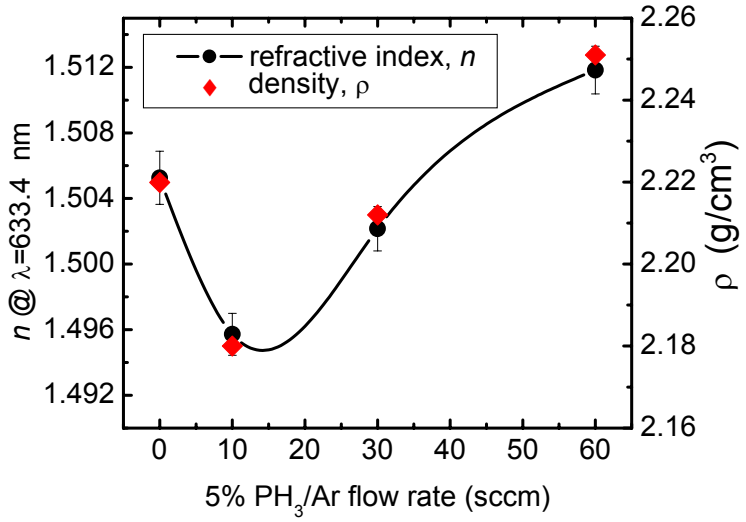

Figure 4.2 refractive index –●– and density ♦ of the studied layers as a function of the PH_3 (5% in Ar) flow ratio

The refractive index, however, increases only after an initial deep decrease. This decrease is unexpected as the index of refraction of phosphorus oxide, P_2O_5 is 1.51, substantially higher than of the SiO_2 (n = 1.457) and of the undoped SiON layer under study (n = 1.505). In order to examine the origin of this initial deep decrease, the densities of the layers were determined. The densities of the P-doped SiON layers was found to have the same trend as the refractive index indicating that the initially decreasing index of refraction is mostly caused by the reduced density of the slightly P-doped layers (Figure 4.2). The deposition rate was found to increase slightly with the P-doping as can be seen in Figure 4.3.

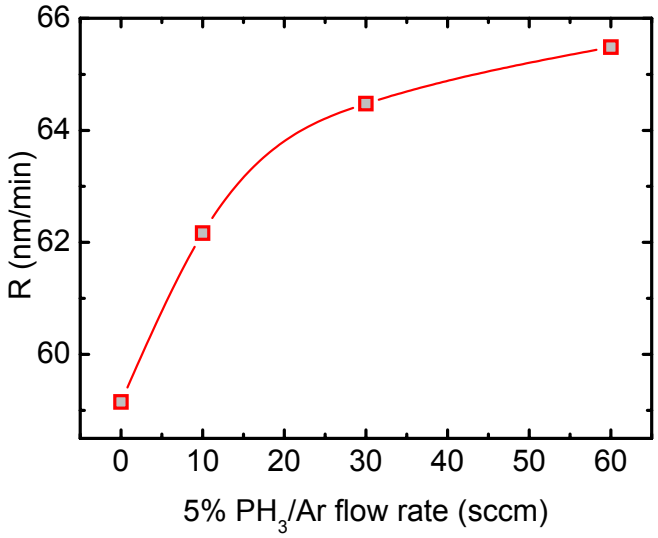

Figure 4.3 Deposition rate of the studied layers as a function of the PH_3 (5% in Ar) flow ratio

With the XPS and RBS analysis the atomic concentration of the heavier elements in the layers could be determined. For the hydrogen concentration and the bond energies FTIR spectroscopy has been used. Figure 4.4 shows FTIR spectra of the P-doped PECVD SiON layers (P-10, P-30, and P-60) in comparison with the undoped layer (P-00). For clarity the curves have been plotted with a vertical offset.

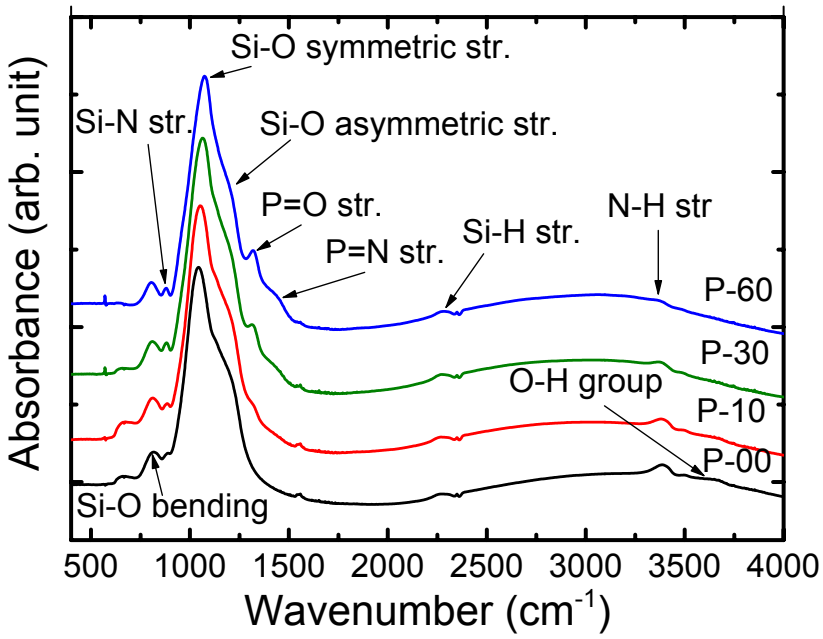

Figure 4.4 FTIR spectra ranging from 400 to 4000 cm^{-1} of the PECVD SiON layers under study with increasing P-doping

The dominant absorption feature in these spectra, a broad peak around 1050 cm^{-1} could be observed in all samples. This peak can be resolved into contributions by Si-O bending, Si-N (1) stretching, Si-N (2) stretching, Si-O symmetric stretching, P-O stretching, N-H bending, P-N stretching, Si-O asymmetric stretching, P=O stretching, and P=N stretching. For a quantitative analysis we used nonlinear curve fitting, assuming that the peaks have a symmetric Gaussian form. The deconvolution of the absorption spectra yields Gaussian peaks whose parameters are summarized in Table 4.1 (see also Figure 4.5). The infrared peak positions are in good agreement with previous studies on undoped SiON and P-doped silica layers [20, 34, 52, 75, 83-86].
Slight shifts were observed in all peaks position with increasing P doping (see Table 4.1). The peak position around 1050 cm^{-1} (the so called Si-O peak, Figure 4.4) is slightly shifting from 1042 to 1075 cm^{-1} with increasing P doping. It has been reported that with increasing oxygen content, the position of the Si-O peaks shifts to high energies [70]. This fact can be attributed to the increase in the electronegativity in the neighborhood of these bonds, since oxygen has higher electronegativity than nitrogen. Also in our case the XPS and the RBS analysis, Figure 4.1 (a) and (b) show a slight increase of the oxygen content with the PH_3 flow rate, this corresponds well with the energy shift.

Table 4.1 Energy of the infrared vibrational modes observed in undoped and P-doped PECVD silicon oxynitride layers.

	Peak frequency (cm^{-1})			
Vibration type	P-00	P-10	P-30	P-60
Si-O bending	817	815	813	808
Si-N (1) stretching	882	883	881	879
Si-N (2) stretching	938	939	948	953
Si-O symmetric str.	1035	1051	1052	1034
P-O stretching	-	-	1085	1090
N-H bending	1135	1130	1128	1130
P-N stretching	-	1155	1151	1152
Si-O asymmetric str.	1174	1203	1197	1191
P=O stretching	-	1315	1318	1319
P=N stretching	-	1386	1397	1407
Si-H(N2Si)	2261	2261	2255	2254
Si-H(N3)	2305	2297	2280	2281
P-H stretching	-	2312	2308	2309
N-H…N stretching	3368	3375	3343	3342
N-H stretching	3408	3411	3386	3382
H-O-H stretching	3497	3498	3489	3482
Si-OH…HOH	3604	3632	-	-
Si-OH (1)	3672	3677	-	-
Si-OH (2)	3749	3748	-	-

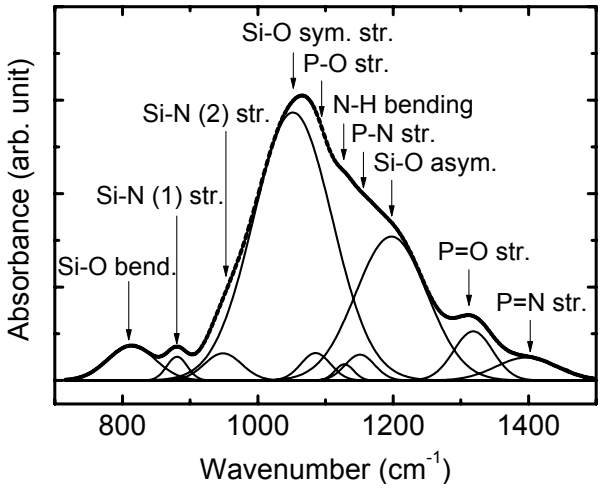

Figure 4.5 The broad IR absorption band between 700 and 1500 cm^{-1} for sample P-30. It is well fitted with 10 Gaussian-shaped absorption bands.

The analysis presented in Table 4.1 shows that no P-O bonds were observed in sample P-10. This provides evidence that nearly no phosphorus oxide, P_2O_5 and phosphate, PO_4 (+5 oxidation state, P with one P=O and three P-O single bonds) are formed in sample P-10 although an increase in oxygen has been observed by XPS with respect to P-00. Moreover, the fitting results show an initial increase and decrease in Si-O and Si-N band areas respectively Figure 4.7(a). It is well known for SiON that the nitrogen atomic concentration is related by the relation: $3[N] = [Si-N] + [N-H]$ (see Equation(3.9)). Based on this relation and the preferred formation of Si-N bonds in comparison to N-H bonds, we suggest the configuration in Figure 4.6(a) being the most probable nitrogen related bond configuration in the undoped SiON layers. This will not be the case when P is present in the reaction since P-N and P=N bonds are more favorable than N-Si and N-H bonds as the bond strength of P-N (617.1 kJ/mol) > Si-N (470.0 kJ/mol) > N-H (339.0 kJ/mol) [64, 87]. This indicates that the silicon and hydrogen bonds in Figure 4.6(a) will be replaced by phosphorus. As a consequence, the Si-O bonds can increasingly be formed at low P-doping as seen for sample P-10, Figure 4.7(a). Nevertheless, at higher P-doping, P-O and P=O are more favorable to be formed. We also suggest that the most probable nitrogen related bonds configuration in the P-doped SiON layers are those presented in Figure 4.6(a) and 4.6(b).

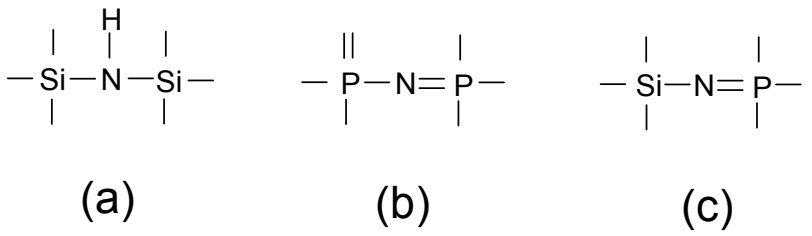

Figure 4.6 The most probable nitrogen related bonds configuration: (a) undoped SiON layers; (b and c) P-doped SiON layers.

The increase in Si-O bonds agrees with the observed refractive index and density behavior of the P-doped PECVD SiON layers when only a small amount of PH_3 is added. The increase in these parameters after adding more PH_3 can be attributed to the increase in the phosphorus content and the simultaneous decrease in silicon content and Si-O bond concentration in the layers as confirmed by the XPS and FTIR measurements. With the increased P content, P_2O_5 can be formed in the SiON matrix as can be seen by the significant increase in P-O bond concentration for sample P-60. The absorption around 1320 and 1400 cm^{-1} in the FTIR spectra can be assigned to the vibrational mode of the P=O and P=N peak respectively. As expected, this

absorption becomes more pronounced with increasing PH_3 flow rate [see Figure 4.4 and 4.7(b)].

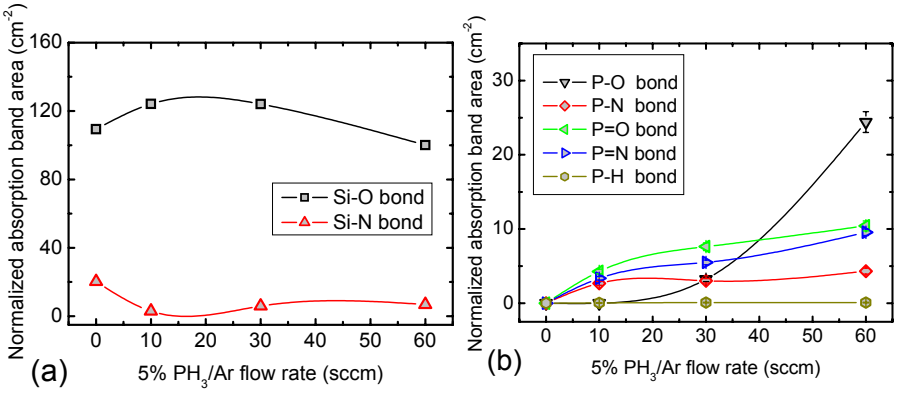

Figure 4.7 Variation of the normalized absorption band area for PECVD SiON layers with increasing PH_3 flow rate: (a) silicon related bonds; (b) phosphorus related bonds.

Another important feature that can be observed in all samples is the absorption due to N-H and Si-H stretching modes in the region 3300 – 3450 cm^{-1} and 2150 – 2300 cm^{-1} respectively. These modes influence largely the performance of devices for applications in optical telecommunication [21, 34, 72, 88], since their overtones contribute to the optical loss at the third telecommunication window around 1550 nm. Therefore, the amount of N-H and Si-H bonds in the layers has been estimated by applying the N-H and Si-H absorption cross-sections as given by Lanford and Rand [54], see Figure 4.8(a).

A significant reduction in N-H bonds concentration was observed for increasing P-doping [Figure 4.8(a)]. This corresponds well with the loss measurements obtained from undoped and P-doped SiON layers [Figure 4.8(b)]. The peak loss at 1505 nm wavelength is reduced from 14.1 dB/cm for undoped samples to 3.5 dB/cm as the 5%PH_3/Ar flow rate increased from 0 to 60 sccm, respectively. Moreover, the optical losses around λ=1400 and 1550 nm were found to decrease from 4.7 to 0.2 dB/cm and from 1.8 to 0.7 dB/cm respectively. This makes P-doped SiON a very promising waveguide material for applications in low-loss integrated optical devices. As mentioned before, the bond strength of P-N > Si-N > N-H and consequently P-N and P=N bonds are more likely be formed instead of N-H bonds. Hence the H atom bonded to nitrogen in the undoped layer will be replaced by a P atom when phosphine is added to the process, as can be clearly seen in Figure 4.4 and 4.8(a).

The simultaneous decrease in the optical loss around λ=1400 nm can be attributed to the elimination of OH related group, since the P-O bonds (599.1 kJ/mol) are energetically more favorable than O-H bonds (427.6 kJ/mol).

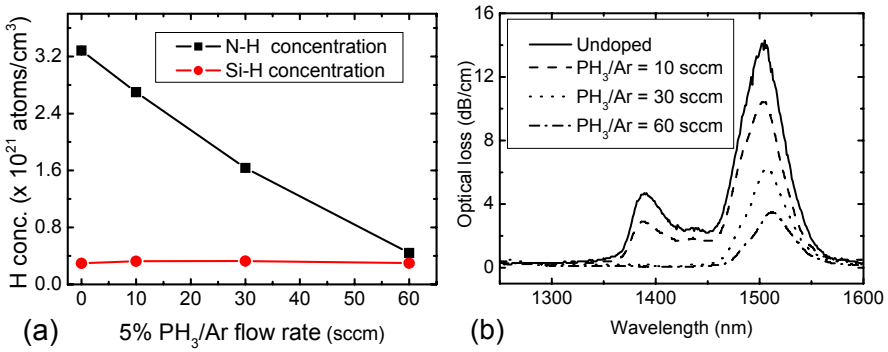

Figure 4.8 The hydrogen bonds concentration and the optical loss of the as-deposited P-doped SiON layers as function of the 5% PH3/Ar flow rate: (a) N-H and Si-H bonds concentration; (b) optical loss as a function of wavelength.

4.1.3 Stability of P-doped SiON layers

As-deposited PECVD P-doped (PSG) and BP-doped SiO_2 (BPSG) are known to have a stability problem with respect to moisture absorption [85]. For P-doped SiON layers, this may result in a refractive index change as a function of time when the layers are exposed to clean-room laboratory air. A comparison was made between the refractive index measured immediately after deposition and some days later. A slight change in refractive indices was observed for sample P-60. For additional stability investigations, P-doped layers (~ 250 nm) with a different refractive index were deposited by adding 50 sccm of 5%PH_3/Ar gas flow rate to the optimized recipes (see Table 4.2).

Table 4.2 Gas flow rates , refractive index for P- doped silicon oxynitride layers and the reduction of N-H bonds concentration of the undoped layers as compared with the P-doped SiON layers.

Sample No.	Gas flow rates (sccm)				*n* @ λ=633. 4 nm	N-H bond conc. (× 10^{21} atoms/cm^3)	
	2%SiH_4 /N_2	N_2O	NH_3	5%PH_3 /Ar		Undoped	P-doped
1	600	600	0	50	1.4906	1.78	0.00
2	600	480	0	50	1.4925	1.91	0.00
3	600	600	25	50	1.5069	3.77	0.98
4	600	360	50	50	1.5492	8.43	2.61

Also, comparisons have been made between refractive indices measured immediately after deposition and when the layers (sample 1, 2, 3 and 4) are exposed to the clean-room laboratory air. Figure 4.9 shows refractive index changes with time for these layers.

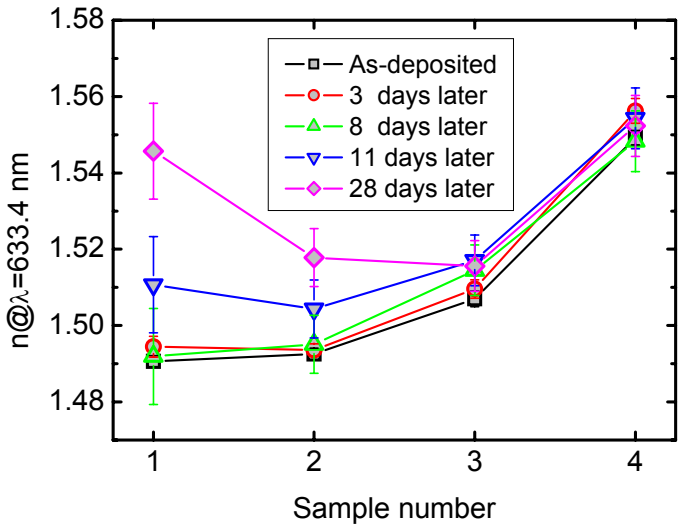

Figure 4.9 Refractive index of different P-doped SiON layers (sample 1, 2, 3 and 4) as a function of time, measured with a spectroscopic ellipsometer.

A large variation in the refractive index was observed in the lower refractive indices layers, as can be clearly seen in Figure 4.9.

The instability of the layers can be attributed to the well-known phenomena of moisture absorption in PSG and BPSG layers [85, 89], which is usually described by the reactions of phosphorus oxides with water molecules:

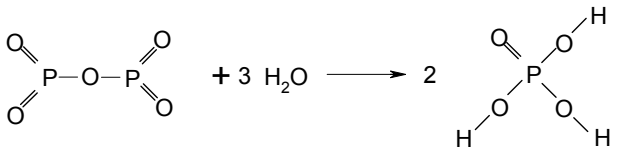

(4.1)

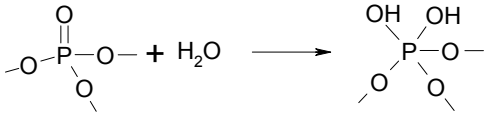

(4.2)

In order to confirm the relevance of the reaction Eqs. (4.1) and (4.2) for our sample we analyzed the unstable layers by FTIR and found indeed a significant increase in P-O bond concentration (see Figure 4.10).

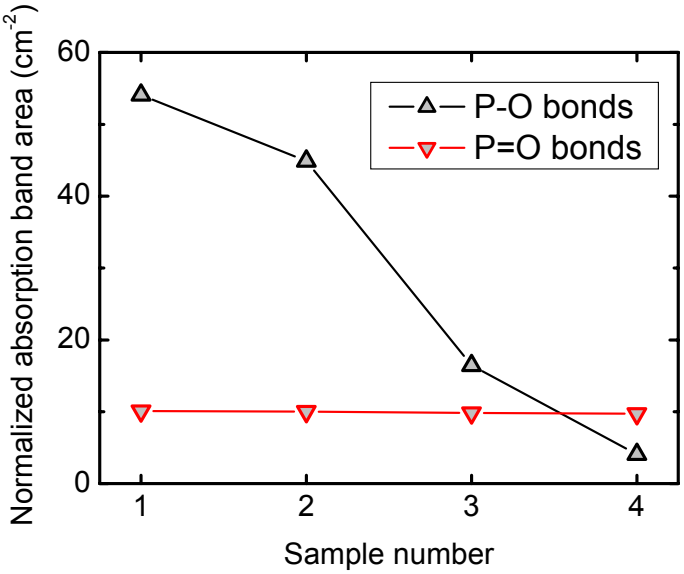

Figure 4.10 Variation of the normalized Phosphorus-oxygen absorption band area for PECVD P-doped SiON layers with increasing refractive index.

This increase in P-O bonds can be taken as evidence for the existence of phosphorus oxides in the highly P-doped low refractive index SiON layers, which was also the case for layer P-60. After long exposition to air (4 months storage time in the clean-room) surface defects were observed on samples 1 and P-60, see optical microscope image, Figure 4.11. This might be an evidence of phosphoric acid on the layer as a result of the reaction of Eq. (4.1).

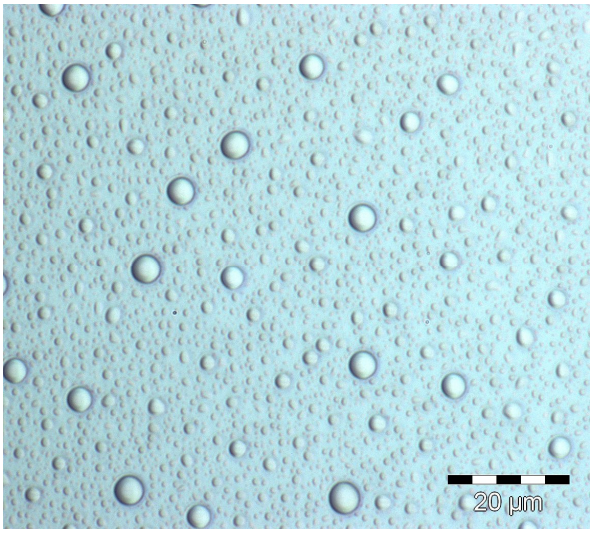

Figure 4.11 Optical microscope image of the surface of sample 1 after 4 months storage time in a clean-room.

Low index PECVD P-doped SiON layers can be deposited without the presence of N-H bonds (see Table 4.2), the stability; however, also in this case stability issues have to be taken into account. It appears that low index P-doped SiON layers with phosphorus concentrations only up to 5.6 at% (~ 20 of 5% PH_3/Ar sccm gas flow rate) were found to be stable.

4.1.4 Effect of post-deposition annealing

In order to study the effects of heat treatment to the hydrogen content and optical losses in P-doped SiON layers, the layers (P-00, P-10, P-30, and P-60) were annealed at four different temperatures of 600, 800, 900, and 1000 °C for 3 hours in a nitrogen atmosphere. A typical example of the FTIR spectrum of as-deposited and annealed undoped (P-00) and P-doped (P-30) SiON layers is shown in Figure 4.12. It appears that the N-H peak is eliminated after annealing at 1000 °C for the doped sample, while for the undoped sample most of the N-H bonds still remain. On the other hand, Si-H bonds have been

eliminated from all samples after annealing at 900 °C. This effect can be attributed to the cross-linking between N-H and Si-H according to Si-H + N-H $\rightarrow$ Si-N + H_2 [31].

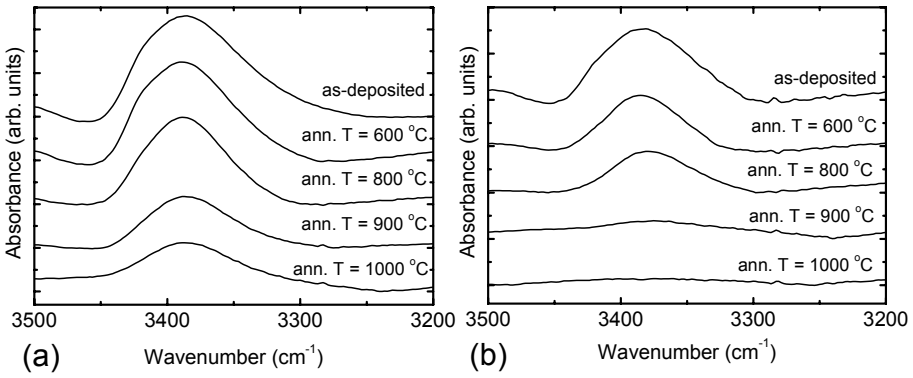

Figure 4.12 Infrared absorption spectra of the N-H region for several annealing temperatures: (a) undoped SiON layer, sample P-00; (b) P-doped SiON layer, sample P-30. Temperatures have been indicated in the figure (For clarity the curves have been plotted with a vertical offset).

The analysis of the FTIR absorption data results in an estimate for the amount of N-H and Si-H bonds of the various as-deposited and annealed layers as is shown in Figure 4.13.

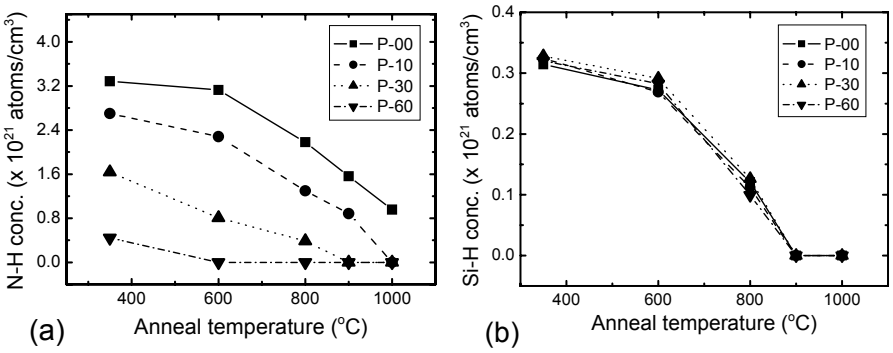

Figure 4.13 The hydrogen bond concentrations of the P-doped SiON layers (P-00 to P-30) as a function of anneal temperature: (a) N-H bond concentration; (b) Si-H bonds concentration.

It can be observed from Figure 4.13, that the bonded hydrogen in all P-doped layers has been eliminated after annealing at 1000 °C, while undoped SiON layers require annealing at 1150 °C [19]. Further, N-H bonds have been removed completely at 600 °C annealing temperature from layer P-60 that contains the highest phosphorus concentration. The annealing temperature that required removing N-H is increasing when the phosphorus concentration decreases. This indicates that the elimination of the N-H bonds at lower annealing temperature is associated with the incorporation of phosphorus in the SiON matrix. It has been reported [85, 90], that the most common bonding orientations for P in BPSG layers are PO_4 with one P=O and three P-O single bonds, and P_2O_5 which could be the case in our layer when more phosphine is added to the process [see Figure 4.7(b)]. It is well known that phosphorus oxides have weaker average bond strengths than silicon oxides resulting, for example, in a boiling point for P_2O_5 as low as 605 °C [64]. Incorporation of phosphorus oxide in the SiON matrix will weaken the nearest neighbors bonds. This might explain the elimination of the N-H bonds at lower temperature for the P-doped SiON in comparison with the undoped layers. This corresponds also well with the optical loss measurements of the annealed undoped and P-doped SiON layers (see Figure 4.14). It can be clearly seen that the optical loss is reduced to below 0.2 dB/cm after annealing at 1000 °C for the doped sample, while in the undoped sample the absorption peak around 1500 nm still remains.

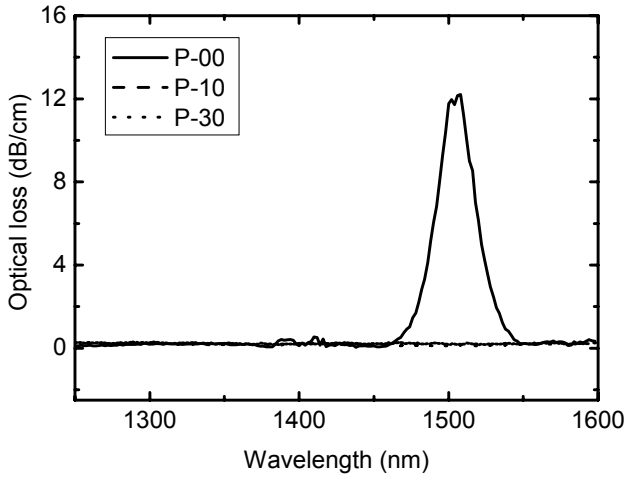

Figure 4.14 Optical loss as a function of wavelength for undoped and P-doped SiON layers annealed at 1000 °C for 3 hours in N_2 atmosphere.

The refractive index and the relative thickness change have also been measured as function of the annealing temperature as shown in Figure 4.15.

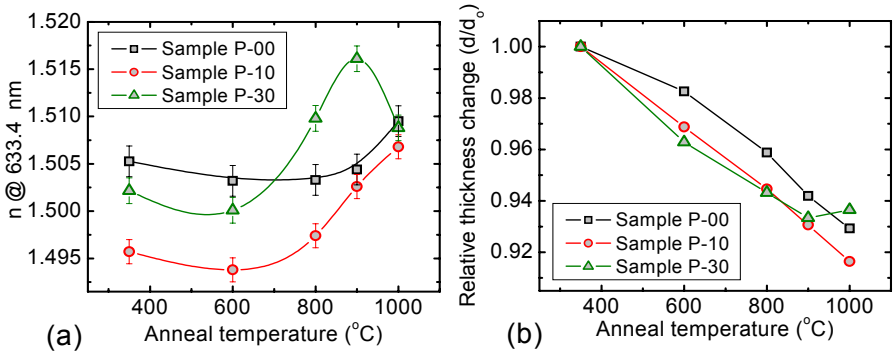

Figure 4.15 Measurements on layers P-00, P-10 and P-30 as a function of the anneal temperature: (a) refractive index; (b) relative thickness change.

From these results three steps in the annealing process can be clearly distinguished for P-doped PECVD SiON: First, at a temperature of 600 °C the hydrogen bonds are broken and reaction products are diffusing out of the layer. From the decrease of the refractive index with simultaneously shrinking of the layer it might be concluded that not only hydrogen is removed, but also other species such as gaseous NH [91]. This is also confirmed by XPS measurements that show a decrease in nitrogen atomic concentration. Second, at temperatures above 600 °C and below 900 °C the material is sintered, which can be explained by the combination of increasing refractive index and shrinkage of the layer. Third, in case of sample P-30, the renewed decrease in the refractive index again at annealing temperature above 900 °C and the increase in layer thickness can be explained by the formation of voids and bubbles in the layer, see scanning electron microscope (SEM) picture Figure 4.16.

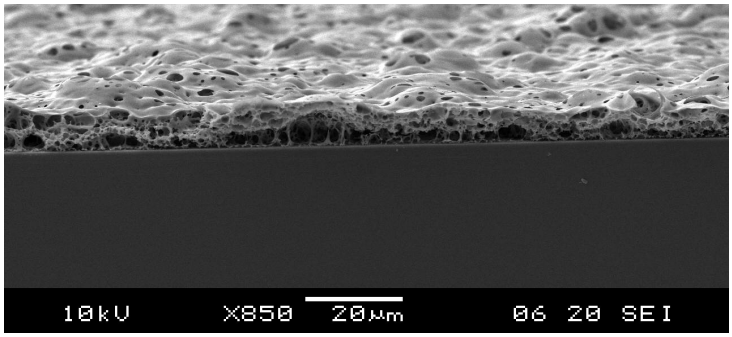

Figure 4.16 SEM image of a P-doped PECVD SiON layer containing 8.6 at% P annealed at 1100 °C for 4 hours in N_2 atmosphere.

The reflowing properties of phosphorus-doped silica (in which P is bonded to oxygen) have been investigated by Mayumi [92] and Feuchter [40]. Feuchter obtained significant reflow for layers containing ~ 5 at% P by heat treatment at 1100 °C for 12 hours.

For phosphorus-doped SiON where nitrogen and hydrogen are present, the influence of phosphorus doping on reflow properties has been investigated by depositing various phosphorus-doped layers on ridges etched in silicon, see Figure 1.6. In Figure 4.17 a cross-section of such a structure is shown before and after annealing for 24 hours at 1100 °C in N_2 atmosphere for 4 µm of P-doped SiON ($n \approx 1.5$) containing 5 at% P.

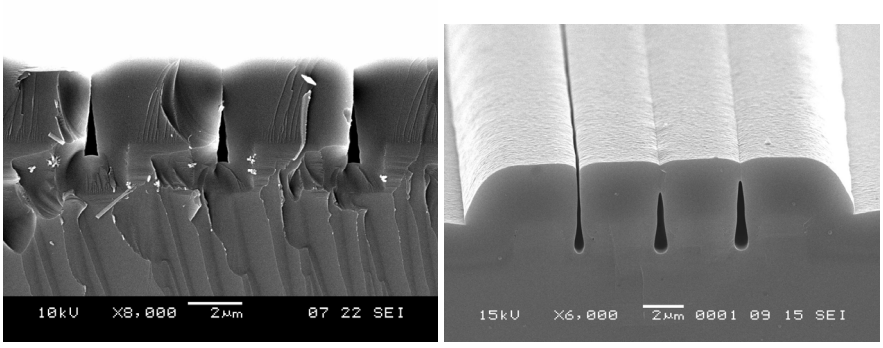

(a) (b)

Figure 4.17 Cross-section of Si-ridges covered with 4 µm of P-doped SiON (n ≈ 1.5) containing 5.6 at% P: (a) before and (b) after heat treatments at 1100 °C in N_2 atmosphere for 24 hours.

As it can be seen from Figure 4.17(b), reflowing of P-doped SiON ($n \approx 1.5$) containing 5.0 at% phosphorus is not enough to fill completely the gaps between two closely spaced steps, but is sufficient to smooth the surface of the P-doped SiON. In order to examine in detail the surface smoothening we performed Atomic Force Microscope (AFM) topographical surface scans on an as-deposited and annealed P-doped SiON layers (~ 5.0 at% P). Fig. 4.17 shows the large decrease in surface roughness as a function of annealing time.

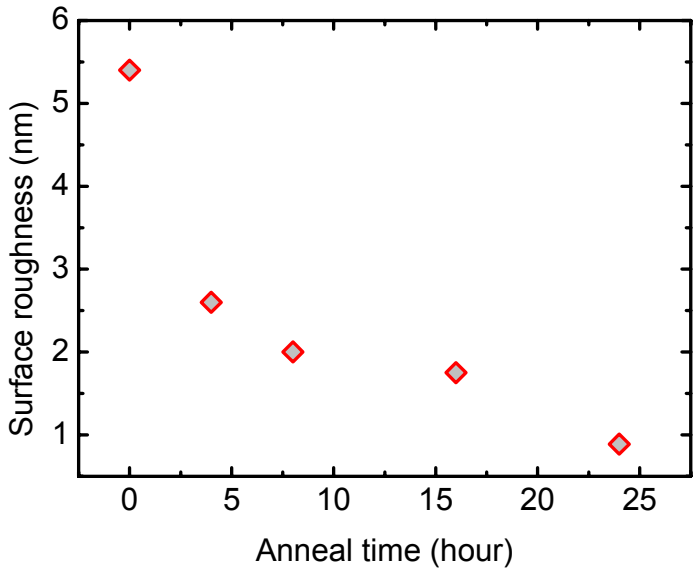

Figure 4.18 Surface roughness of the P-doped SiON layer (5.6 at% P) as a function of the annealing time at 1100 °C measured by AFM

The reflow temperature can be reduced by increasing the phosphorus concentration in the layers. However, as has been explained before, for high phosphorus concentrations the layers become hygroscopic, see section. Moreover, voids and bubbles are formed upon annealing of these layers (see Figure 4.19).

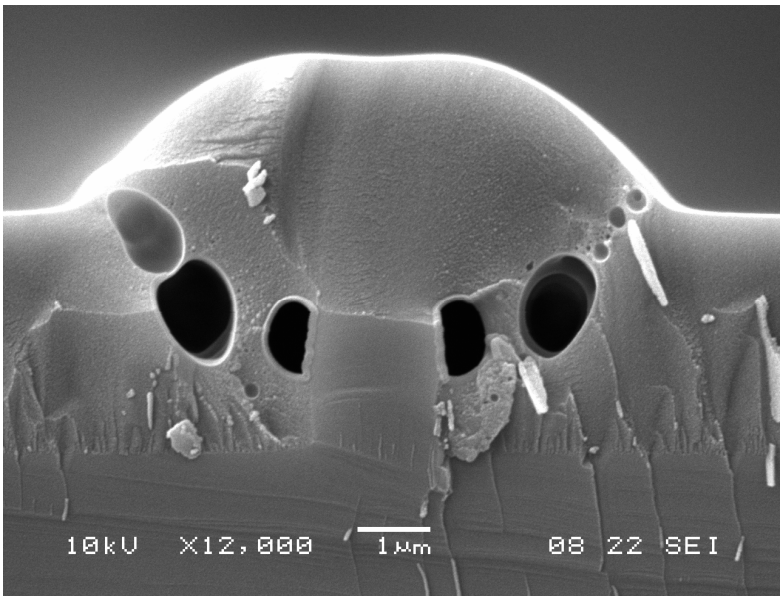

Figure 4.19 Micrograph of voids formation in P-doped SiON (n ≈ 1.49) containing 8.0 at% P annealed at 1100 °C in N_2 atmosphere for 7 hours

The voids formation seems to be correlated to the phosphorus concentration. For P-doped SiON layers containing less than 5.0 at% phosphorus no such effects have been noticed. Such layers will be used for further co-doping with boron, which will be described in chapter 5.

4.2 Deposition of high index P-doped SiON layers

PECVD undoped and P-doped SiON layers with a refractive index ~ 1.60 were deposited on p-type <100> oriented 100 mm silicon wafers at a substrate temperature of 300 °C, a chamber pressure of 86.6 Pa and RF power of 60 W (LF). Optimized undoped SiON layers (P2-00) could be obtained by gas mixtures of 600 sccm of silane (2% SiH_4 diluted in N_2) and 180 sccm of N_2O. Phosphorus doping was obtained by adding phosphine (5% PH_3 diluted in Ar) to the gas mixtures. In total 5 compositions of phosphorus- doped layers P2-20, P2-40, P2-60, P2-80 and P2-100 were deposited by adding 20, 40, 60, 80 and 100 sccm, respectively, of phosphine (5% PH_3 diluted in Ar) to the gas mixtures.

4.2.1 Characterization of as-deposited layers

After deposition, the as-deposited layers were analyzed and showed a refractive index in-homogeneity of less than 0.002 and a thickness non-uniformity of 1% over 50×50 mm² and less than 3% over 70×70 mm² area for the entire layers. Figure 4.20 shows the atomic concentration determined by XPS.

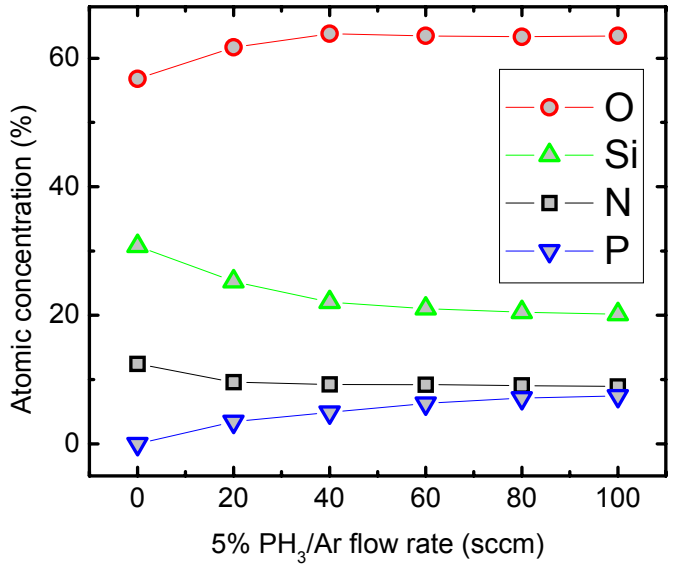

Figure 4.20 Atomic concentration of the studied layers (P2-00 to P2-100) as a function of the PH_3 (5% in Ar) flow ratio measured by XPS

The atomic phosphorus concentration increases, as expected, with increasing PH_3/Ar gas flow rate. Figure 4.21 shows the refractive index obtained by spectroscopic ellipsometry of the PECVD SiON layers with increasing P-doping. The refractive index increases with P-doping (phosphorus concentration) as expected.

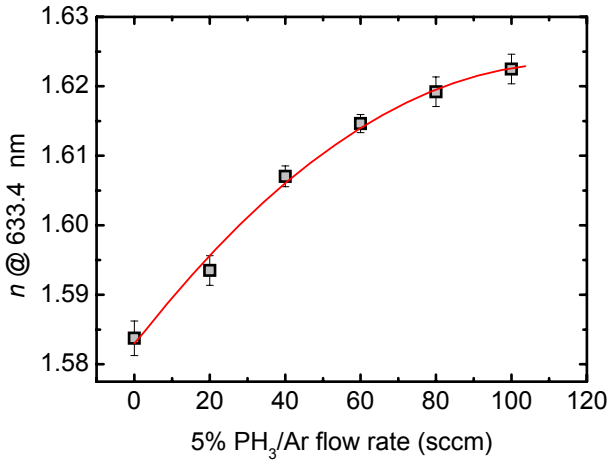

Figure 4.21 Refractive index of the studied layers (P2-00 to P2-100) as a function of the PH_3 (5% in Ar) flow ratio.

With the XPS analysis the atomic concentration of the heavier elements in the layers could be determined. For the hydrogen concentration and the bond energies FTIR spectroscopy has been used. Figure 4.22 shows FTIR spectra of the P-doped PECVD SiON layers (P2-20, P2-40, P2-60, P2-80 and P2-100) in comparison with the undoped layer (P2-00). For clarity the curves have been plotted with a vertical offset.

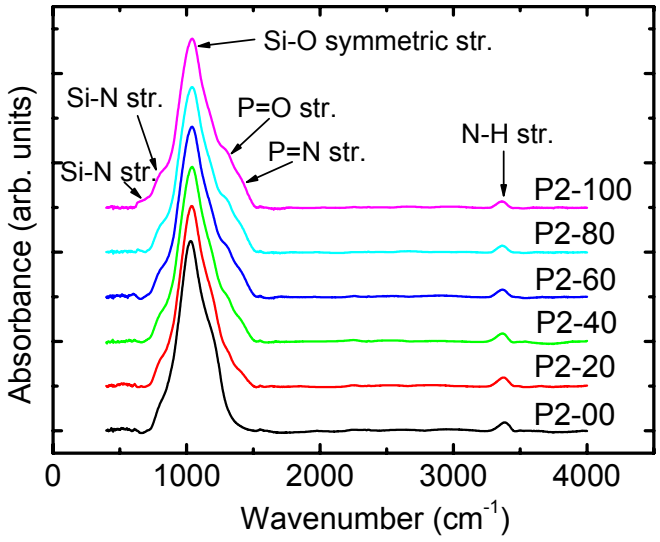

Figure 4.22 FTIR spectra ranging from 400 to 4000 cm^{-1} of the PECVD SiON layers under study with increasing P-doping.

The dominant absorption feature in these spectra, a broad peak around 1050 cm^{-1} could be observed in all samples. This peak can be resolved into contributions by Si-O bending, Si-N (1) stretching, Si-N (2) stretching, Si-O symmetric stretching, P-O stretching, P-N stretching, Si-O asymmetric stretching, P=O stretching, and P=N stretching. For a quantitative analysis we used nonlinear curve fitting, assuming that the peaks have a symmetric Gaussian form. The deconvolution of the absorption spectra yields Gaussian peaks whose parameters are summarized in Table 4.3. The infrared peak positions are in good agreement with previous studies on undoped SiON and P-doped silica layers [20, 34, 52, 75, 83-86].

Table 4.3 Energy of the infrared vibrational modes observed in undoped and P-doped PECVD silicon oxynitride layers.

	Peak frequency (cm^{-1})					
Vibration type	P2-00	P2-20	P2-40	P2-60	P2-80	P2-100
Si-O bending	802	796	793	791	789	787
Si-N (1) str.	864	880	871	860	850	841
Si-N (2) str.	955	947	945	947	946	946
Si-O sym. str.	1034	1027	1008	1004	1009	1016
P-O stretching	-	1067	1074	1079	10769	1072
P-N stretching	-	1143	1138	1136	11359	1135
Si-O asym. str.	1146	1206	1195	1177	1172	1170
P=O stretching	-	1291	1287	1290	1291	1291
P=N stretching	-	1409	1414	1416	1416	1417
N-H…N str.	3359	3344	3340	3335	3334	3329
N-H stretching	3400	3385	3380	3378	3377	3374

Another important feature that can be observed in all samples is the absorption due to N-H stretching modes in the region 3250 – 3450 cm^{-1}, whereas the Si-H bonds are below the FTIR detection limit in the studied samples. As it has been mentioned in the previous section, the N-H modes influence largely the performance of devices for applications in optical telecommunication. Therefore, the amount of N-H bonds in the layers has been estimated.

Figure 4.23 shows the infrared absorption spectra of the N-H region for the various as-deposited layers and the corresponding N-H bonds concentration with increasing P-doping.

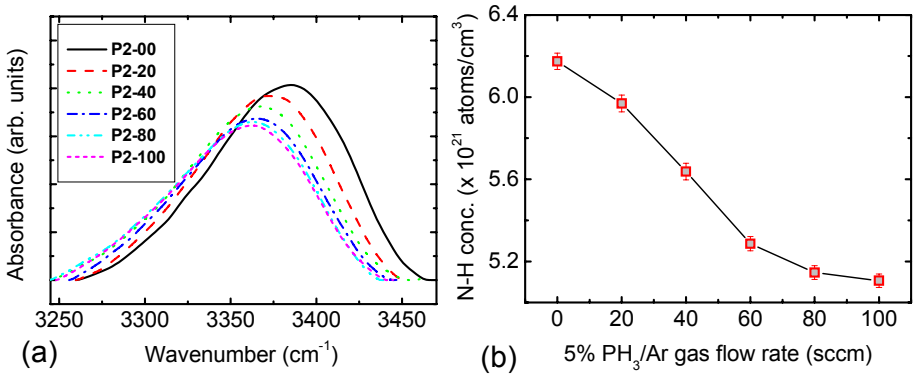

Figure 4.23 Reduction of N-H bonds in P-doped SiON layers (P2-00 to P2-100) (a) infrared absorption spectra; (b) bonds concentration with increasing P-doping.

A significant reduction in N-H bonds concentration was observed for increased P-doping (see
Figure 4.23) and an N-H peak shifts from 3386 to 3361 cm^{-1}. The N-H bands are observed to consist of an asymmetric peak with a tail extending on the low wavenumber side. This asymmetry has been attributed to hydrogen bonding (H atoms in N-H) and lone-pair electrons on nearby N atoms, which is indicated by the notation N-H···N [93].

Sample P2-40 was found to be stable and not sensitive to air, this layer has been taken for further investigation.

4.2.2 Effect of post-deposition annealing

In order to study the effects of heat treatment on the hydrogen content and optical losses in high index P-doped SiON layer (P2-40), layers similar to P2-00 and P2-40 (thickness ≈ 2 μm) were deposited and annealed at four different temperatures of 600, 800, 1000 and 1100 °C for 3 hours in a nitrogen atmosphere. The N-H peak is eliminated after annealing at 1000 °C for the doped samples, while for the undoped samples most of the N-H bonds still remain (Figure 4.24).

The P-doped SiON layers were intact after annealing at all temperatures, whereas at 1100°C annealing temperature cracks occurred in the undoped sample.

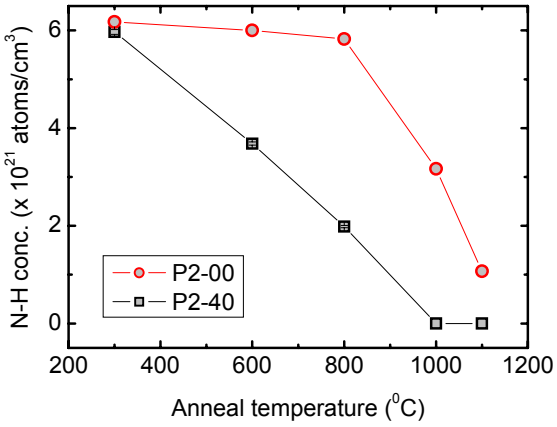

Figure 4.24 N-H bonds concentration of the undoped (P2-00) and P-doped (P2-40) SiON layers as a function of anneal temperature.

The elimination of the hydrogen at 1000°C corresponds well with the loss measurements obtained from as-deposited and annealed P-doped SiON layers (see Figure 4.25). It can clearly be seen that the optical loss is reduced to below 0.2 dB/cm after annealing at 1000°C for 3 hours in N_2 atmosphere.

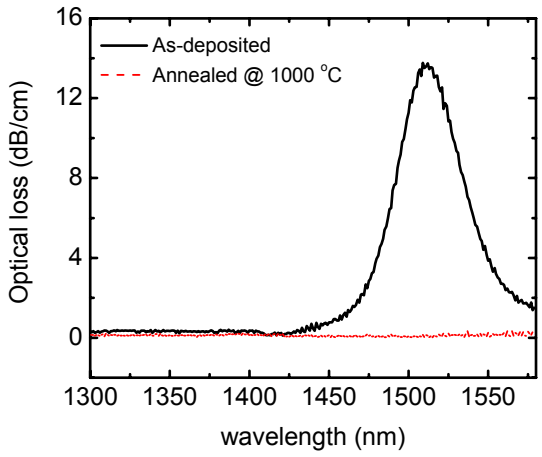

Figure 4.25 Optical loss as a function of wavelength for as-deposited and annealed P-doped SiON layer (sample P2-40)

The refractive index of as-deposited and annealed P-doped SiON layers (P2-40) was measured by the prism coupling technique at wavelengths of 632.8, 830, 1300 and 1550 nm. The results were used to fit the Cauchy coefficients, Eq. (2.9) in order to obtain the refractive index dispersion, see Figure 4.26.

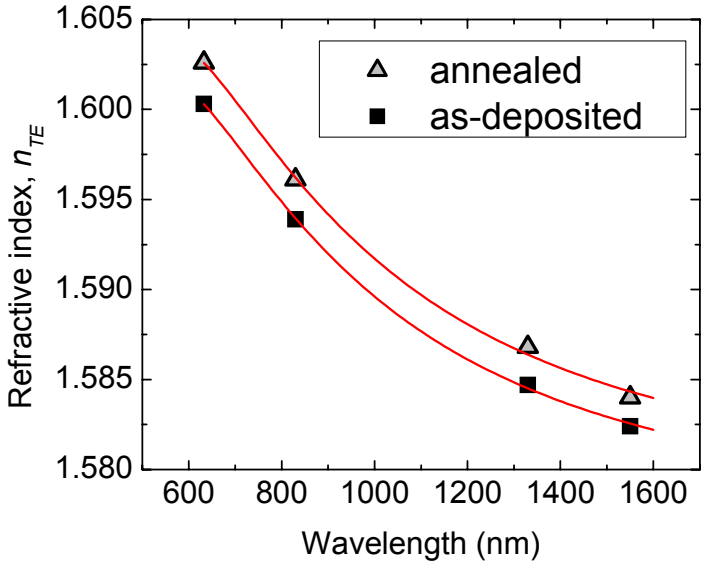

Figure 4.26 Refractive index as a function of wavelength for as-deposited and annealed P-doped SiON layer (sample P2-40)

An increase in refractive index of 0.023 and shrinkage of the layer thickness of 9.2% after annealing were observed for the studied layer. From the refractive index values for TE and TM polarized light, the materials birefringence $(\Delta n_{TM-TE} = n_{TM} - n_{TE})$ was found to be 15×10^{-4} for the as-deposited sample and 4.0×10^{-4} for the annealed (1000°C) sample. The materials birefringence is known to be caused by the mechanical stress in the layers. This stress can be determined by measuring the radius of curvature of the wafer before and after deposition and after annealing for the annealed layers. The stress as a function of annealing temperature for sample P2-40 is shown in Figure 4.27. The stress in the as deposited layer is ~ -140 MPa, a compressive stress which is plotted at the anneal temperature of 300°C (the deposition temperature). The stress becomes tensile upon annealing at 600°C, and then decreases with increasing annealing temperature. The stress reaches a value close to zero at an anneal temperature of 1000°C. This decrease in the stress has been attributed to the relaxation of the material [94] at this anneal temperature. The decrease in the

birefringence for the annealed layer can probably be related to the decrease in stress.

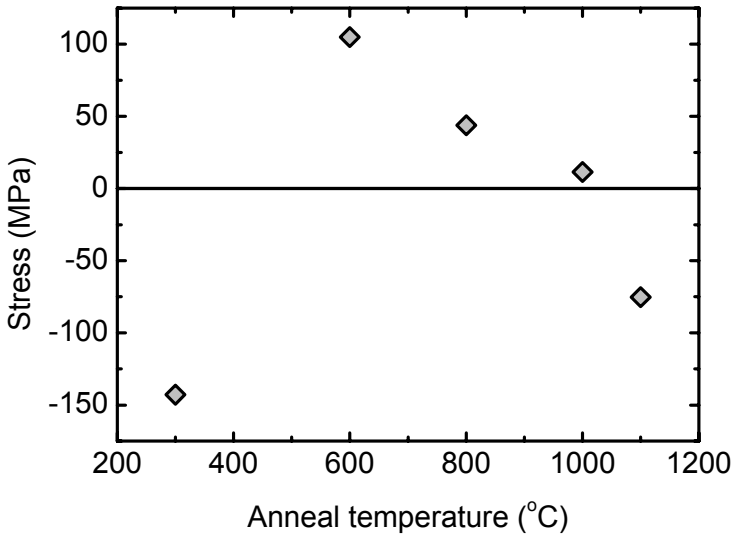

Figure 4.27 Mechanical stress as a function of anneal temperature for sample P2-40 (as-deposited stress is plotted at 300°C)

Also low loss (< 0.2 dB/cm) P-doped layers with a refractive index up to 1.73 were obtained without cracks after annealing at 1000°C for layer thickness up to 1 μm.

PECVD undoped and P-doped SiON layers with a refractive index ~ 1.73 were deposited on p-type <100> oriented 100 mm silicon wafers at a substrate temperature of 300 °C, a chamber pressure of 86.6 Pa and RF power of 60 W (LF). Optimized undoped SiON layers (P3-00) could be obtained by gas mixtures of 1000 sccm of silane (2% SiH_4 diluted in N_2) and 125 sccm of N_2O. Phosphorus doping was obtained by adding phosphine (5% PH_3 diluted in Ar) to the gas mixtures. In total 5 compositions of phosphorus- doped layers P3-20, P3-40, P3-60, P3-80 and P3-100 were deposited by adding 20, 40, 60, 80 and 100 sccm, respectively, of phosphine (5% PH_3 diluted in Ar) to the gas mixtures. Figure 4.28 shows the refractive index obtained by spectroscopic ellipsometry of the PECVD SiON layers with increasing P-doping. The refractive index increases with P-doping.

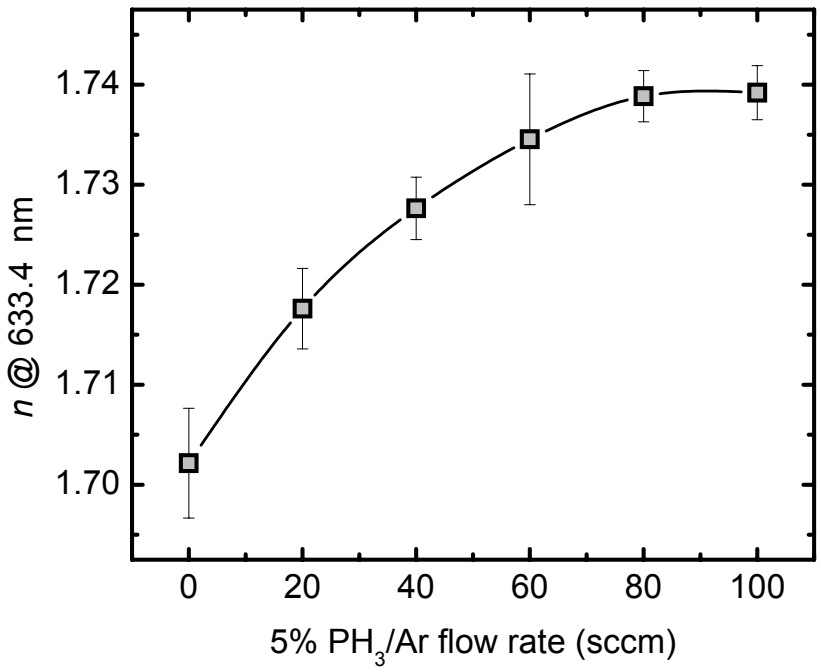

Figure 4.28 Refractive index of the studied layers (P3-00 to P3-100) as a function of the PH_3 (5% in Ar) flow ratio.

In order to study the effect of heat treatment on the hydrogen content and optical losses in P-doped SiON with a refractive index around 1.73, layers with the same composition as P3-20, P3-40, P3-60, and P3-100 were deposited and annealed at 1000 °C for 3 hours in a nitrogen atmosphere. The FTIR spectra show no N-H and Si-H peaks after annealing at 1000 °C for P-doped samples P3-40, P60, and P3-100, while N-H bonds still remain for the undoped sample and P3-20 sample (see Figure 4.29).

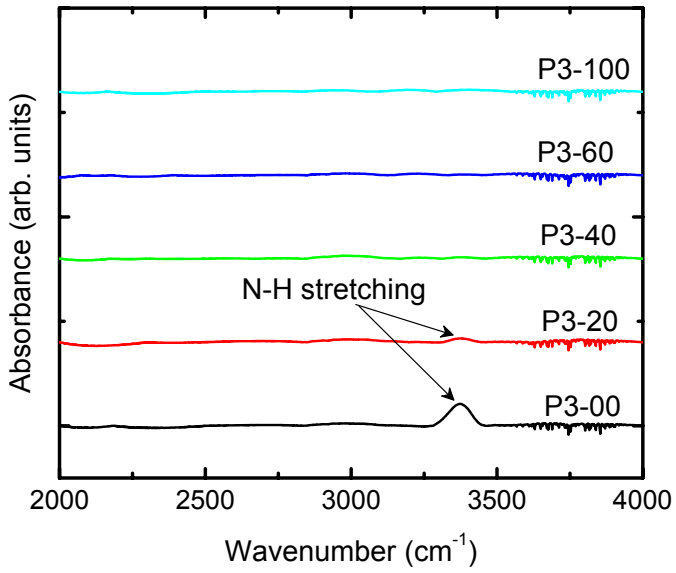

Figure 4.29 FTIR spectra ranging from 2000 to 4000 cm^{-1} of the annealed P-doped SiON layers (P3-00, P3-20, P3-40, P3-60 and P3-100). The layers were annealed at 1000 °C in N_2 atmosphere for 3 hours.

Figure 4.30 present the total hydrogen concentration in the layers before and after heat treatment.

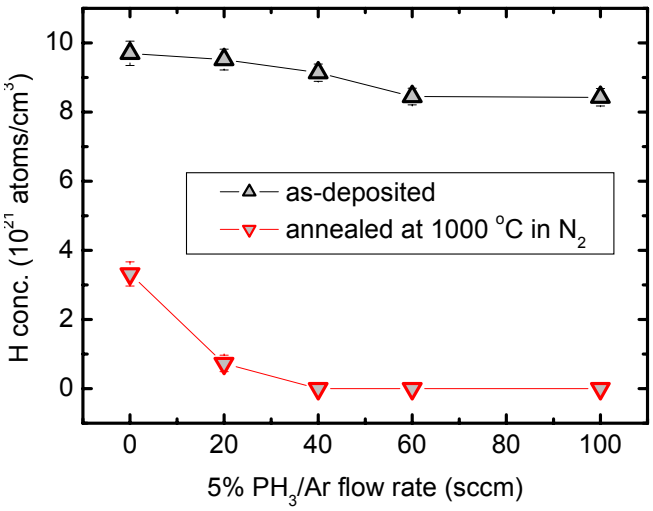

Figure 4.30 Total hydrogen concentration of the as-deposited and annealed P-doped SiON layers (P3-00, P3-20, P3-40, P3-60 and P3-100). The layers were annealed at 1000 °C in N_2 atmosphere for 3 hours.

The elimination of the hydrogen at 1000 °C corresponds well with the loss measurements obtained from as-deposited and annealed P-doped SiON layer sample P3-40 (see Figure 4.31). It can clearly be seen that the optical loss is reduced to below 0.2 dB/cm after annealing at 1000 °C for 3 hours in N_2 atmosphere.

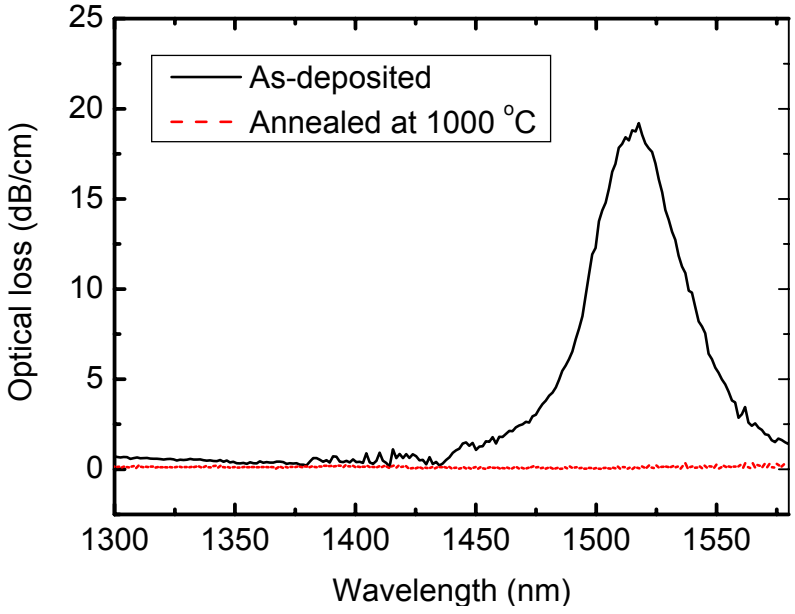

Figure 4.31 Optical loss as a function of wavelength for as-deposited and annealed P-doped SiON layer (sample P3-40)

4.3 Summary and conclusions

Phosphorus-doped silicon oxynitride layers for integrated optics applications have been deposited from 2%SiH_4/N_2 + N_2O + 5% PH_3/Ar and 2%SiH_4/N_2 + NH_3 + N_2O + 5% PH_3/Ar.

The phosphorus concentration was found to increase steadily with the phosphine flow rate. Special attention has been given to the presence of hydrogen bonds that lead to unwanted optical absorption in telecommunication applications. A significant reduction in N-H and O-H bonds concentration was observed for the P-doped SiON layers, when compared to undoped samples. Thus, a significant reduction in the optical loss of slab-type waveguides at λ=1505 nm was obtained for the P-doped SiON

layers, when compared to undoped samples. Moreover, the optical loss below λ=1400 nm was reduced to below 0.2 dB/cm.

The annealing experiments show that the H bonds in the P-doped layers can completely be eliminated by annealing at 1000 °C. In that case, the optical losses in the entire range from 1300 to 1600 nm (including the third telecommunication window) are reduced to below 0.2 dB/cm for slab-type P-doped SiON waveguides with refractive indices up to 1.73. It therefore can be concluded that this material is well suited for applications in telecommunication devices. Moreover, the influence of phosphorus doping on the reflowing properties has been investigated. The reflowing temperature was found to decrease with increasing the phosphorus concentration in the layer.

5 Boron-phosphorus doped PECVD silicon oxynitride

This chapter describes our results on the PECVD deposition and reflowing of SiON doped with boron and phosphorus. We first focus on the composition and the chemical environment of boron, phosphorus, silicon, oxygen, nitrogen, and hydrogen in these layers. These data were obtained by XPS and FTIR. Thereafter an analysis is given for the as-deposited as well as annealed layers with respect to reflow properties, the hydrogen content and optical losses.

5.1 Experimental procedure

Low index PECVD P-doped and BP-doped SiON layers were deposited on p-type <100> oriented 100 mm silicon wafers at a substrate temperature of 350 °C, a chamber pressure of 140 Pa and RF power of 20 W (HF). Optimized P-doped SiON layers (B1-00) could be obtained by gas mixtures of 600 sccm of 2% SiH_4/N_2, 600 sccm of nitrous oxide (N_2O), and 20 sccm of 5% PH_3/Ar (see Section 4.1). Boron-Phosphorus doping was obtained by adding diborane (5% B_2H_6 diluted in Ar) to the gas mixtures. Three types of boron phosphorus-doped layers B1-10, B1-20, and B1-30 were deposited by adding 10, 20, and 30 sccm of diborane (5% B_2H_6 diluted in Ar) to the gas mixtures.

In order to determine the composition and optical properties of the layers, several depositions of B1-00, B1-10, B1-20, and B1-30 type layers were carried out. The layer thickness and the index of refraction have been determined by spectroscopic ellipsometry on approximately 250 nm thin layers directly deposited on silicon wafers. Relatively thick layers (~ 1200 nm) deposited directly on silicon were used for the atomic concentrations measurements, whereas for the optical loss measurement sufficiently thick layers on thermally oxidized wafers were prepared.

The nature of the hydrogen bonds and the hydrogen concentration of the layers were determined with FTIR. The atomic concentrations of Si, O and N of the layers were determined by XPS. The optical loss measurements were performed on the fundamental mode using the sliding prism method (see Section 2.2.3).

5.2 Characterization of as-deposited layers

In order to study the boron and phosphorus-doping effect on the PECVD SiON layer properties, a series of PECVD BP-doped SiON layers (B1-10, B1-20, and B1-30) were deposited. The as-deposited layers were analyzed and showed a refractive index in-homogeneity of less than 0.002 and a thickness non-uniformity of 1% for the entire layers. Figure 5.1 shows the atomic concentration determined by XPS. The atomic boron concentration increases with increasing B_2H_6/Ar gas flow rate.

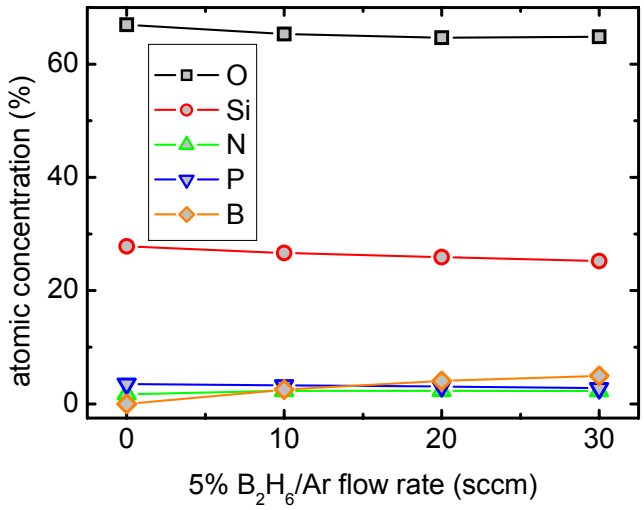

Figure 5.1 Atomic concentration of the studied layers as a function of the B_2H_6 (5% in Ar) flow ratio measured y XPS.

Figure 5.2 shows the refractive index obtained by spectroscopic ellipsometry of the PECVD SiON layers with increasing B-doping.

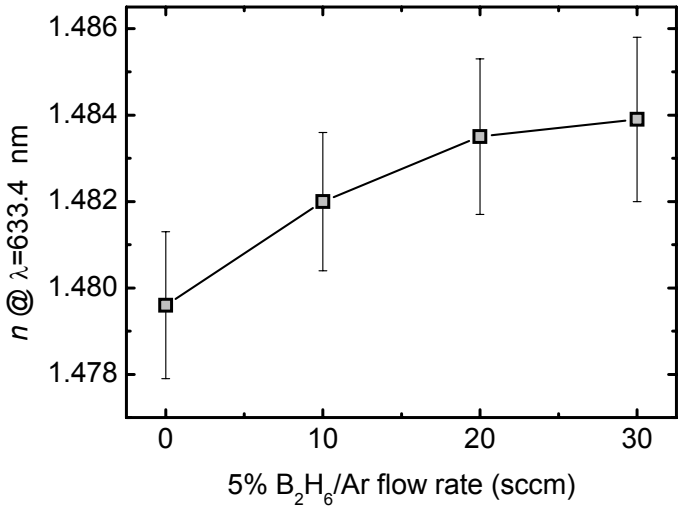

Figure 5.2 Refractive index of the studied BP-SiON layers as a function of the B_2H_6 (5% in Ar) flow ratio.

The refractive index was found to increase slightly with the B-doping as can be seen in Figure 5.2. This increase is unexpected as the index of refraction

of boron oxide, B_2O_3 is 1.43, substantially lower than of the SiO_2 (n = 1.457) and of the P-doped SiON layer under study (n = 1.48). It is well known that the refractive index of the layer is strongly influence by its structure and composition. In particular, increasing the layer density and the nitrogen content or decreasing the oxygen content will result in an increased refractive index value. XPS analysis, indeed, has shown a slight increase in nitrogen content with increasing B_2H_6 flow rate.

For the bond configuration and the hydrogen concentration FTIR spectroscopy has been used. Figure 5.3 shows FTIR spectra of the B-doped PECVD SiON layers (B1-10, B1-20, and B1-30) in comparison with the P-doped layer (B1-00). For clarity the curves have been plotted with a vertical offset.

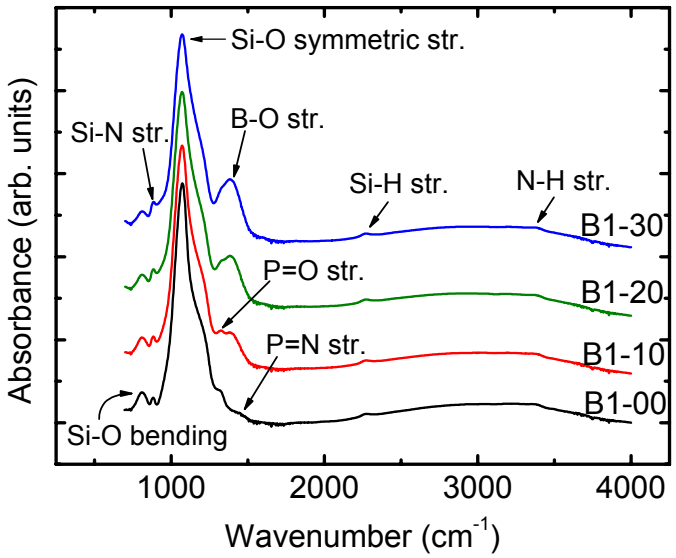

Figure 5.3 FTIR spectra ranging from 700 to 4000 cm^{-1} of the PECVD P-doped SiON layers under study with increasing B-doping.

The dominant absorption feature in these spectra, a broad peak around 1050 cm^{-1} could be observed in all samples. This peak can be resolved into contributions by Si-O bending, Si-N (1) stretching, Si-N (2) stretching, Si-O symmetric stretching, P-O stretching, P-N stretching, Si-O asymmetric stretching, P=O stretching, B-O stretching and P=N stretching. For a quantitative analysis we used nonlinear curve fitting, assuming that the peaks have a symmetric Gaussian form. The deconvolution of the absorption spectra yields Gaussian peaks whose parameters are summarized in Table 5.1 (see also Figure 5.4). The infrared peak positions are in good agreement with previous studies on undoped SiON, P-doped silica and BP-doped silica layers [20, 34, 52, 75, 83-86].

Table 5.1 Energy of the infrared vibrational modes observed in P-doped (B1-00) and BP-doped PECVD silicon oxynitride layers.

	Peak frequency (cm^{-1})			
Vibration type	B1-00	B1-10	B1-20	B1-30
Si-O bending	811	811	811	812
Si-N (1) stretching	882	882	882	881
Si-N (2) stretching	956	947	943	937
Si-O symmetric str.	1077	1074	1071	1071
P-O stretching	1138	1135	1134	1133
P-N stretching	1165	1162	1161	1159
Si-O asymmetric str.	1212	1208	1205	1203
P=O stretching	1314	1322	1323	1322
B-O stretching	-	1403	1400	1399
P=N stretching	1413	1458	1456	1460
Si-H(N_2Si)	2250	2246	2245	2243
Si-H(N_3)	2268	2266	2266	2263
N-H…N stretching	3346	3350	3354	3352
N-H stretching	3388	3392	3394	3396
H-O-H stretching	3498	3495	3499	3499
Si-OH…HOH	3557	-	-	-

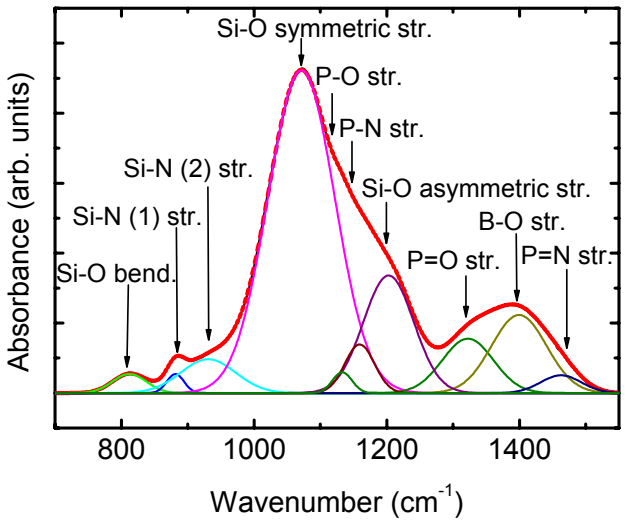

Figure 5.4 The broad IR absorption band between 700 and 1500 cm^{-1} for sample B1-30. It is well fitted with 10 Gaussian-shaped absorption bands.

The increase in the broad peak shoulder with the B-doping can be explained by the appearance of B-O stretching bonds at 1400 cm^{-1} with increasing B_2H_6 flow rate. The fitting results show an increase in B-O band area (see Figure 5.5).

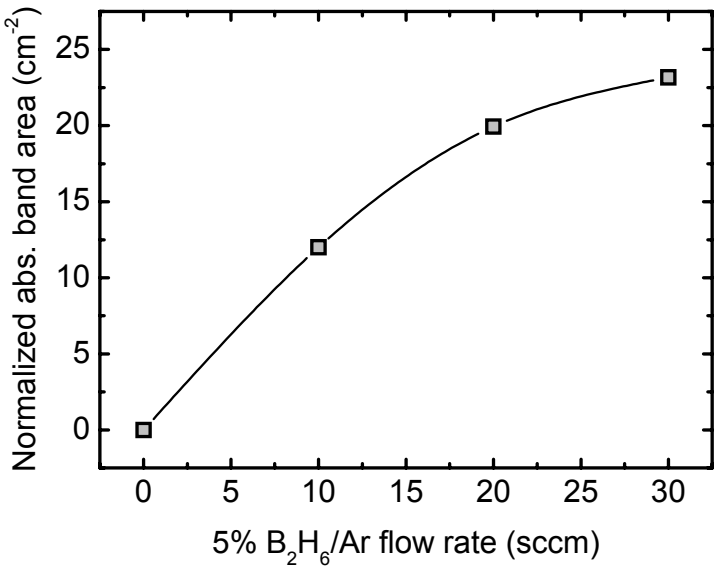

Figure 5.5 Variation of the normalized B-O absorption band area for PECVD P-doped SiON layers with increasing B_2H_6 flow rate.

In order to explain the increase of the nitrogen content with B_2H_6 flow rate, the following reactions for N_2O was proposed [95]:

$$N_2O \rightarrow O + N_2 \tag{5.1}$$

$$N_2O + O \rightarrow 2NO \tag{5.2}$$

$$NO + O \rightarrow NO_2 \tag{5.3}$$

The oxygen atom initially removed from N_2O by reaction (5.1) is used either for the layer formation or it can react with N_2O by equation (5.2) to form a NO radical, which gets absorbed in the layer as a source of nitrogen. Concurrent to reaction (5.2), reaction (5.3) diminishes the amount of oxygen. When B_2H_6 is added to the gas mixture, boron is present in the layer and

oxygen is bonded to boron as B-O together with Si-O bonds. It should be mentioned that the bond strength of B-O (808.8 kJ/mol) is comparable with that of Si-O (799.6 kJ/mol) and stronger than Si-N (470.0 kJ/mol) [64]. Therefore, increasing B_2H_6 flow rate may consume the oxygen atoms due to formation of B-O and/or boron oxide (B_2O_3). The deficient in oxygen would raise the probability to absorb the NO radical in the layer [95].

Another features that can be observed in all samples (B1-00 to B1-30) are the absorption due to N-H and Si-H stretching modes in the region 3300 – 3450 cm^{-1} and 2150 – 2300 cm^{-1} respectively. These peaks were not influenced by the B-doping.

5.3 Effect of post-deposition annealing

The melting point of B_2O_3 is 450 °C [64]. Incorporation of boron oxide in the SiON matrix will reduce the SiON reflowing temperature. The annealing properties of BSG and BPSG have been investigated by [40, 96]. There is, however, a discrepancy about the reflow temperature in literature. Osorio [90] have reported that B-doping of silica reduces the reflowing temperature to below 900 °C. However, Feuchter [40] obtained significant reflow for BPSG layers by heat treatment for 12 hours at temperatures as high as 1100 °C.

5.3.1 Reflow of boron-phosphorus doped SiON

In our study boron doping has been introduced in order to improve the reflow properties of PECVD P-doped SiON layers. The influence of boron doping on the reflow properties has been investigated by depositing various boron phosphorus-doped SiON layers (B1-10, B1-20 and B1-30) on ridges etched in silicon, and consequent annealing at 1000°C in a nitrogen atmosphere for 17 hours.

A significant improvement in the reflow properties was observed for sample B1-30 and the gaps are completely filled. This can be seen in Figure 5.6, where a cross section of our test structure before and after annealing is given. The excellent reflow properties can be attributed to the increase of B_2O_3 in the BPSG, see also ref. [97].

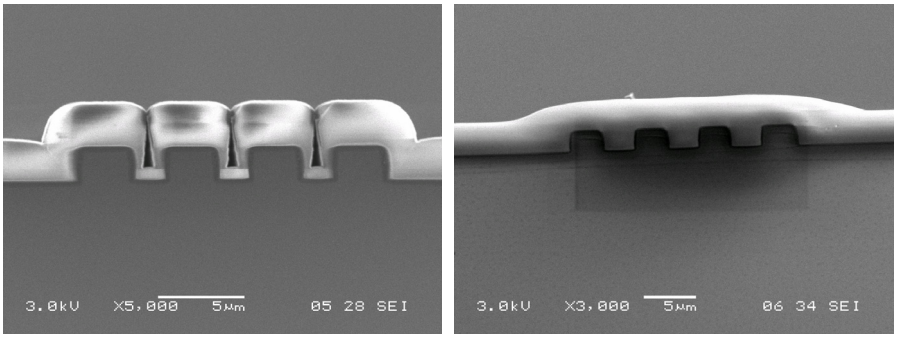

(a) (b)

Figure 5.6 Cross-section of Si-rides covered with 4 µm of BP-doped SiON (Sample B1-30): (a) before and (b) after heat treatments at 1000 °C in N_2 atmosphere for 17 hours

As it has been explained before (see Sections 4.1 and 5.3) the incorporation of P_2O_5 and B_2O_3 in the SiON matrix are crucial for reducing the reflow temperature. As a consequence, it would be difficult to reduce the reflow temperature of SiON layers with higher refractive indices, where less oxygen radicals are present. Moreover, the deficiency in oxygen radicals increase the probability of boron nitride to be formed in the SiON matrix, that may lead to increased hardening of layers.

In order to study the reflow properties of higher refractive indices BP-doped SiON oxynitride layers, depositions of B1-30, B2-30, B3-30 and B4-30 type layers were carried out. The gas flow rates of the 4 samples are given in Table 5.2. All layers were deposited at a substrate temperature of 350°C, a chamber pressure of 140 Pa and RF power of 20 W (HF).

Table 5.2 Gas flow rates for the BP-doped silicon oxynitride layers B1-30 to B4-30.

	Gas flow rates				
Sample	N_2O (sccm)	2% SiH_4/N_2 (sccm)	5% PH_3/Ar (sccm)	5% B_2H_6/Ar (sccm)	n @ λ=633 nm
B1-30	600	600	20	30	1.4819
B2-30	330	600	20	30	1.4917
B3-30	260	600	20	30	1.4980
B4-30	200	600	20	30	1.5147

The reflow properties of channel waveguides etched in BP-doped SiON (B1-30, B2-30, B3-30 and B4-30) were investigated by annealing at 1000°C in a nitrogen atmosphere. As expected the lower index layers show better reflow properties. This can clearly be seen in Figure 5.7(a-d), which show BP-doped SiON ridge waveguides before and after annealing.

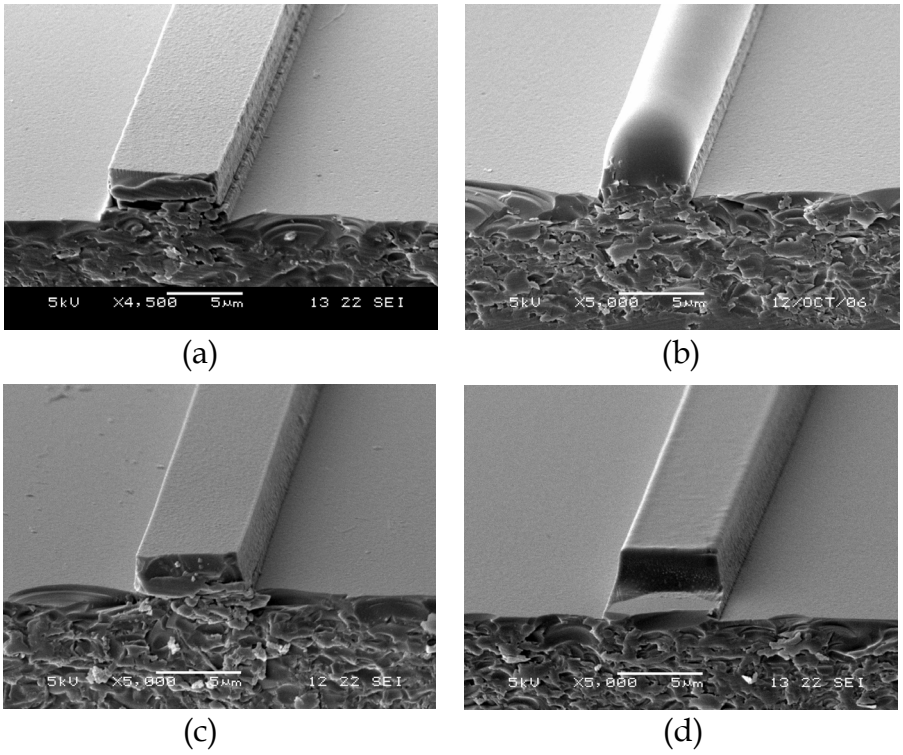

Figure 5.7 SEM photograph of BP-doped SiON channel waveguides (a) sample B1-30 before; (b) sample B1-30 after; (c) sample B3-30 before; (d) sample B3-30 after annealing at 1000°C in N_2 atmosphere for 17 hours.

It can clearly be seen in Figure 5.7(a-d) that the surface roughness has been largely reduced by surface tension induced smoothening (see Leinse et al. [98] for similar results in Polymers). Moreover, especially in (b), the large change in the cross-sections from rectangular to nearly elliptical shape can be observed.

In order to examine in detail the surface tension induced smoothening we performed Atomic Force Microscope (AFM) topographical surface scans on as-deposited and annealed BP-doped SiON layers. Figure 5.8(a-d) shows AFM images of 1×1 μm² surfaces of BP-doped (sample B3-30) before and after annealing at 1000°C in N_2 for 17 hours.

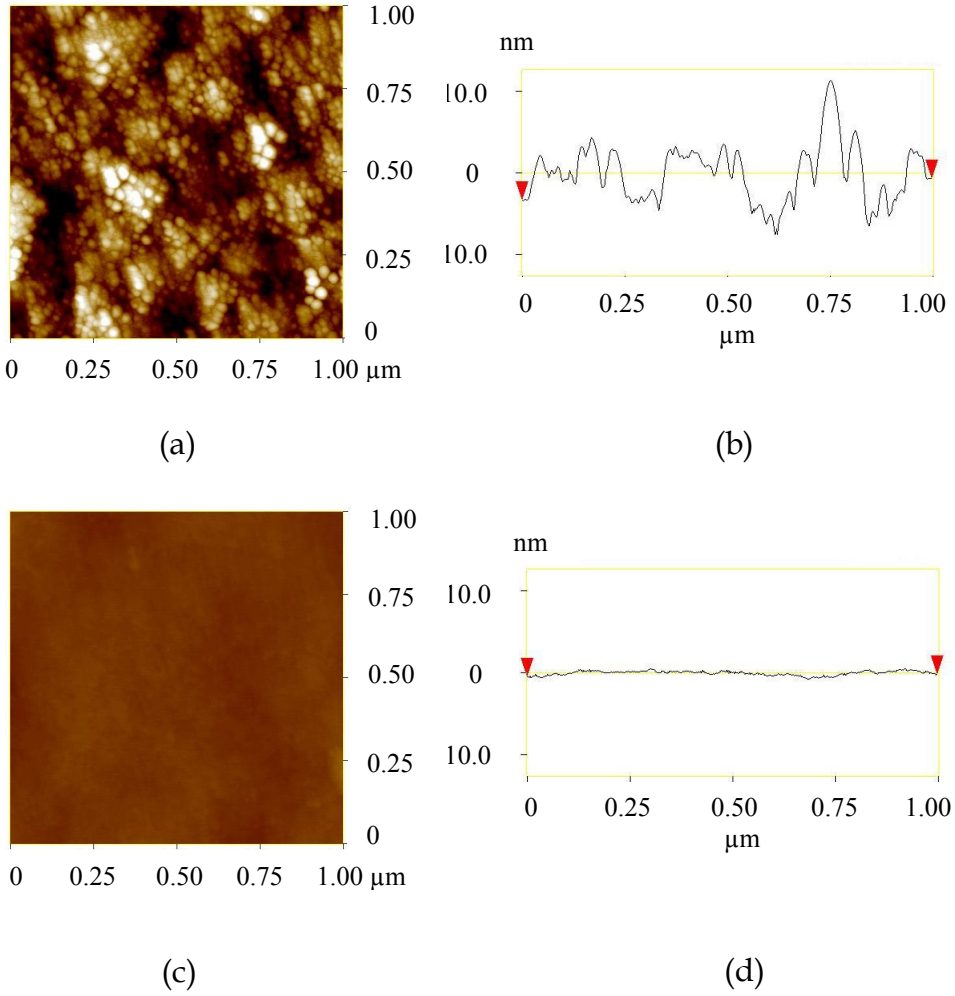

Figure 5.8 AFM images of the BP-doped SiON (sample B3-30) surface demonstrating the effect of annealing at 1000 °C in N_2 atmosphere for 17 hours (a) area scan before annealing; (b) linear scan before annealing; (c) area scan after annealing; (d) linear scan after annealing

An analysis of the AFM scans show a large decrease in the root-mean-square surface roughness upon annealing from 1.66 and 2.81 nm to 0.16 and 0.23 nm for sample B1-30 and B3-30 respectively. However, for sample B4-30 (n=1.51) no reflow could be observed at 1000 °C anneal temperature. This layer has been treated at higher anneal temperature, at 1050 °C as well as 1100 °C. A significant reflow was obtained at 1100 °C reflow temperature, see Figure 5.9.

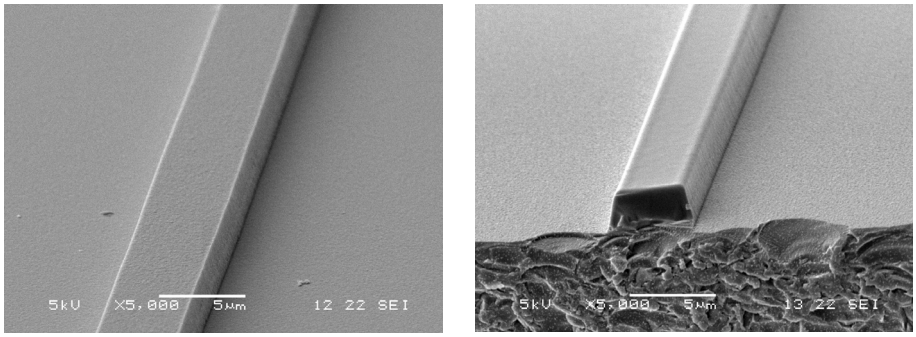

(a) (b)

Figure 5.9 SEM photograph of BP-doped SiON channel waveguide (sample B4-30) (a) before; (b) after annealing at 1100 °C in N_2 atmosphere for 17 hours.

5.3.2 Hydrogen induced losses

In order to study the effect of heat treatment on the hydrogen content and optical losses in BP-doped SiON, layers with the same composition as B1-30, B2-30, B3-30 and B4-30 were deposited and annealed at 1000 °C for 3 hours in a nitrogen atmosphere. The FTIR spectra show no N-H and Si-H peaks after annealing at 1000 °C for all BP-doped samples (B1-30 – B4-30). Figure 5.10 present the total hydrogen concentration in the layers before and after heat treatment.

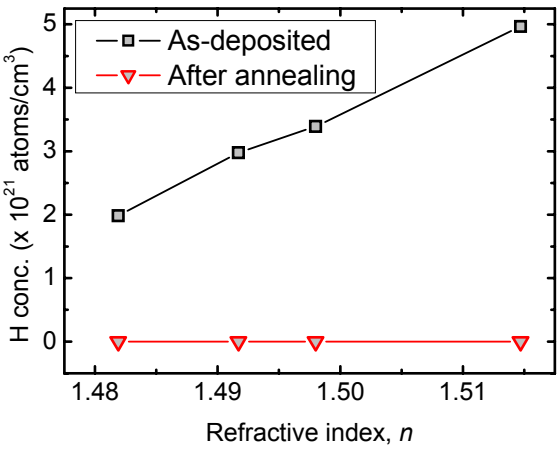

Figure 5.10 Total hydrogen concentration of the as-deposited and annealed BP-doped SiON layers (B1-30 –B4-30). The layers were annealed at 1000 °C in N_2 atmosphere for 3 hours.

The elimination of the hydrogen at 1000 °C corresponds well with the loss measurements obtained from as-deposited and annealed BP-doped SiON layers (see Figure 5.11). It can clearly be seen that the optical loss is reduced to below 0.2 dB/cm after annealing at 1000 °C for 3 hours in N_2 atmosphere.

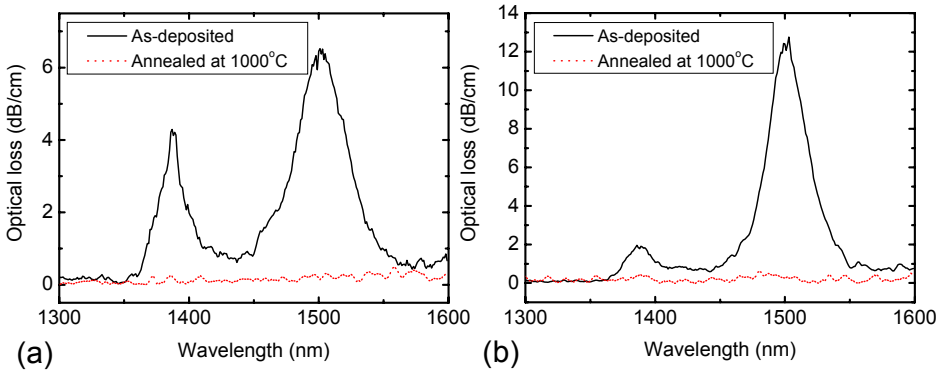

Figure 5.11 Optical loss as a function of wavelength for as-deposited and annealed BP-doped SiON layers (a) sample B1-30; (b) sample B3-30

The refractive index, the thickness and the materials birefringence of as-deposited and annealed (1000 °C) BP-doped SiON layers were measured by the prism coupling technique at wavelengths of 632.8 nm. The results are listed in Table 5.3.

Table 5.3 Refractive index, layer thickness and the materials birefringence for BP-doped SiON layers as-deposited and after annealing at 1000 °C for 17 hours; measured by ATR at a wavelength of 632.8 nm.

	As-deposited			After annealing		
Sample	n_{TE}	d (μm)	Δn_{TM-TE}	n_{TE}	d (μm)	Δn_{TM-TE}
B1-30	1.4782	4.005	-0.0004	1.4793	3.860	0.0000
B2-30	1.4897	4.025	-0.0002	1.4969	3.787	0.0002
B3-30	1.4964	4.089	-0.0003	1.5158	3.628	0.0001

An increase in refractive index and shrinkage of the layer thickness after annealing were observed for the studied layer. The materials birefringence was found to decrease upon annealing at 1000 °C. As it has been discussed in the previous chapter this decrease in the birefringence for the annealed layers can probably be related to the decrease in stress.

5.4 Summary

Boron phosphorus-doped silicon oxynitride layers for integrated optics applications have been deposited from 2%SiH_4/N_2 + N_2O + 5% PH_3/Ar and 5% B_2H_6/Ar. The influence of boron and phosphorus-doping to the PECVD SiON layer properties has been investigated.

The boron concentration was found to increase steadily with the diborane flow rate. Special attention has been given to the reflow properties and the presence of hydrogen bonds that lead to unwanted optical absorption in telecommunication applications. The reflow properties of P-doped SiON layers have been improved by B-doping. A significant material reflow was obtained for BP-doped SiON containing ~ 3 at% P and ~ 5 at% B by heat treatment at 1000°C in N_2 atmosphere for 17 hours. Also the sidewall surface roughness of the BP-doped channel waveguides with a refractive index up to 1.51 has been smoothed. Moreover, the hydrogen induced losses have been eliminated at 1000 °C. In that case, the optical losses in the entire range from 1300 to 1600 nm (including the third telecommunication window) are reduced to below 0.2 dB/cm for slab-type BP-doped SiON waveguides. It therefore can be concluded that this material is very promising for applications in low-loss integrated optical devices.

6 Summary and conclusions

Development and improvement of optical materials is one of the challenges in integrated optics, since materials issues in the fabrication of waveguiding layer structures are of great importance for getting high-quality integrated optical components. As explained in Chapter 1, these materials must satisfy certain requirements with respect to high transparency, possibility for accurate waveguide definition, high physical, chemical, mechanical and thermal stability, compatibility with other materials used in microelectronics and fiber technology, easy processing and reasonably low cost. In particular, silicon oxynitride grown by CVD has been emerging as a technologically reliable material for integrated optics application.

The scope of this thesis is to develop new processes for the realization of PECVD silicon oxynitride layers for use in low loss optical waveguides. A serious drawback of the chosen deposition process is the incorporation of undesirable N-H and Si-H bonds in the layers which significantly increase the optical loss in the spectral region of interest (around 1550 nm wavelength) for telecom applications. Phosphorus and boron doping was considered and optimized as a way to reduce the hydrogen content and the reflow temperature of the SiON layers. In order to optimize the fabrication of passive optical waveguides, a number of physical parameters of the deposited layers are characterized. Methods and experimental setups for the determination of the properties of slab-waveguides are described in chapter 2. The refractive index and the layer thickness are both determined by spectroscopic ellipsometry and prism coupler techniques. The atomic composition of the layer material is characterized by XPS and RBS. The hydrogen induced optical losses are determined by FTIR spectroscopy in the deep infrared, whereas the overtone absorption of these hydrogen bonds is measured by the prism coupler technique in the near infrared.

In our study the process development includes the optimization of the undoped SiON layers, which have been taken as a starting point for phosphorus and boron doping. This optimization is described in chapter 3. Optimized PECVD silicon oxynitride layers for integrated optics application have been deposited from 2%SiH_4/N_2 + N_2O and 2%SiH_4/N_2 + NH_3 + N_2O. The uniformity and homogeneity of the deposited layers and the reproducibility of the process are good. The optical properties of SiON layers were found to depend largely on the deposition parameters, especially on the N_2O/SiH_4 gas flow ratio. The concentrations of the HF SiON layers deposited with high N_2O/SiH_4 flow ratio (> 20) can be described with the SiO_xN_y stoichiometric model. The deviation from the stoichiometric composition at

lower N_2O/SiH_4 gas flow ratio is due to the formation of silicon rich silicon oxynitride. An increase of silicon content in the layers is accompanied by an increase in the number of Si-H bonds. The excess of silicon and the hydrogen content are responsible for raising the optical losses in the layers at wavelengths of 632.8 and 1550 nm, respectively. Both silicon and hydrogen increase with decreasing N_2O/SiH_4 gas flow ratio. PECVD SiON layers have been deposited without Si-Si bond by adding NH_3 to the (N_2O + SiH_4/N_2) gas mixture. PECVD silicon oxynitride with lower hydrogen concentration and without Si-Si bonds have been obtained by using a LF RF generator. That means that LF RF plasma is suitable for deposition of high refractive index SiON layers.

Chapter 4 deals with deposition and characterization of low and high index P-doped SiON layers. In the first stage we have investigated the composition and the chemical environment of phosphorus, silicon, oxygen, nitrogen, and hydrogen in these layers. The phosphorus concentration was found to increase steadily with the phosphine flow rate. Special attention has been given to the presence of hydrogen bonds that lead to unwanted optical absorption in telecommunication applications. A significant reduction in N-H and O-H bonds concentration was observed for the P-doped SiON layers, when compared to undoped samples. Thus, a significant reduction in the optical loss of slab-type waveguides at λ=1505 nm was obtained for the P-doped SiON layers, when compared to undoped samples. Moreover, the optical losses below λ=1400 nm were reduced to below 0.2 dB/cm.

The annealing results show that the H bonds in the P-doped layers can completely be eliminated by annealing at 1000 °C. In that case, the optical losses in the entire range from 1300 to 1600 nm (including the third telecommunication window) are reduced to below 0.2 dB/cm for slab-type P-doped SiON waveguides with refractive indices up to 1.73. It therefore can be concluded that this material is well suited for applications in telecommunication devices. Moreover, the influence of phosphorus doping on the reflow properties has been investigated. The reflow temperature was found to decrease with increasing phosphorus concentration in the layers.

In chapter 5 we present our results on the deposition and reflowing of BP-doped SiON layers for integrated optics applications. The PECVD layers have been deposited from 2%SiH_4/N_2 + N_2O + 5% PH_3/Ar and 5% B_2H_6/Ar. The influence of boron and phosphorus-doping to the layer properties has been investigated. First, we focused on the composition and the chemical environment of boron, phosphorus, silicon, oxygen, nitrogen, and hydrogen in these layers. The boron concentration was found to increase steadily with the diborane flow rate. Special attention has been given to the reflow properties and the presence of hydrogen bonds that lead to unwanted optical absorption in telecommunication applications. The reflow properties of P-doped SiON layers have been improved by B-doping. A significant materials reflow was obtained for BP-doped SiON containing ~ 3 at% P and ~ 5 at% B by heat

treatment at 1000 °C in N_2 atmosphere for 17 hours. Also the sidewall surface roughness of the BP-doped channel waveguides with a refractive index up to 1.51 has been reduced by surface tension induced smoothening. Moreover, the hydrogen induced losses have been eliminated at 1000 °C. In that case, the optical losses in the entire range from 1300 to 1600 nm (including the third telecommunication window) are reduced to below 0.2 dB/cm for slab-type BP-doped SiON waveguides. It therefore can be concluded that this material is very promising for applications in low-loss integrated optical devices.

Samenvatting en conclusies

Ontwikkeling en verbetering van optische materialen is één van de uitdagingen van geïntegreerde optica, daar de materiaal eigenschappen bij de fabricage van golfgeleidende laag structuren van groot belang zijn om hoog kwalitatieve geïntegreerde optische componenten te verkrijgen. Zoals uitgelegde in Hoofdstuk 1, dienen deze materialen te voldoen aan zekere eigenschappen met betrekking tot transparantie, mogelijkheid voor nauwkeurige golfgeleider definitie, hoge fysische, chemische, thermische stabiliteit, compatibiliteit met andere materialen gebruikt in micro-elektronica en glasvezel technologie, makkelijke fabricage en redelijke lage kosten. Met name silicium oxynitride, gegroeid in CVD, heeft zich ontpopt als technologisch betrouwbare materiaal voor toepassingen in de geïntegreerde optica.

Het doel van dit proefschrift is het ontwikkelen van nieuwe processen voor de realisatie van PECVD silicium oxynitride lagen voor het gebruik in optische golfgeleiders met lage verliezen. Een nadeel van de gekozen depositieproces is de incorporatie van ongewenste N-H en Si-H verbindingen in de lagen hetgeen de optische verliezen significant doet toenemen in het gebruikte spectrale gebied (rond 1550 nm golflengte) voor telecom toepassingen. Als een methode om waterstof te verminderen en de reflow temperatuur van de SiON te verlagen, werd doping met fosfor en borium onderzocht en geoptimaliseerd. Om de fabricage van de passieve optische golfgeleiders te optimaliseren, werd een aantal fysische parameters van de gedeponeerde lagen gekarakteriseerd. Methoden en experimentele opbouw voor de bepaling van de eigenschappen van de vlakke golfgeleiders worden beschreven in Hoofdstuk 2. De brekingsindex en de laagdiktes worden bepaald door spectroscopische ellipsometrie en prisma inkoppel technieken. De atomaire samenstelling van de materiaal laag wordt gekarakteriseerd door XPS en RBS. De door waterstof veroorzaakte optische verliezen worden bepaald met FTIR spectroscopie in het gebied van diep- infrarood, terwijl de boventoon absorptie van deze waterstof verbindingen wordt gemeten met de prisma inkoppel techniek in het nabije infrarood gebied.

In ons onderzoek omvat de proces ontwikkeling het optimaliseren van de niet -gedopte SiON lagen als startpunt voor de doping met fosfor en borium. Deze optimalisatie wordt beschreven in Hoofdstuk 3. Geoptimaliseerde PECVD silicium oxynitride lagen voor toepassing in geïntegreerde optica zijn gegroeid met 2%$SiH_4/N_2 + N_2O$ en 2%$SiH_4/N_2 + NH_3 + N_2O$. De uniformiteit en de homogeniteit van de gedeponeerde lagen en de reproduceerbaarheid van het proces zijn goed. De optische eigenschappen van SiON lagen bleek

voor een groot deel af te hangen van de depositieparameters, met name van de verhouding N_2O/SiH_4 gas flow. De concentraties van de HF SiON lagen, gedeponeerd met een hoge N_2O/SiH_4 gas stroom verhouding (>20), kan worden beschreven met het SiO_xN_y stoichiometrische model. De afwijking van de stoichiometrische samenstelling bij lagere N_2O/SiH_4 gas stroom is te wijten aan de vorming van silicium rijk oxynitride. Een toename van het silicium gehalte in de lagen gaat gepaard met een toename van het aantal Si- H verbindingen. De overvloed van silicium en waterstof gehalte is verantwoordelijk voor de toename van optische verliezen in de lagen bij golflengtes van respectievelijk 632.8 en 1550 nm. Zowel silicium als waterstof nemen toe bij de afname van N_2O/SiH_4 gas stroom verhouding. PECVD SiON lagen zijn gedeponeerd zonder Si-Si verbinding door het toevoegen van NH_3 aan de (N_2O + SiH_4/N_2) gas samenstelling. PECVD silicium oxynitride met lage waterstof concentratie en zonder Si-Si verbindingen werden verkregen door het gebruik van de LF RF generator. Dat betekent dat het LF RF plasma geschikt is voor depositie van hoge brekingsindex SiON lagen.

Hoofdstuk 4 handelt over depositie en karakterisatie van lage en hoge index P- gedoteerde SiON lagen. In de eerste fase hebben wij de compositie en de chemische omgeving van fosfor, silicium, zuurstof, stikstof en waterstof in deze lagen onderzocht. De fosfor concentratie bleek gestaag toe te nemen met de fosfine stroom snelheid. Speciale aandacht werd gegeven aan de aanwezigheid van waterstof verbindingen die tot ongewenste optische absorptie leiden in telecommunicatie toepassingen. Een significante reductie van N-H en O-H verbindingen concentratie werd waargenomen voor de P-gedoteerde SiON lagen, in vergelijking met de niet- gedoteerde preparaten. Dus een significante reductie van optische verliezen van slab- type golfgeleiders bij λ=1505 nm werd verkregen voor P- gedoteerde SiON lagen in vergelijking met niet gedoteerde lagen. Bovendien, werden de optische verliezen beneden λ=1400 nm gereduceerd tot beneden 0.2 dB/cm.

De resultaten van het annealen laten zien dat de H verbindingen in de P-gedoteerde lagen volledig kunnen worden geëlimineerd door te uitgloeien bij 1000 ^{0}C. In dat geval worden de optische verliezen voor het hele gebied van 1300 tot 1600 nm (inclusief het derde telecommunicatie window) gereduceerd tot beneden 0,2 dB/cm voor slab-type P- gedoteerde SiON golfgeleiders met brekingsindices tot 1.73. Het kan daarom worden geconcludeerd dat dit materiaal goed geschikt is voor toepassingen in telecommunicatie componenten. Daarnaast werd de invloed van de fosfor dotering op de reflow eigenschappen onderzocht. Het bleek dat de reflow temperatuur afnam met de toename van de fosfor concentratie in de lagen.

In Hoofdstuk 5 presenteren wij de resultaten van de depositie en reflow van BP- gedoteerde SiON lagen voor geïntegreerde optische toepassingen. De PECVD lagen werden gedeponeerd met 2%SiH_4/N_2 + N_2O + 5% PH_3/Ar en 5% B_2H_6/Ar. De invloed van borium en fosfor- dotering op de laageigenschappen werd onderzocht. We focusseerden eerst op de

samenstelling en de chemische omgeving van borium, fosfor, silicium, zuurstof, stikstof en waterstof in deze lagen. De borium concentratie bleek gestaag to te nemen met de diboraan stroom snelheid. Speciale aandacht werd gegeven aan de reflow eigenschappen en de aanwezigheid van waterstof verbindingen die tot ongewenste optische absorptie in de telecommunicatie toepassingen leiden. De reflow eigenschappen van P- gedoteerde SiON lagen werden verbeterd door B- dotering. Een significante materiaal reflow werd verkregen voor BP- gedopte SION met ~ 3 at% P en ~ 5 at% B bij een warmtebehandeling van 1000 ^{0}C in N_2 omgeving gedurende 17 uur. Ook de zijwand ruwheid van de BP- gedopte golfgeleiders met een brekingsindex tot 1.51 werd verminderd door glad strijken door middel van oppervlakte spanning. Daarnaast werden de door de waterstof veroorzaakte verliezen tegengegaan bij 1000 ^{o}C. In dat geval worden de optische verliezen voor het hele gebied van 1300 tot 1600 nm (inclusief het derde telecommunicatie venster) gereduceerd tot beneden 0, 2 dB/cm voor slab- type BP- gedoteerde SiON golfgeleiders. Het kan daarom worden geconcludeerd dat dit materiaal veelbelovend is voor toepassingen in laag- verlies geïntegreerd optische componeneten.

References

[1] S. E. Miller, "Integrated optics: an introduction," *Bell Syst. Tech. J.*, vol. 48, pp. 2059, 1969.

[2] K. Kashiwagi and S. Yamashita, "Fabrication of silica-based glass optical waveguide by UV beam scanning," *Japanese Journal of Applied Physics Part 1-Regular Papers Short Notes & Review Papers*, vol. 43, pp. 5850-5853, 2004.

[3] D. Y. Kim, H. Du, G. R. Kowach, C. A. White, and D. J. McGee, "Fabrication and optical measurements of germanium-doped silica ridge waveguides using a colloidal suspension approach," *Applied Physics Letters*, vol. 87, pp. 121114, 2005.

[4] J. W. Lee, S. S. Kim, B. T. Lee, and J. H. Moon, "Ge-doped SiO2 glass films prepared by plasma enhanced chemical vapor deposition for planar waveguides," *Applied Surface Science*, vol. 228, pp. 271-276, 2004.

[5] M. R. Poulsen, P. I. Borel, J. Fage-Pedersen, J. Hubner, M. Kristensen, J. H. Povlsen, K. Rottwitt, M. Svalgaard, and W. Svendsen, "Advances in silica-based integrated optics," *Optical Engineering*, vol. 42, pp. 2821-2834, 2003.

[6] L. T. Zhang, W. F. Xie, J. Wang, A. W. Li, H. Xing, W. Zheng, and Y. S. Zhang, "Thermal annealing in FHD Ge-doped SiO2 film for applications in optical waveguides," *Applied Surface Science*, vol. 228, pp. 48-52, 2004.

[7] Q. Y. Zhang, K. Pita, C. K. F. Ho, N. Q. Ngo, L. P. Zuo, and S. Takahashi, "Low optical loss germanosilicate planar waveguides by low-pressure inductively coupled plasma-enhanced chemical vapor deposition," *Chemical Physics Letters*, vol. 368, pp. 183-188, 2003.

[8] P. F. Hu, T. C. Chong, and L. P. Shi, "Fabrication and characterization of ion-exchanged optical waveguides in potassium lithium niobate crystal substrates," *Japanese Journal of Applied Physics Part 1-Regular Papers Short Notes & Review Papers*, vol. 41, pp. 155-159, 2002.

[9] A. Kaplan and S. Ruschin, "Optical switching and power control in LiNbO3 coupled waveguide arrays," *IEEE Journal of Quantum Electronics*, vol. 37, pp. 1562-1573, 2001.

[10] J. S. Selvan, M. Fujimura, and T. Suhara, "Fabrication of Zn-indiffused LiNbO3 optical waveguides using ZnS as diffusion source," *Japanese Journal of Applied Physics Part 1-Regular Papers Brief Communications & Review Papers*, vol. 44, pp. 3075-3076, 2005.

[11] W. Sohler, B. K. Das, D. Dey, S. Reza, H. Suche, and R. Ricken, "Erbium-doped lithium niobate waveguide lasers," *IEICE Transactions on Electronics*, vol. E88c, pp. 990-997, 2005.

[12] T. C. Kleckner, A. S. Helmy, K. Zeaiter, D. C. Hutchings, and J. S. Aitchison, "Dispersion and modulation of the linear optical properties of GaAs-AlAs superlattice waveguides using quantum-well intermixing," *IEEE Journal of Quantum Electronics*, vol. 42, pp. 280-286, 2006.

[13] H. Nakajima, "Development on guided-wave switch arrays," *IEICE Transactions on Electronics*, vol. E82C, pp. 297-304, 1999.

[14] D. J. Blumenthal and M. Masanovic, "LSOR (Label switched optical Router): Architecture and underlying integration technologies," presented at 31st European Conference on Optical Communications Glasgow, 2005.

[15] J. R. Bonar, R. Childs, and R. I. Laming, "Advancements in passive planar lightwave circuits and hybrid integration devices," *Comptes Rendus Physique*, vol. 4, pp. 51-64, 2003.

[16] J. H. C. van Zantvoort, F. M. Huijskens, C. G. P. Herben, and H. de Waardt, "Fiber-array pigtailing and packaging of an InP-based optical cross-connect chip," *IEEE Journal of Selected Topics in Quantum Electronics*, vol. 5, pp. 1255-1259, 1999.

[17] R. Varrazza, T. Bricheno, and S. Y. Yu, "A fully packaged 4x4 integrated optical switch matrix," *IEEE Journal of Selected Topics in Quantum Electronics*, vol. 11, pp. 1248-1254, 2005.

[18] D. Peters, K. Fischer, and J. Muller, "Integrated-Optics Based on Silicon Oxynitride Thin-Films Deposited on Silicon Substrates for Sensor Applications," *Sensors and Actuators a-Physical*, vol. 26, pp. 425-431, 1991.

[19] K. Wörhoff, A. Driessen, P. V. Lambeck, L. T. H. Hilderink, P. W. C. Linders, and T. J. A. Popma, "Plasma enhanced chemical vapor deposition silicon oxynitride optimized for application in integrated optics," *Sensors and Actuators a-Physical*, vol. 74, pp. 9-12, 1999.

[20] F. Ay and A. Aydinli, "Comparative investigation of hydrogen bonding in silicon based PECVD grown dielectrics for optical waveguides," *Optical Materials*, vol. 26, pp. 33-46, 2004.

[21] K. Wörhoff, L. T. H. Hilderink, A. Driessen, and P. V. Lambeck, "Silicon oxynitride - A versatile material for integrated optics applications," *Journal of the Electrochemical Society*, vol. 149, pp. F85-F91, 2002.

[22] R. M. de Ridder, K. Wörhoff, A. Driessen, P. V. Lambeck, and H. Albers, "Silicon oxynitride planar waveguiding structures for application in optical communication," *IEEE Journal of Selected Topics in Quantum Electronics*, vol. 4, pp. 930-937, 1998.

[23] M. G. Hussein, K. Wörhoff, C. G. H. Roeloffzen, L. T. H. Hilderink, R. M. de Ridder, and A. Driessen, "Characterization of thermally treated PECVD SiON layers," Proceedings of the 6th Annual Symposium IEEE/LEOS Benelux Chapter, Brussels, Belgium, p.265-268, Nov. 2001.

[24] A. Stoffel, A. Kovacs, W. Kronast, and B. Muller, "LPCVD against PECVD for micromechanical applications," *Journal of Micromechanics and Microengineering*, vol. 6, pp. 1-13, 1996.

[25] J. Yota, J. Hander, and A. A. Saleh, "A comparative study on inductively-coupled plasma high-density plasma, plasma-enhanced, and low pressure chemical vapor deposition silicon nitride films," *Journal of Vacuum Science & Technology A*, vol. 18, pp. 372-376, 2000.

[26] M. I. Alayo, D. Criado, L. C. D. Goncalves, and I. Pereyra, "Deposition and characterization of silicon oxynitride for integrated optical applications," *Journal of Non-Crystalline Solids*, vol. 338-40, pp. 76-80, 2004.

[27] A. Sassella, P. Lucarno, A. Borghesi, F. Corni, S. Rojas, and L. Zanotti, "Silicon Oxynitride Study by the Tetrahedron Model and by Spectroscopic Ellipsometry," *Journal of Non-Crystalline Solids*, vol. 187, pp. 395-402, 1995.

[28] O. P. Agnihotri, S. C. Jain, J. Poortmans, J. Szlufcik, G. Beaucarne, J. Nijs, and R. Mertens, "Advances in low temperature processing of

silicon nitride based dielectrics and their applications in surface passivation and integrated optical devices," *Semiconductor Science and Technology*, vol. 15, pp. R29-R40, 2000.

[29] A. Sassella, "Tetrahedron Model for the Optical Dielectric Function of H-Rich Silicon Oxynitride," *Physical Review B*, vol. 48, pp. 14208-14215, 1993.

[30] W. A. P. Claassen, H. A. J. T. Vanderpol, A. H. Goemans, and A. E. T. Kuiper, "Characterization of Silicon-Oxynitride Films Deposited by Plasma-Enhanced Cvd," *Journal of the Electrochemical Society*, vol. 133, pp. 1458-1464, 1986.

[31] C. M. M. Denisse, K. Z. Troost, F. H. P. M. Habraken, W. F. van der Weg, and M. Hendriks, "Annealing of plasma silicon oxynitride films," *Journal of Applied Physics*, vol. 60, pp. 2543, 1986.

[32] C. M. M. Denisse, K. Z. Troost, J. B. Oude Elferink, F. H. P. M. Habraken, and M. Hendriks, "Plasma-enhanced growth and composition of silicon oxynitride films," *Journal of Applied Physics*, vol. 60, pp. 2536-2542, 1986.

[33] C. M. M. Denisse, J. F. M. Janssen, F. H. P. M. Habraken, and W. F. Vanderweg, "Infrared-Absorption Study of N-H Bonds in Plasma-Deposited Silicon Oxynitride Films," *Applied Physics Letters*, vol. 52, pp. 1308-1310, 1988.

[34] G. L. Bona, R. Germann, and B. J. Offrein, "SiON high-refractive-index waveguide and planar lightwave circuits," *IBM Journal of Research and Development*, vol. 47, pp. 239-249, 2003.

[35] P. Blochl, R. Germann, B. J. Offrein, I. Massarek, and H. W. M. Salemink, "Material with reduced optical Absorption," in *PCT Publication* Nr. WO 99/44937. European Patent Application, 1998.

[36] M. G. Hussein, K. Worhoff, G. Sengo, and A. Driessen, "Deposition and characterization of PECVD phosphorus-doped silicon oxynitride layers for integrated optics," presented at Proceedings of EUROCVD-15, The Electrochemical Society, Bochum, Germany, 2005.

[37] M. G. Hussein, K. Worhoff, G. Sengo, and A. Driessen, "Reduction of hydrogen-induced optical losses of plasma-enhanced chemical vapor deposition silicon oxynitride by phosphorus doping and heat treatment," *Journal of Applied Physics*, vol. 101, pp. 023517, 2007.

[38] S. Shanfield and S. Bay, "Process characterization of PSG and BPSG plasma deposition," *Journal of the Electrochemical Society*, vol. 131, pp. 2202-2203, 1984.

[39] J. E. Tong, K. Schertenleib, and R. A. Carpio, "Process and film characterization of PECVD borophosphosilicate films for VLSI application," *Solid State Technology*, 1984.

[40] T. Feuchter, "Active and passive optical waveguides by PECVD," Ph.D thesis: The Technical University of Denmark, 1996.

[41] M. K. Smit and C. van Dam, "PHASAR-based WDM-devices: Principles, design and applications," *IEEE Journal of Selected Topics in Quantum Electronics*, vol. 2, pp. 236-250, 1996.

[42] S. M. Rossnagel, J. J. Cuomo, and W. D. Westwood, *Handbook of plasma processing technology: Fundamentals, Etching, Deposition, and Surface Interaction*. New Jersey: Noyes Publications, 1990.

[43] R. Syms and J. Cozens, *Optical guided waves and devices*. London: McGraw-Hill, 1992.

[44] J. A. C. Woollam, Inc, "Maintenance and operation Manual M-44 Ellipsometer," 1996.

[45] R. M. Azzam and N. M. Bashara, *Ellipsometry and Polarized Light*: North-Hooland Publishing Co., 1977.

[46] S. T. Kirsch, "Determining the refractive index and thickness of thin films from prism coupler measurements," *Applied Optics*, vol. 20, pp. 2085, 1981.

[47] R. Ulrich and R. Torge, "Measurement of thin film prameters with a prism coupler," *Applied Optics*, vol. 12, pp. 2901, 1973.

[48] D. L. Lee, *Electromagnetic principles of integrated optics*. New York: John Wiley & sons, Inc., 1986.

[49] T. Tamir and R. C. Alferness, *Guided wave optoelectronics*. Berlin: Springer-Verlag, 1990.

[50] "Indexfit software," 0.23 ed: Devoloped at University of Twente, Department of Applied Physics, 2000.

[51] A. Fadini and F. M. Schnepel, *Vibrational Spectroscopy methods and applications*: Ellis Horwood Ltd, 1989.

[52] G. Sogarates, *Infrared characteristic group frequencies*. New York: John Wiley & Sons, 1994.

[53] B. C. Smith, *Fundamentals of Fourier Transform Infrared Spectroscopy*: CRC Press, Inc., 1996.

[54] W. A. Lanford and M. J. Rand, "The Hydrogen content of plasma-deposited silicon nitride," *J. Appl. Phys.*, vol. 49, pp. 2473-2477, 1978.

[55] J. R. Shallenberger, D. A. Cole, and S. W. Novak, "Characterization of silicon oxynitride thin films by x-ray photoelectron spectroscopy," *Journal of Vacuum Science & Technology a-Vacuum Surfaces and Films*, vol. 17, pp. 1086-1090, 1999.

[56] R. P. Vasquez, M. H. Hecht, F. J. Grunthaner, and M. L. Naiman, "X-ray photoelectron spectroscopy study of the chemical structure of thermally nitrided SiO_2," *Applied Physics Letters*, vol. 44, pp. 969 - 971, 1984.

[57] J. Viard, E. Beche, D. Perarnau, R. Berjoan, and J. Durand, "XPS and FTIR study of silicon oxynitride thin films," *Journal of the European Ceramic Society*, vol. 17, pp. 2025-2028, 1997.

[58] J. F. Moulder, F. S. William, P. E. Sobol, and D. B. Kenneth, *Handbook of X-ray Photoelectron Spectroscopy*. Eden Prairie, Minnesota: Perkin-Elmer Corporation, Physical Electronics Division, 1992.

[59] M. Ribeiro, I. Pereyra, and M. I. Alayo, "Silicon rich silicon oxynitride films for photoluminescence applications," *Thin Solid Films*, vol. 426, pp. 200-204, 2003.

[60] W. L. Scopel, M. C. A. Fantini, M. I. Alayo, and I. Pereyra, "Structural investigation of Si-rich amorphous silicon oxynitride films," *Thin Solid Films*, vol. 425, pp. 275-281, 2003.

[61] R. G. Hunsperger, *Integrated optics: Theory and Technology*, 5th ed. Berlin: Springer, 2002.

[62] D. R. Cote, S. V. Nguyen, A. K. Stamper, D. S. Armbrust, D. Tobben, R. A. Conti, and G. Y. Lee, "Plasma-assisted chemical vapor deposition of dielectric thin films for ULSI semiconductor circuits," *IBM Journal of Research and Development*, vol. 43, pp. 5-38, 1999.

[63] J. M. Austin and A. L. Smith, "Decomposition of N_2O in a glow discharge," *J. Phys. D: Appl. Phys.*, vol. 6, pp. 2236 - 2241, 1973.

[64] D. R. Lide, *Handbook of chemistry and Physics*, 84th ed. New York: CRC Press LLC, 2004.

[65] M. I. Alayo, I. Pereyra, W. L. Scopel, and M. C. A. Fantini, "On the nitrogen and oxygen incorporation in plasma-enhanced chemical vapor deposition (PECVD) SiOxNy films," *Thin Solid Films*, vol. 402, pp. 154-161, 2002.

[66] W. A. P. Claassen, "Ion Bombardment-Induced Mechanical Stress in Plasma-Enhanced Deposited Silicon Nitride and Silicon Oxynitride Films," *Plasma Chemistry and Plasma Processing*, vol. 7, pp. 109 - 124, 1987.

[67] W. A. P. Claassen, W. G. J. N. Valkenburg, M. F. C. Willemsen, and W. M. v. d. Wijgert, "Influence of Deposition Temperature, Gas Pressure, Gas Phase Composition, and RF Frequency on Composition and Mechanical stress of Plasma Silicon Nitride Layers," *Journal of the Electrochemical Society*, vol. 132, pp. 893-898, 1985.

[68] A. Sassella, A. Borghesi, F. Corni, A. Monelli, G. Ottaviani, R. Tonini, B. Pivac, M. Bacchetta, and L. Zanotti, "Infrared study of Si-rich silicon oxide films deposited by plasma-enhanced chemical vapor deposition," *Journal of Vacuum Science & Technology a-Vacuum Surfaces and Films*, vol. 15, pp. 377-389, 1997.

[69] B. Chapman, *Glow discharge processes*. New York: John Wiley and Sons, Inc., 1980.

[70] J. Campmany, J. L. Andujar, A. Canillas, J. Costa, and E. Bertran, "Optical, Vibrational and Compositional Study of Amorphous-Silicon Oxynitride Thin-Films Grown by an Rf Plasma Using N_2O+SiH_4 Gas-Mixtures," *Applied Surface Science*, vol. 70-1, pp. 695-700, 1993.

[71] Y. Cros, N. Jaffrezicrenault, J. M. Chovelon, and J. J. Fombon, "Study of PECVD Silicon Oxynitride Thin-Layers as Isfet Sensitive Insulator Surface for Ph Detection," *Journal of the Electrochemical Society*, vol. 139, pp. 507-511, 1992.

[72] A. L. Zhang, K. T. Chan, M. S. Demokan, V. W. C. Chan, P. C. H. Chan, and A. H. P. Chan, "Annealing effects on the loss and birefringence of silicon oxynitride rectangular optical waveguides," *Applied Physics Letters*, vol. 87, pp. 101105-1 - 101105-3, 2005.

[73] E. M. Bartee, *Engineering experimental Design fundamentals*. New Jersey: Prentice-Hall, Inc., 1968.

[74] C. R. Hicks, *Fundamental concepts in the design of experiments*. New York: Saunders College Publishing, 1993.

[75] M. Futatsudera, T. Kimura, A. Matsumoto, T. Inokuma, Y. Kurata, and S. Hasegawa, "Defects in silicon oxynitride films," *Thin Solid Films*, vol. 424, pp. 148-151, 2003.

[76] D. C. Montgomery and G. C. Runger, *Applied Statistics and Probability for Engineers*. New York: John Wiley & Sons, Inc., 2003.

[77] A. L. Edwards, *An introduction to linear regression and correlation*, 2nd ed. New York: Freeman, 1984.

[78] Y. T. Kim, S. M. Cho, Y. G. Seo, H. D. Yoon, Y. M. Im, and D. H. Yoon, "Influence of hydrogen on SiO_2 thick film deposited by PECVD and FHD for silica optical waveguide," *Crystal Research and Technology*, vol. 37, pp. 1257-1263, 2002.

[79] Y. Cros, J. C. Rostaing, J. Peisner, G. Leveque, and C. Ance, "Optical properties of plasma-enhanced chemical vapor deposited silicon-oxynitride films," *J. Appl. Phys.*, vol. 62, pp. 4538-4544, 1987.

[80] R. Germann, H. W. M. Salemink, R. Beyeler, G. L. Bona, F. Horst, I. Massarek, and B. J. Offrein, "Silicon oxynitride layers for optical waveguide applications," *Journal of the Electrochemical Society*, vol. 147, pp. 2237-2241, 2000.

[81] M. G. Hussein, K. Wörhoff, G. Sengo, and A. Driessen, "Influence of phosphorus doping on hydrogen content and optical losses in PECVD silicon oxynitride," Proceedings of the 10th Annual Symposium IEEE/LEOS Benelux Chapter, Mons, Belgium, pp.101-104, Dec. 2005.

[82] M. Jozwik, P. Delobelle, C. Gorecki, A. Sabac, L. Nieradko, C. Meunier, and F. Munnik, "Optomechanical characterisation of compressively prestressed silicon oxynitride films deposited by plasma-enhanced chemical vapour deposition on silicon membranes," *Thin Solid Films*, vol. 468, pp. 84-92, 2004.

[83] D. E. C. Corbide and E. J. Lowe, "Infra-red Spectra of Inorganic Phosphorus Compounds.," *Journal of the Chemical Society*, pp. 4555-4564, 1956.

[84] M. K. Gunde and M. Macek, "Infrared optical constants and dielectric response functions of silicon nitride and oxynitride films," *Physica Status Solidi a-Applied Research*, vol. 183, pp. 439-449, 2001.

[85] A. G. Thorsness and A. J. Muscat, "Moisture absorption and reaction in BPSG thin films," *Journal of the Electrochemical Society*, vol. 150, pp. F219-F228, 2003.

[86] C. K. Wong, H. Wong, C. W. Kok, and M. Chan, "Silicon oxynitride prepared by chemical vapor deposition as optical waveguide materials," *Journal of Crystal Growth*, vol. 288, pp. 171-175, 2006.

[87] P. Patnaik, *Handbook of inorganic chemicals*. New York: McGraw-Hill, 2002.

[88] R. M. de Ridder, K. Worhoff, A. Driessen, P. V. Lambeck, and H. Albers, "Silicon oxynitride planar waveguiding structures for application in optical communication," *IEEE Journal of Selected Topics in Quantum Electronics*, vol. 4, pp. 930-937, 1998.

[89] V. Y. Vassiliev, J. Z. Zheng, S. K. Tang, W. Lu, J. Hua, and Y. S. Lin, "Growth kinetics and deposition-related properties of subatmospheric pressure chemical vapor deposited borophosphosilicate glass film," *Journal of the Electrochemical Society*, vol. 146, pp. 3039-3051, 1999.

[90] S. Rojas, R. Gomarasca, L. Zanotti, A. Borghesi, A. Sassella, G. Ottaviani, L. Moro, and P. Lazzeri, "Properties of Borophosphosilicate Glass-Films Deposited by Different Chemical Vapor-Deposition Techniques," *Journal of Vacuum Science & Technology B*, vol. 10, pp. 633-642, 1992.

[91] K. E. Mattsson, "Plasma-Enhanced Growth, Composition, and Refractive-Index of Silicon Oxy-Nitride Films," *Journal of Applied Physics*, vol. 77, pp. 6616-6623, 1995.

[92] S. Mayumi and S. Ueda, "PSG Flow in High-Pressure Steam," *Japanese Journal of Applied Physics Part 1-Regular Papers Short Notes & Review Papers*, vol. 29, pp. 645-649, 1990.

[93] Z. Yin and F. W. Smith, "Optical Dielectric Function and Infrared-Absorption of Hydrogenated Amorphous-Silicon Nitride Films - Experimental Results and Effective-Medium-Approximation Analysis," *Physical Review B*, vol. 42, pp. 3666-3675, 1990.

[94] D. Criado, M. I. Alayo, M. C. A. Fantini, and I. Pereyra, "Study of the mechanical and structural properties of silicon oxynitride films for optical applications," *Journal of Non-Crystalline Solids*, vol. 352, pp. 2319-2323, 2006.

[95] R. H. Horng, F. Chen, D. S. Wuu, and T. Y. Lin, "Refractive index behavior of boron-doped silica films by plasma-enhanced chemical vapor deposition," *Applied Surface Science*, vol. 92, pp. 387-390, 1996.

[96] S. P. A. Osorio, I. Montero, J. Perriere, and J. M. Martinezduart, "Effect of Annealing on the Composition of Pecvd Borosilicate and Borophosphosilicate Glasses," *Applied Surface Science*, vol. 70-1, pp. 772-776, 1993.

[97] R. R. A. Syms, W. Huang, and V. M. Schneider, "Optimisation of borophosphosilicate glass compositions for silica-on-silicon integrated optical circuits fabricated by the sol-gel process," *Electronics Letters*, vol. 32, pp. 1233-1234, 1996.

[98] A. Leinse, M. B. J. Diemeer, and A. Driessen, "Scattering loss reduction in polymer waveguides by reflowing," *Electronics Letters*, vol. 40, pp. 992-993, 2004.

Acknowledgements

A journey is easier when you travel together. This thesis is the result of four and half years of work, whereby I have been accompanied and supported by many people. It is a pleasant that I have now the opportunity to express my sincere gratitude to all of them.

First, I would like to thank my promotor Prof. Dr. Alfred Driessen who has been always supportive in my research. Without his valuable guidance this work could not have been done. I would like to acknowledge his fruitful discussions. I would also like to appreciate his patience in reading and criticizing the manuscript of this thesis.
I'm grateful to my assistant promotor Dr. Kerstin Wörhoff, for her support and encouragement since 2001 when I started my MSc assignment. She has given me many useful advices during my research.
I would like to thank all members of my graduation committee for their willingness to examine this thesis, the efforts in proof-reading and providing me with valuable comments on the manuscript of this thesis.
I have enjoyed working in IOMS group; I would like to give my sincere thanks to Markus Pollnau, Hugo Hoekstra and René de Ridder.
I wish to express my sincere gratitude to IOMS secretary Rita ter Weele, for the excellent administrative support.
I'm very grateful to Anton Hollink for his technical support. Whenever I needed something in the lab, the great Anton was there to deliver it as quickly as possible.
I'm indebted to Luice Hilderink for her technical assistance during my MSc and PhD research. I enjoyed a lot talking with her about our and the Dutch social life. Bedankt Lucie!
I would like to thank Gabriel Sengo for his technical assistance in the cleanroom and for translating the summary into Dutch.
I'm very grateful to the technical assistance from Henk van Wolferen (everything is so easy with his sense of humor), Robert Wijn and Meindert Dijkstra.
I wish to express my sincere gratitude to Ronald Dekker for help with spectraloss software, dicing and for sharing the RIM practical supervision with me. Also I would like to thank him for patiently answering my questions related to the PhD graduation procedure.
I would like to thank Edwin Klein for help in mask design and for sharing supervision of MSc assignment of Dorleta Oregui. Thanks to Dorleta for her work on boron-phosphorus doped silicon oxynitride waveguides.

My sincere thanks are devoted to Mart Diemeer, Henry Kelderman, Muralidharan Balakrishnam and Jing Yang for the useful discussions in the IOMS-II cavity meetings.
I'm very thankful to Henri Uranus for many pleasant and fruitful discussions and the good friendship.
It has been an extraordinary pleasure to stay 6 years (MSc plus PhD) in one office (Hogekamp, room 7102A) and to share the office with Cazimir Gabriel Bostan for four years. I'm very grateful for all things we have shared and the friendship developed during that time.
I would like to thank Feridun Ay for many pleasant and interesting discussions and for his friendship.
Thanks to Ton Koster, Arne Leinse, Chaitanya Dongre, Alexander Iskandar and Gan shuyi, my current and former office-mates for very good atmosphere in "7102A" and for the many stimulating discussions.
I wish to express my sincere gratitude to Chris Roeloffzen, who guided my first steps into the world of integrated optics and I have learned lots from him during my MSc period.
Life would have been difficult in the Netherlands without my close friend and colleague Sami Musa, he gently offer counsel and unconditional support at each turn of the road, "Shukran ya abu alsamasim".
I would like to extend my thanks to current and former members of LDG/IOMS group who made my stay enjoyable and memorable: Marcel Hoekman, Wico Hopman, Jonathan Bradley, Lasse Kauppinen, Dimitri Geskus, Shanmugam Aravazhi, Tom Blauwendraat, Douwe Geuzebroek, Geert Altena, Didit Yudistira, Joris van Lith, Freddy Tan, Dion Klunder, Remco Stoffer, Els Kok, Webin Hu, Boudewijn and Shankar Selvaraja.
I would like to thank René Heideman for his encouragement and support on my work.
I would like to give my sincere thanks to all cleanroom staff for making MESA+ an excellent working environment.
I wish to express my warm and sincere thanks to Hala Bakri, for rendering me the sense of brotherhood. I'm glad to know her in Twente.
Omer Adam (Abu Ali) was great and true friend. I would like to thank him and his wife Wijdan for all their support.
I would like to thank Saravanan for his friendship and for all things we have shared during the past 6 years, wish you a good stay and work in Singapore.
I wish to thanks all my Romanian friends that I have met in Twente for the good time and support: Diana Bostan, Liviu, Georgiana and Aurelian Galca.
It has been a great pleasure to meet Pierre-Olivier Logerais and Josef Wagner in EUROCVD-15 conference. Thanks for the wonderful moments in Bochum, Germany and for keeping our contact.
I would like to express my most sincere gratitude to Marten Durieux for many ways of support. Without his efforts and the financial support from "De

Stichting Steunfonds Soedanese Studenten" during my MSc program, the possibility to start a PhD in the Netherlands would have been very difficult.
I would like to extend my sincere gratitude to all my Dutch friends that I have met in Sudan and/or in the Netherlands for their many ways of support: Bert and Ina Zwart, Rob Koorders, Harry, Willem, Ron, Maurits Wijzenbeek, Metje Postma, Olga, Elizabeth and René.
I'm very thankful to Mohammed, Ursula, Sami and Tariq Elmusharaf for the good time we have together and for their full support.
I would like to express my sincere gratitude to Siddig Tawer for his good friendship and for the nice time we had in Leiden.
Mohsen Tambel was magnificent, helpful and good fried. I would like to thank him for his endless support.
I would like to thank all members of Al Neelain University, Khartoum, Sudan for their support and encouragements.
I have enjoyed my visit to Berlin. Special thanks to Noha & Mohamed Yahia, Ali Esawi and Prof. Badr Eldin for the wonderful time and for their support.
I feel a deep sense of gratitude to "majmoaat 99": Sarah Hamza (Enschede), Mohamed Kamil, Hala Artoli, Alarees Obai (wish you and Hadeel a happy life), AmiR Abdalla, Elmuez Dawi, Azza & Amjed, Elhaseen, Sarah (Rotterdam) and Mozamel (Delft). Thanks for all the "gezellige" moments and for their support.
The presence of Sudanese friends in the Netherlands was very important for emotional composure; "lakum meni Khalis Al-shukr": Nouralla (Abu Alanoaar), Abdel Monim Artoli, Hassan Idris & Limya, Sir Elkhatim Elsayed, Mohamed Abdo, Ibrahim Idris, Tino, Aldosh & Iglal, Isam Obeid & Dalal, Tarig & Wafaa, Isam & Mona, Mojahid (Alzaiem), Yazeed, Mohamed & Dalia, Yasir Abbas & Amani, Hassan & Ikhlas, Afifi & Tahani, Kushaib & Fatima, Hamdi Alajab, Wali & Nidal, Esia & Itimad, Khaled Elraid, Mobarak & Mai, Yousif Elsheikh, Ahmed & Khalda, Abdelsalam & Mona, Kamal & Jehaan, Nasir Kashkash, Tagiq Abasia, Kuri Family, Aymen Kamal, Hussein Suliman, Izzeldin (Ya wad Madani) and Osama (Oldenzaal)...
Above all, without the extra support of my lovely wife, Nagla, I could not accomplish my work for PhD. She has always encouraged and refreshed me with love. My daughter Lara joined our family in my last year in the PhD. The presence of her has been a great tonic to our couple. I finally thank from heart all members of my family in Sudan for continuous support and encouragements. I'm glad to be one of them.

Mohamed Gamar Hussein

Enschede, January 2007

Publications

- M.G. Hussein, K. Wörhoff, D. Oregui, E. Klein, L.T.H. Hilderink, and A. Driessen, "Deposition and characterization of PECVD boron-phosphorus doped silicon oxynitride layers for integrated optics," To be published (2007).

- M.G. Hussein, K. Wörhoff, G. Sengo, and A. Driessen, "Reduction of hydrogen-induced optical losses of plasma-enhanced chemical vapor deposition silicon oxynitride by phosphorus doping and heat treatment," *Journal of Applied Physics,* vol. 101, pp. 023517, 2007.

- M. G. Hussein, K. Wörhoff, G. Sengo, and A. Driessen, "Optimization of plasma-enhanced chemical vapor deposition Silicon Oxynitride layers for integrated optics applications" (Accepted for publication in *Thin Solid Films*, 2006).

- M. G. Hussein, K. Wörhoff, G. Sengo, and A. Driessen, "Influence of phosphorus doping on hydrogen content and optical losses in PECVD silicon oxynitride," Proceedings of the 10th Annual Symposium IEEE/LEOS Benelux Chapter, Mons, Belgium, pp.101-104, Dec. 2005.

- M.G. Hussein, K. Wörhoff, G. Sengo, and A. Driessen, "Deposition and characterization of PECVD phosphorus-doped silicon oxynitride layers for integrated optics," Proceedings of EUROCVD-15, The Electrochemical Society, Bochum, Germany, Sept. 2005.

- M.G. Hussein, K. Wörhoff,, G. Sengo, and A. Driessen, "Fabrication and characterization of PECVD phosphorus-doped silicon oxynitride layers for integrated optics application," Proceedings of the 9th Annual Symposium IEEE/LEOS Benelux Chapter, December 2-3 2004, Pp. 91-94, Ghent University, Ghent, Belgium, ISBN Number: 9076546061, Dec. 2004.

- M.G. Hussein, K. Wörhoff, G. Sengo, and A. Driessen, "Stability of low refractive index PECVD silicon oxynitride layers," Proceedings of the 8th Annual Symposium IEEE/LEOS Benelux Chapter, University of Twente, Enschede, The Netherlands, Pp. 77-80, Nov. 2003

- K. Wörhoff, M. G. Hussein, C.G.H. Roeloffzen, and L.T.H. Hilderink, "Properties of annealed silicon oxynitride layers for optical applications" (Invited), Editors: R.E. Sah, K.B. Sundaram, M.J. Deen, D. Landeer, W.D. Brown and D. Misra, The Electrochemical Society, Proceedings 7th Conference Electrochemical Society "Silicon Nitride and Silicon Dioxide Thin Insulating Films, Paris, France, Pp. 406-417, ISBN 1-56677-347-4, (2003, April 27- May 2).

- K. Wörhoff, P. V. Lambeck, D. J. W. Klunder, R. M. de Ridder, R. G. Heideman, C. G.H. Roeloffzen, M.G. Hussein, S. Musa, H. J. van Weerden, and A. Driessen, "Planar waveguide devices on an Si-compatible technology platform," Proceedings The electrochemical society 2002-4 (invited), First international symposium on integrated optics, Philadelphia, USA, pp. 279-312, 2002.

- M.G. Hussein, K. Wörhoff, C.G.H. Roeloffzen, L.T.H. Hilderink, R.M. de Ridder and A. Driessen, "Characterization of thermally treated PECVD SiON layers," Proceedings of the 6th Annual Symposium IEEE/LEOS Benelux Chapter, Brussels, Belgium, p.265-268, Nov. 2001.